Cluster Mean Field Approach to Low Dimensional Quantum Magnets

Ayushi Singhania

A thesis submitted for the partial fulfillment of

the degree of Doctor of Philosophy

Department of Physical Sciences,
Indian Institute of Science Education and Research Mohali

Knowledge City, Sector 81, SAS Nagar, Manauli PO, Mohali 140306, Punjab, India.

February, 2021

Dedicated to mummy,
who always dreamt of the day I made something of myself,
and to papa and bhai for their support.

Declaration

The work presented in this thesis has been carried out by me under the guidance of Dr. Sanjeev Kumar at the Indian Institute of Science Education and Research Mohali. This work has not been submitted in part or in full for a degree, a diploma, or a fellowship to any other university or institute. Whenever contributions of others are involved, every effort is made to indicate this clearly, with due acknowledgment of collaborative research and discussions. This thesis is a bonafide record of original work done by me and all sources listed within have been detailed in the bibliography.

Ayushi Singhania

In my capacity as the supervisor of the candidate's thesis work, I certify that the above statements by the candidate are true to the best of my knowledge.

Dr. Sanjeev Kumar

Acknowledgements

I would like to begin by expressing my sincere gratitude to my advisor Dr. Sanjeev Kumar. This thesis would not have been written, were it not for his guidance and constant encouragement. He has taught me the art of approaching a research problem from basics. I am especially grateful for his incredible patience and calm nature which has made the journey of Ph.D. very comfortable.

I would also like to thank my doctoral committee, Dr. Yogesh Singh and Dr Rajeev Kapri for monitoring my progress throughout my journey as a research scholar. I also thank Dr. Gautam Sheet for giving me an opportunity to gain hands-on experience with numerous experimental techniques like AFM and STM during a summer project. I would like to extend my gratitude towards Dr. Abhishek Chaudhuri for his sincere comments and motivation. I am grateful to all the faculty members of IISER Mohali for the courses they have taught me. My sincere thanks to Dr. Satoshi Nishimoto for giving me an opportunity to present my work at IFW Dresden. I would also like to extend my gratitude towards him for his inputs and collaborations in one of my projects. I also thank Dr. F. Assad for hosting me at the University of Wurzburg and for his comments on my work. I would like to present my deepest gratitude to Kanhaiya sir, without whose efforts I wouldn't have ever become capable of achieving this. I would also like to thank Rajeev sir for motivating me to take this as a career path.

I would like to acknowledge IISER Mohali for research fellowship and high-performance computing facilities useful for conducting my research. I appreciate IISER Mohali and CSIR for supporting my travel to present my research at conferences in Germany and Portugal.

I would like to thank my group members Arnob, Swagatam, Deepak, Abhinay, Sanjib, Kanika, and Preeti for delightful discussions. I cannot thank Sudhanshu and Arnob enough for always helping me with technical issues, I don't know what I would have done without you both. I have been fortunate to have friends like Sanchi, Shivangi and Sambit for always supporting me. Sambit plays an instrumental role in making Physics more interesting for me. Samridhi has been with me since the day I entered IISER, I cannot thank her enough for being there with me in all the ups and downs I have faced in this very long journey. I thank Poulami, Jaskaran, Mayank, Vikas(h), Shivam, Sujoy, Manaoj, Ankit and Anubhav for making IISER a second home. I thank Shashi and Pranay for becoming my doubt centre and for all those entertaining Skype calls.

A big thanks to my mother for her dream to make me an independent and a confident woman. None of this would have been possible without my father's love and support. I thank my brother for being the pillar of my strength. I wish my mama Arvind Jain could see me finally finishing my degree.

I am grateful to have met Pranay, which wouldn't have been possible if not for this degree. I would like to thank him for making me look at the brighter side on my bad days and being there (virtually) to celebrate my happiness.

In the end I would like to extend my gratitude to all the people with whom I have crossed paths in the last seven years. The journey is more important than the destination, and I have learned a lot in these years academically and personally, the credit for which goes to each one of them.

Ayushi Singhania

Abstract

Collective behaviour of large number of interacting particles results in fascinating phenomena ranging from as simple as freezing of water to as complex as appearance of superconductivity. Magnetism is a remarkable example of how quantum physics can spring up new surprises even in cases where relevant particles remain immobile. It covers wide scale of complexity, from magnets sticking to our household fridges to the exotic quantum spin liquid phases that define the forefront of current research in quantum magnetism. Low dimensional spin-1/2 magnetic systems are ideal candidates for observing and uncovering mysteries of quantum physics as the combination of low dimensionality and low spin quantum number enhances quantum fluctuations. Motivated by their importance in understanding fundamental aspect of quantum mechanics and potential applications, a plethora of low dimensional magnetic materials have been discovered and studied experimentally. However, strictly 1D or 2D magnets are almost never realized in real materials, as contribution from spins in neighboring chains or planes affect the magnetic ordering. This often leads to unexpected ordering and phase transitions. This thesis attempts to understand such low temperature behaviour of real materials, in terms of quasi-1D and 2D model spin Hamiltonians studied using cluster mean field theory (CMFT). The key idea of CMFT is to treat all interaction links located within the cluster exactly, and to make use of the conventional mean field decoupling for interaction links connecting the cluster and the environment. The approach allows for an accurate treatment of short range spatial correlations, as well as thermodynamic behavior, in the mean field spirit. The technique captures the subtle competition between different possibilities of magnetic ordering at the level of finite-size calculations. CMFT successfully explains the origin of low-temperature peak observed in specific heat data reported in the experiments performed on $CuInVO_5$. For the frustrated ferromagnet $\beta-TeVO_4$, CMFT is able to uncover multiple phase transitions in the absence of applied field. In presence of field, it identifies complex orders such as quadrupolar and vector chiral orders along with specific anomalies like re-entrant transition similar to experimental observations. Furthermore, a problem of disordered antiferromagnetic spin chain with anisotropic impurities is explored. CMFT analysis reveals that a fraction of anisotropic impurities is capable of inducing a Néel type ordering. In addition to providing a satisfactory understanding of observations on $CuInVO_5$ and β-$TeVO_4$, this thesis highlights that CMFT can become a powerful tool in understanding the nature of magnetic order emerging at low temperatures in frustrated as well as disordered magnets.

List of Publications

Singhania, A., Kumar, S., "Cluster mean-field study of the Heisenberg model for $CuInVO_5$", ***Phys. Rev. B*** 98, (2018) 104429

Singhania, A., Kumar, S., "Multiple phase transitions and high-field quadrupolar order in a model for β-$TeVO_4$", ***Phys. Rev. B*** 101, (2020) 064403

"Effect of XXZ anisotropies on a spin-1/2 Heisenberg chain", ***manuscript in preparation***

List of Acronyms

AFM	Antiferromagnet
BPW	Bethe Peierls Weiss
βTVO	β-$TeVO_4$
CMF	Cluster Mean Field
CMFT	Cluster Mean Field Theory
CCMFT	Correlated Cluster Mean Field Theory
D	Dimensional
DMRG	Density matrix renormalization group
ED	Exact Diagonalization
FM	Ferromagnet
LRO	Long Range Order
MBS	Many body system
MFT	Mean Field Theory
NMR	Nuclear magnetic resonance
NN	Nearest neighbor
NNN	Next nearest neighbor
OBC	Open boundary conditions
PBC	Periodic boundary conditions
PO	Partially ordered
PM	Paramagnet
Q1D	Quasi-one-dimensional
QCCMFT	Quantum correlated Cluster Mean Field Theory
QCP	Quantum critical point
QOP	Quadrupolar order parameter
SCCF	Self Consistent Correlated Mean Field theory
SDW	Spin density wave
TFIM	Transverse field Ising Model
VBS	Valence bond solid
VC	Vector Chiral

Contents

Chapter 1

Introduction

Collective behavior of many interacting quantum particles is full of surprises. The properties of the phases appearing due to interactions bear little resemblance to those of the independent degrees of freedom. Many fascinating phenomena such as fractional quantum Hall effect, Kondo effect, high-temperature superconductivity, etc. [1, 2] are a result of strongly correlated electrons. Interestingly, even strongly insulating systems where itinerancy aspect of electrons is inactive, manifest various surprises of quantum physics. They host a rich variety of phenomena ranging from conventional ordered magnetic states to exotic magnetic states and disordered states such as spin glass. In recent years quantum spin liquid states have emerged as a new state of quantum matter where spins neither order nor freeze down to very low temperatures. Theoretical and experimental investigations on low dimensional (D) spin systems have attracted considerable attention recently [3], due to the desire to understand fundamental concepts as well to investigate the relevance of the materials to possible technological applications. Low dimensional magnets exhibit stronger quantum fluctuations compared to their higher dimensional analogues [4]. These systems host a rich variety of phases arising as a combination of lower dimensionality, interactions, effective masses, orbital overlap and spin sizes [3, 5]. Various low dimensional materials with strong frustrating effects have potential use in nano-technologies [6], quantum computing [7], refrigerating due to enhanced magneto-caloric effect [8, 9] etc. Spin chains offer an intriguing solid-state alternative for short-range quantum communication [10]. In addition to being of fundamental interest in their own right, spin systems also describe parent states of many important phases. Lanthanum cuprates ($La_{2-x}Sr_xCuO_4$) turned out to be an ideal platform for exploring quantum effects like destruction of Néel order on introduction of holes in planar spin-1/2 antiferromagnets with isotropic nearest-neighbor coupling [11].

Theoretically, the phenomena of magnetism is studied utilizing model Hamiltonians of atomic sized magnets (spins) localized on lattice and interacting via mechanics governed by quantum principles. The topic of lattice quantum spin systems, in itself is a fascinating branch of theoretical physics [12]. Not only do these constitute the basic models of quantum magnetic insulators relevant to many magnetic materials, but also serve as prototypical models of quantum systems as they are conceptually simple, yet demonstrates surprisingly rich physics. The field can be traced back to 1925 when Ernst Ising followed a suggestion of his academic teacher Lenz to investigate the one-dimensional (1D) version of the model which is now well known by his name [13]. Using analytical and computational techniques, magnetic models are investigated to study critical and scaling phenomena. Exact (analytical) solutions of the low dimensional models are available for very few magnetic models. Therefore, sophisticated computational approaches are often employed to solve variety of magnetic models.

The field of quantum many body physics is characterized by fruitful interplay between theory and experiments. One of the aims of this research field is to build realistic models of physical processes often driven by experimental findings. Magnetic properties observed in naturally occurring magnetite (commonly known as Lodestone) marks the beginning of magnetic materials [14]. It exhibited the remarkable property to attract metals without external influence, the phenomenon was later understood as spontaneous alignment of magnetic moments into finite sized domain. Absence of such a magnetic order was the reason why the discovery of antiferromagnets was delayed. During the period of seventies and eighties, interests in low dimensional models gained practical relevance as real materials appeared which resembled the behaviour predicted by theoretical 1D and 2D models [15]. Magnets in restricted dimensions exist as real bulk crystals with exchange interactions resulting in magnetic coupling much stronger only in one or two spatial directions. Therefore, low-dimensional magnets often have all the advantages of bulk materials in providing sufficient experiments investigating thermal properties (e.g. specific heat), as well as dynamical properties [16]. In addition, experimental techniques, such as, Nuclear Magnetic Resonance (NMR) and Neutron scattering directly couple to magnetic order parameter and are employed to study spatial or temporal correlations [17]. Magnetic insulators can often be described by simple spin Hamiltonians with few experimentally measurable parameters, which allows for a quantitative comparison of experimental data with theory and numerical simulations. In the following section a brief overview of theoretical models relevant for magnetic ordering arising in the material is presented.

1.1 Magnetic Interactions

One of the profound "Surprises in Theoretical Physics" [18] is that magnetism is a quantum mechanical effect. From a classical perspective, magnetic moments originate from electric currents, which interact via dipole interaction. The magnetostatic interaction energy of two moments $\boldsymbol{\mu}_1$ and $\boldsymbol{\mu}_2$ separated by a distance r is

$$U \propto \frac{\boldsymbol{\mu}_1 \cdot \boldsymbol{\mu}_2 - 3(\boldsymbol{\mu}_1 \cdot \hat{\mathbf{r}})(\boldsymbol{\mu}_2 \cdot \hat{\mathbf{r}})}{r^3}. \tag{1.1}$$

Magnetostatic energy of two atomic moments of the order of $\mu_B = e\hbar/mc$ at distances of the order of Bohr radius $r \sim a_0 = \hbar^2/me^2$, is $U \approx 10^{-4}eV(\sim 1K)$. This long range interaction is too weak and only allows for magnetic orders at very low temperatures. Since, magnetic ordering observed in real materials, e.g. in magnetite (Fe_3O_4) persist till about 860K, the phenomenon has to be other than magnetostatic interaction of dipoles. Nevertheless, magnetic dipolar interaction can be significant to the properties of materials ordering at milliKelvin temperatures.

Heisenberg Model:

Heisenberg model is an interaction model discovered by Werner Heisenberg in 1926 [19]. He correctly identified that interaction between magnetic moments arises due to Coulomb repulsion and is therefore, electrostatic in nature. To understand the origin of interaction we consider two isolated electrons. Following Heitler-London theory, orbital wave functions of two single electron system can be constructed from the linear combinations of $\psi_i(r_1)\psi_j(r_2), \psi_i(r_2)\psi_j(r_1)$, where r_1, r_2 are the locations of the two electrons in space. In addition to the orbital part, it is important to consider the spin part of the wave function which can be either $\uparrow$ or $\downarrow$. The total wave function of this two-electron system, which is a combination of the orbital and spin wave functions, must obey Pauli exclusion principle. Pauli exclusion principle imposes that the wave function of two electron system to vanish if both the electrons are in same state. As a consequence, the possible wave functions are:

$$\psi_1(r_1, r_2) = \psi_-(r_1, r_2)S_T \tag{1.2}$$

$$\psi_2(r_1, r_2) = \psi_+(r_1, r_2)S_S \tag{1.3}$$

where ψ_- (ψ_+) is the anti-symmetrical (symmetrical) combination of orbital wave function, and S_T (S_S) is the symmetrical triplet state (anti-symmetrical singlet state). Eigenenergies corresponding to ψ_1, ψ_2 can be obtained by solving the Schrodinger equation.

Heisenberg pointed out that the exchange integral (J_{ij}) appearing in the eigen energy for the singlet and triplet state of two-electron system is the origin of magnetic phenomena [20]. The integral reads as,

$$J_{ij} = \int d^3r_1 d^3r_2 \psi_i^*(\mathbf{r}_1)\psi_j^*(\mathbf{r}_2)V(\mathbf{r}_1,\mathbf{r}_2)\psi_j(\mathbf{r}_1)\psi_i(\mathbf{r}_2) \tag{1.4}$$

where V represents the Coulomb interactions between the particles. Notice that $\psi_i^*(r_1)$ couples to $\psi_j(r_1)$ while $\psi_j^*(r_2)$ couples to $\psi_i(r_2)$, this is of purely quantum mechanical origin and has no classical analogue. Strength of the interaction is governed by this exchange integral which decays exponentially with distance. This direct overlap of wave functions results in magnetic interaction leading to spontaneously orientation of neighboring magnetic dipoles at temperatures significantly higher than the dipole interaction.

Heisenberg model can also be arrived at as a limiting case of a well known Hubbard model, which was presented in the early 1960s by J. Hubbard [21]. Hubbard model is the most fundamental model to study strongly correlated electron systems, it describes the basic competition of the kinetic energy as well as the electrostatic repulsion energy of many electron system. Heisenberg model is an effective low-energy description of the half-filled Hubbard model for $U >> t$. In this limit, the interaction energy is minimized thereafter treating kinetic energy as a perturbation. Interaction energy can be reduced to zero by restricting doubly occupied sites, which can be achieved exactly at half-filling. Interaction energy remains unaffected by the spin arrangement of the electrons. Now any hopping of electron will be energetically costly ($\sim U$). If the neighbouring electrons have opposite spins then electron can *virtually* hop to neighbouring site and back. This virtual delocalization treated in the sense of 2^{nd} order perturbation theory reduces the kinetic energy. However, if the neighbouring spins are parallel, then such a hopping will be forbidden by Pauli exclusion principle. This results in an effective interaction which favours antiparallel orientation of electrons on nearest neighbours. Therefore, exactly at half filling the charge fluctuations cease to exist, and the model maps onto a pure spin model described by the isotropic Heisenberg Hamiltonian. Using perturbation theory, the resultant Hamiltonian for spin-1/2 quantum Heisenberg antiferromagnet reads as,

$$\mathcal{H} = \sum_{\langle i,j \rangle} \frac{4t_{ij}^2}{|U|} \mathbf{S}_i \cdot \mathbf{S}_j \equiv \sum_{\langle i,j \rangle} J_{ij} \mathbf{S}_i \cdot \mathbf{S}_j \tag{1.5}$$

Therefore, the underlying mechanisms that gives rise to magnetic order are based on pure quantum mechanical effects [22]. The exchange interaction J is a cumulative effect of of the delocalization energy, electron spin, Heisenberg's uncertainty principle, Pauli's

exclusion principle, and the Coulomb repulsion between electrons. Since forces of electrical origin are much stronger than those of magnetic origin, this explains the existence of room temperature magnetism. Magnetic properties of many insulating crystals can be quite well described by Heisenberg-type models of interacting spins

A general Heisenberg model for spins in zero field can be written as :

$$\mathcal{H} = \sum_{\langle i,j \rangle} J^{\alpha} \mathbf{S}_i \cdot \mathbf{S}_j \tag{1.6}$$

$$= \sum_{\langle i,j \rangle} J^x S_i^x S_j^x + J^y S_i^y S_j^y + J^z S_i^z S_j^z \tag{1.7}$$

where S_i^{α} are the components of quantum spin operators $\mathbf{S}$ with spin S at site i. J^{α} describes the magnetic coupling between the $\alpha-$component of the spin. The sign of the exchange coupling governs the nature of order, for antiferromagnetic (ferromagnetic) coupling J is positive (negative). $\langle i,j \rangle$ indicates the summation over nearest-neighbour pairs of spin. Ground state order further depends on dimensionality and the geometry of lattice. The operator $\mathbf{S^2}$ have eigenvalue $S(S+1) = S^2(1+\frac{1}{S})$, where $(1+\frac{1}{S})$ is taken as the correction factor due to quantum nature of the spins. In the limit $S \to \infty$, the quantum correction factor becomes 1, hence the large spin-S limit allows for a classical treatment of spins. In this limit, the spins can be considered as three dimensional vectors. To understand the Hamiltonian clearly, consider two atoms with spin-1/2 interacting with an isotropic exchange interaction J is

$$\mathcal{H} = J\mathbf{S_1} \cdot \mathbf{S_2} \tag{1.8}$$

Classically, the spins are treated as angular momentum vectors and the energy of the system depends on the angle between them

$$E_{class} = \frac{1}{4} J \cos\theta. \tag{1.9}$$

All the energies between $+\frac{1}{4}J$ and $-\frac{1}{4}J$ are possible since $-1 \leq \cos\theta \leq 1$.

Quantum mechanically all the eigenstates of the system have to be found by diagonalizing $\mathcal{H}$ matrix, which is written using a complete set of orthonormal basis. Basis vectors can be chose as : $|\uparrow\uparrow\rangle, |\uparrow\downarrow\rangle, |\downarrow\uparrow\rangle, |\downarrow\downarrow\rangle$, where $\uparrow$ ($\downarrow$) stands for $m = +1/2(-1/2)$.

It is useful to rewrite the Hamiltonian as follows

$$\begin{aligned} \mathcal{H} &= J(S_1^x S_2^x + S_1^y S_2^y + S_1^z S_2^z) \\ &= J\left(S_1^z S_2^z + \frac{1}{2}\left(S_1^+ S_2^- + S_1^- S_2^+\right)\right) \end{aligned} \tag{1.10}$$

where $S^{\pm} = S^x \pm iS^y$. After diagonalization, eigenspectrum of the Hamiltonian is:

$$\begin{aligned} E_{1,2,3} = \frac{J}{4} : |E_1\rangle &= |\uparrow\uparrow\rangle, \\ |E_2\rangle &= \frac{1}{\sqrt{2}}(|\uparrow\downarrow\rangle + |\downarrow\uparrow\rangle), \\ |E_3\rangle &= |\downarrow\downarrow\rangle, \\ E_4 = -\frac{3J}{4} : |E_4\rangle &= \frac{1}{\sqrt{2}}(|\uparrow\downarrow\rangle - |\downarrow\uparrow\rangle) \end{aligned} \tag{1.11}$$

The maximum eigenvalue is $\frac{J}{4}$, but the minimum eigenvalue is $-\frac{3J}{4}$, which is much lower than the classical counterpart. For $J < 0$ the system is ferromagnetic with three-fold degenerate ground state that correspond to three possible orientations of total spin $S_{tot} = S_1 + S_2 = 1$. In a ferromagnet, because all the individual moments are aligned in the same direction, there is a net total moment even in the absence of a magnetic field. For $J > 0$, alternating spin orientations on neighboring sites would minimize the total energy to $-|JS^2|$ per spin, the state is called Néel state, named after Louis Néel. The antiferromagnetic state consists of two sublattices, where the ions of the nearest neighbors have antiparallel spin having mutually compensating magnetic moments. Thus, the net magnetic moment of such type of solids is zero. The simplest examples of ferromagnetically ordered crystals are Fe, Ni and Co; on the other hand for antiferromagnets, the prominent examples are the transition metal oxides and fluorides.

When spins are treated quantum mechanically, it turns out Néel state is not the eigenstate of the Hamiltonian (see E_4 in 1.11). Instead spins would form a many body analogue of the spin singlet state, known as a *valence bond*, with no orientation ($S_{tot} = S_1 - S_2 = 0$). The exact analytic result of a general $S = 1/2$ antiferromagnetic Heisenberg models is not yet known. Néel state has been found as true order of spins in neutron diffraction experiments in a wide range of three-dimensional antiferromagnetic materials. However, the magnitude of the ordered magnetic moment is less than $\sqrt{S(S+1)}$ Bohr magneton. The reduction in the ordered magnetic moment is understood as a result of zero-point fluctuations, which is a consequence of quantum mechanical nature of the ground state.

Ising Model:

Ising model is the first well studied model to study ferromagnetism. It was first studied in 1925 by Lenz and Ising, who showed that in dimension, $D = 1$ the model does not show a phase transition for $T > 0$. In Ising model, the local magnetic moment on each lattice site can take two discrete values, i.e. $\sigma_i = \pm 1$, corresponding to spin pointing either up or down. Hamiltonian of Ising model with general interactions J_{ij} between all spins on an arbitrary lattice with an uniform external field h is:

$$\mathcal{H} = -\frac{1}{2}\sum_{i=1}^{N}\sum_{j=1, j\neq i}^{M} J_{ij}\sigma_i\sigma_j - h\sum_{i=1}^{N}\sigma_i \tag{1.12}$$

The factor of $1/2$ compensates for over counting of interacting pairs in the sum. Although the model was introduced to study ferromagnetism and phase transitions [23], it has been very useful in describing the essential features of real systems where strong uniaxial anisotropy locks magnetic moments along one crystallographic axis (usually the z-axis). [24].

A completely isotropic Heisenberg model 1.7 with $J_x = J_y = J_z$ is referred as XXX model. For $J_x = J_y = 0$ the model reduces to Ising model, the opposite limit of dominating transverse components ($J_z = 0$) leads to XY model relevant for materials with strong easy-plane anisotropy. Isotropic Heisenberg model is an ideal model to describe magnetically ordered solids. However, exchange interactions in real materials depends on orbital overlap of magnetic ions. Due to the highly complex structure of these overlaps or other stronger couplings such as spin-orbit coupling, real materials usually do not possess continuous symmetry. In real materials, various other antisymmetric exchanges are observed such as Dzyaloshinskii-Moriya $\mathbf{D}_{ij} \cdot (\mathbf{S}_i \times \mathbf{S}_j)$ [25] and Biquadratic interactions Biquadratic $K_{ij}(\mathbf{S}_i \cdot \mathbf{S}_j)^2$. Furthermore, presence of magnetic anisotropy in the Hamiltonian has a potential to alter the state of the system completely. It can aid in development of long range order or introduce frustration to an otherwise unfrustrated isotropic system. Anisotropic XXZ model with $J_x = J_y \neq J_z = \Delta$ is a classic example of one-dimensional integrable quantum spin systems. The XXZ model with periodic boundary conditions (PBC) and in a pure longitudinal magnetic field is known to be exactly solvable by the Bethe ansatz [26].

Usually, short-range interactions, e.g., nearest neighbor and next nearest neighbor interactions, are sufficient for appropriate descriptions of the major magnetic properties of real materials. Presence of further neighbor interactions modifies the energy spectrum of the system, for instance it opens a spin gap in an otherwise gapless spin-1/2 chain

system. Competition arises when both nearest neighbor J_{nn} and next-nearest neighbor J_{nnn} interactions are active. In 1D, for $J_{nnn}/J_{nn} = 0.5$ the model is known as Majumdar–Ghosh model [27]. This is a special model as the ground state of this model is exactly known as the product of singlet pairs on even and odd sites [28].

Heisenberg model in principle can be studied for any spin value. It was pointed out by Haldane in 1983 that the phenomena by which magnetic spins order can be dependent on the spin value [29]. He conjectured that the ground state of integer differ from half-integer spin chains. It has been very well established theoretically [30] as well as experimentally [31] that spin-1/2 antiferromagnetic Heisenberg chain is gapless with fractionalized excitations (*spinons*) carrying spin $S = 1/2$. However, integer spin chains have a non-degenerate singlet ground state with a triplet state at finite excitation gap, named after him, *Haldane gap*, above the ground state [32]. Furthermore, the spin correlation function quickly decays exponentially unlike spin-1/2 chain where correlations decay with power law. Experimentally, the Haldane phase was most comprehensively studied in the $S = 1$ chain material $Ni(C_2H_8N_2)_2NO_2ClO_4$ (NENP), confirming the theoretical predictions [33, 34].

1.2 Magnetic ordering

A collection of spins are considered magnetically ordered if the interaction among magnetic spins separated by distance become correlated resulting in a pattern. Correlation among magnetic spins in this ordered arrangement may be long range or limited to short distances. Some of the conventional orders appearing in magnetic systems are ferromagnets (FM) where all magnetic moments spontaneously align in the same direction (see Fig. 1.1(a)). Other types of orders are antiferromagnets (AFM) with antiparallel arrangements of spins on neighboring sites (see Fig. 1.1(d)). While magnitude of spontaneous magnetization on such a bipartite lattice remains same in AFM, the case of unequal magnetic moments with anti-parallel orientation is known as ferrimagnets (see Fig. 1.1(b)). Magnetic orders possible in a lattice are not limited to the conventional ordered patterns [35]. A rich variety of magnetic orders are possible where the angle between the neighboring magnetic moments are allowed to vary between zero and π known as spiral orders (see Fig. 1.1(c)). Furthermore, there exists highly correlated exotic states, such as spin ice, spin liquid, unusual partial orders, which do not posses a finite magnetic moment even at zero temperature. These interesting states arise when competing forces in a system are not simultaneously satisfied, the phenomena is known

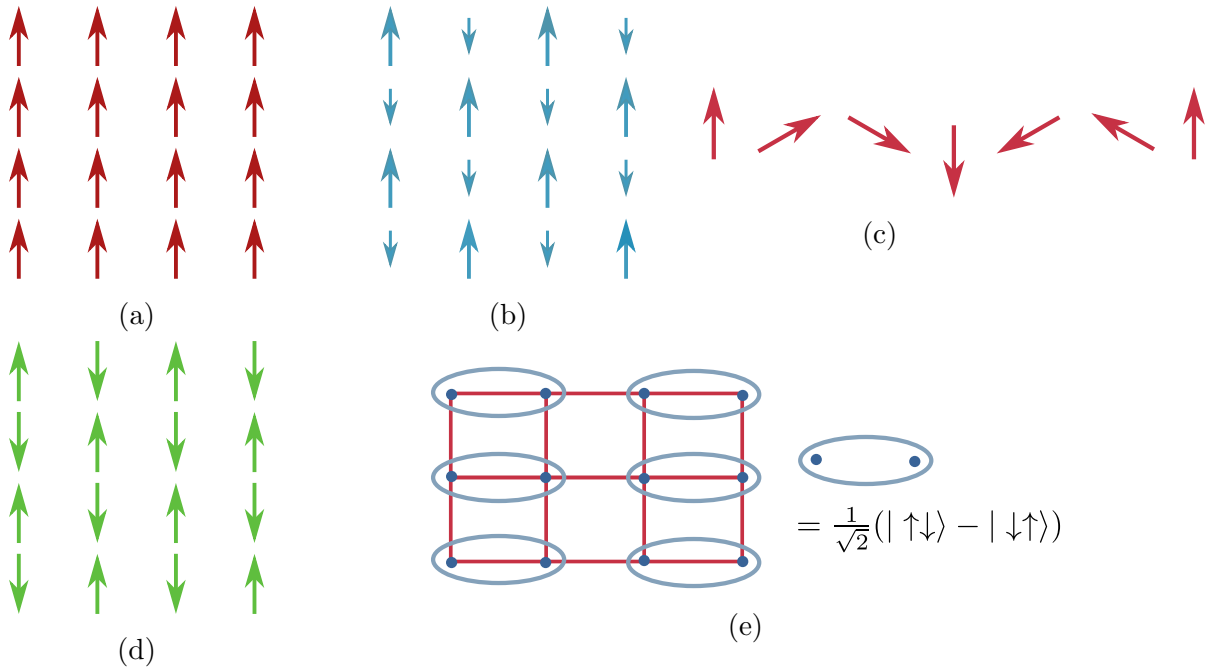

Figure 1.1: A schematic diagram representing various magnetic orders:(a) ferromagnetic, (b) ferrimagnetic, (c) spiral (d) antiferromagnetic and (e) valence bond solid.

as *frustration* [36, 37]. Antiferromagnet on a 2D triangular plaquette with Ising spins is a prototype of frustration as, three spins on a triangle cannot all be anti-parallel (see Fig. 1.2(a)). This is referred to as *geometric frustration* as the frustration is of geometric origin. This phenomena can be observed in other lattice geometries with triangular motifs such as, kagome, Shastry-Sutherland and pyrochlore lattices.

It was pointed out by Wannier in 1950 [38], that this model possess a macroscopic number of degenerate states with ground state entropy equal to 0.323 k_BN where k_B is the Boltzmann constant and N is the number of spins. As a result, spins continue to fluctuate at low temperatures, however in a correlated manner. The state is called as 'spin liquid' or cooperative paramagnet, analogous to the ordinary liquid where molecules form highly correlated state with no static order. The spatially anisotropic triangular antiferromagnet Cs_2CuCl_4 is extensively studied for its rich behavior due to frustration. Experiments have revealed exotic magnetic phases and quasi particle excitations [39, 40] in this material.

In addition to geometry, frustration can also be realized on unfrustrated lattices with a mixture of AF and FM interactions with nearest or next nearest neighbor (NNN) spins. A situation with AF interaction bonds on nearest and next nearest neighbor results in a frustrated spin system similar to the case in geometric frustration with triangular motifs. Model describing such type of interactions are $J_1 - J_2$ models with both interactions being AFM have been extensively studied on 1D chain (see Fig. 1.2(c)) and various geometries

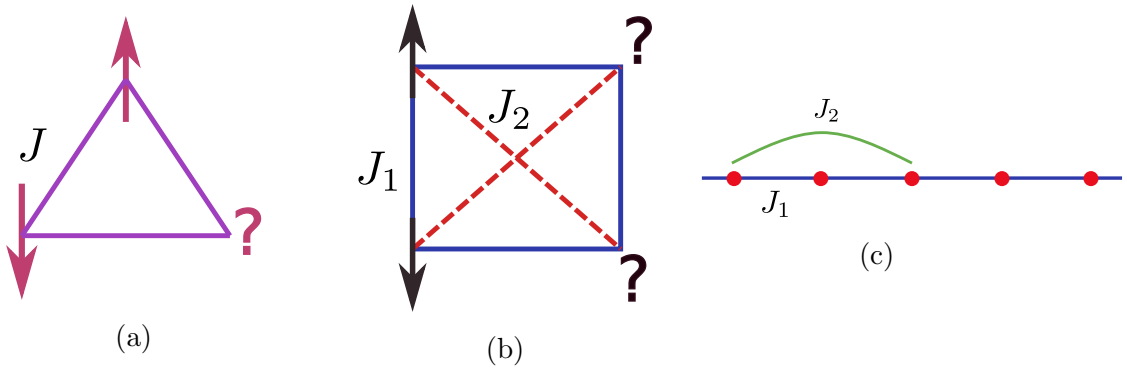

Figure 1.2: (a) Ising spins on a triangular lattice interacting via antiferromagnetic interaction (J). Frustrated spins with both nearest neighbor (J_1) and next nearest neighbor (J_2)interactions on (b) a square lattice and (c) one-dimensional chain.

in 2D like square (see Fig. 1.2(c)), honeycomb, etc. In some cases, valence bond solid (VBS) (see Fig. 1.1) may emerge as a ground state of spin-1/2 antiferromagnetic model on square lattice with frustrating further neighbor interactions. A VBS state is a product of singlets where each site participates in one and only one singlet and which leads to a lack of magnetic order. Materials hosting such type of interactions are of particular interest as they might show spin liquid orders.

While low dimensional Hamiltonians are very interesting from a theoretical perspective, truly 1D or 2D materials are almost never realised. Weak inter-chain or inter-plane interactions are always present which may either spoil the order by introducing competing interactions or they may aid in stabilizing orders. Progress of material science has further allowed to study spin ladders which are objects staying in between one and two dimensions [41]. Presence of magnetic field further leads to a number of ground states, for example, spin-spiral states, the spin multi-polar phases (spin nematic phases), etc. which are observed in models with competing interaction [42, 43].

1.3 Phase Transitions

The phenomena by which collective behavior of large number of interacting particles change their certain properties when subjected to an external influence, such as temperature or pressure, is known as phase transitions. These are frequently observed in nature, ranging from freezing of water into ice to the development of superconductivity [44]. A phase is usually associated with an order parameter that allows a distinction between an ordered and a disordered phase. A first (second) order phase transition is

characterized by an observable changing discontinuously (continuously) in the vicinity of the critical point. The order parameter associated to transitions like melting of ice or boiling of water is density of the system. They involves phase coexistence and latent heat, therefore are categorized as first-order phase transitions. Other types of transitions are characterized as continuous, their signature is reflected as power-law decay of correlations, divergences in the susceptibility and specific heat near criticality. Second order phase transitions are observed in magnetic phase transitions. The hallmark of magnetism is the existence of an ordered arrangement of magnetic moments over macroscopic length scales, this spontaneous magnetization is considered as the order parameter for magnetic systems. Long range magnetic orders such as ferromagnets and antiferromagnets exists below certain temperature known as the Curie temperature (T_C) [45] and Néel temperature (T_N) respectively. Above these temperatures, thermal fluctuations with energy scale k_BT, overwhelm the spin-spin exchange energy J leading to a paramagnetic state, through a second order phase transition.

The properties of magnetic systems are usually associated with their symmetry and dimensionality D of the Hamiltonian. For example, ground state of a uniform S=1/2 chain for Ising model and Heisenberg model are different. Ising model with discrete symmetry becomes ordered at $T = 0$ in $D = 1$ while the symmetry cannot be broken at finite T. On the other hand, Heisenberg model posses continuous symmetry (SU(2)), which cannot be broken in $D = 1$ even at $T = 0$ but for $D = 2$ the system spontaneously orders at $T = 0$. The interplay of symmetry breaking and dimensionality is governed by *Mermin Wagner theorem*. The theorem was formulated in 1966, it states no one-dimensional or two-dimensional isotropic Heisenberg spin system can order at non zero temperatures [46]. However, at zero temperature magnetic long range order may still be allowed depending on the strength of quantum fluctuations.

Unlike classical transitions, where destruction of the order is driven by thermal fluctuations, phase transitions can also be observed at $T \to 0$ upon changing parameters like magnetic field, chemical doping and pressure. These zero temperature, second-order phase transitions are driven by quantum fluctuations arising due to non-commuting terms in the Hamiltonian, which are mandated by the Heisenberg uncertainty principle. At zero temperature, the system prefers a ground state dictated by the parameters of the Hamiltonian describing the system. The system can be driven to another phase by tuning the control parameter which regulates the amplitudes of quantum fluctuations. One might think that such phase transitions are not relevant to the real world due to the unattainability of zero temperature. However, it has been found that many finite temperature properties of a system can be explained by understanding its quantum critical point

(QCP) [47, 48]. This is because, unlike classical finite-temperature phase transitions, their dynamic and static critical behaviors are intimately intertwined [49]. Quantum mechanical aspects are important as long as $\hbar\omega_c >> k_BT$, where ω_c is the frequency associated with the relaxation time required to decay to ground state from an excited state. One of the prototypical models capturing the essence of quantum phase transitions is the transverse field Ising model (TFIM). The well known mapping to a $D+1$ dimensional classical statistical mechanics problem allows the study of this model. The model is also referred to as Quantum Ising Model, its Hamiltonian is written as :

$$\mathcal{H} = -J\sum_{\langle i,j\rangle}^{N}\sigma_i^z\sigma_i^z - \Gamma\sum_{i=1}^{N}\sigma_i^x \tag{1.13}$$

where Γ is the transverse magnetic field. Transverse magnetic field, induces quantum fluctuations between up and down state. At $\Gamma = J$, the model exhibits phase transition from a polarized state ($\Gamma > J$) to a symmetry broken ground state ($\Gamma < J$). Experimental evidences of quantum phase transitions have been reported in low dimensional magnets such as $LiHoF_4$, $TlCuCl_3$, $KCuCl_3$, $LiCuVO_4$, $CoNb_2O_6$, etc.

1.4 Thesis Overview

A comprehensive introduction of various magnetic orders and phase transition phenomena observed in the field motivates to study of the underline concept behind them. However, the central challenge in the field of strongly correlated electron systems is solving the problem of thermodynamically large number of spins. Due to lack of analytical tools and computational limitations of numerical methods, often approximate methods are employed to understand the effects of correlations in many body systems. Mean field theory serves as a starting point for understanding the behavior of large number of interacting particles. More accurate description of correlations in an interacting system can be achieved by retaining the quantum nature of the coupling. Based on this concept, a method known as Cluster mean field theory (CMFT) is designed which treats interactions in a cluster exactly while taking into account effect of interactions outside the cluster the via mean fields. In *Chapter 2*, a brief account of mean field theory and its extensions are provided. A detailed comparison of CMFT with other methods are also discussed, justifying the utilization of CMFT as the main method of calculation.

Quasi-1D magnets are very interesting as they can host highly correlated phases such

as quantum spin liquids and non-trivial excitations such as spinons and longitudinal excitations. Experimental studies on various materials show unusual magnetic orders at low temperatures. Thermodynamic measurements on $CuInVO_5$ is a spin-1/2 tetramer compound, hints the presence of a long range ordered antiferromagnetic state below 2.7K. However, prototypical isotropic Heisenberg model on a 1D chain will not order at finite temperature. Presence of a long range order at low temperature in $CuInVO_5$ hints the presence of inevitable weak inter-chain couplings. Motivated by this material, CMFT is applied to a quasi-1D model spin Hamiltonian of weakly interacting tetramers. For the material specific choice of interaction parameters, CMFT is put to test to check if it can explain the results obtained experimentally. The most important experimental observation being the presence of low temperature peak in specific heat results. A microscopic picture of the ordered state and its evolution with magnetic field and temperature is discussed in *chapter 3*.

Frustrated low-dimensional spin systems are the centre of research in the field of strongly correlated systems, theoretical as well as experimental techniques are constantly developing to identify highly frustrated phases. J_1-J_2 Heisenberg model on a chain is the simplest model with frustrating interactions which has been extensively studied numerically. Interests in systems with one of the interaction in the above model being FM gained interest with the discovery of materials hosting exotic phenomena where NN interaction is FM and the NNN is AFM. $\beta-TeVO_4$ is a material belonging to the family of materials hosting frustrated ferromagnetic interactions. Experimental reports on $\beta-TeVO_4$ reveals the presence of exotic phases like, vector chiral, spin density wave, spin stripe and quadrupolar orders. In *chapter 4*, CMFT is implemented to a minimal anisotropic Heisenberg model for coupled zigzag chains in two dimensions aiming to capture the dominating interactions in $\beta-TeVO_4$. We calculate temperature and field dependent observables and lookout for features observed experimentally which has been captured by CMFT.

Presence of impurities in materials are known to alter qualitative behaviour such as conductivity of a material. In insulators impurities can affect the ground state properties as well as the excitation spectrum [50]. Furthermore, impurity induced effects gets enhanced in low-D systems as the interplay of strong quantum effects and the disorder physics. Recently, a number of studies have focused on embedding magnetic and non-magnetic impurities in spin-1/2 chain materials like Sr_2CuO_3 [51]. In *chapter 5*, we study impurity effects in an isotropic Heisenberg model on a chain. The impurity introduced has an unusual effect of modifying the anisotropy of the neighboring bonds. We utilize CMFT to understand the resultant ground state of such a system and its dependence on

impurity density and anisotropy strength. Moreover, signatures of ordering and phase transitions at finite temperatures in presence of magnetic field are also explored.

Chapter 2

Methods

Once, the relevant interactions in the system are known, the challenge is to solve the model Hamiltonian. The first breakthrough towards solving the Heisenberg model was introduced by Hans Bethe [52] in 1931 to find exact quantum mechanical ground state of one-dimensional antiferromagnetic Heisenberg model. The method is now known as "Bethe ansatz". Since then the method has been extended to other models in one dimension like the anisotropic Heisenberg chain (XXZ model), the Hubbard model, the Kondo model, the Anderson impurity model, etc. Exact solution of the $2D$ Ising model by Onsager in 1944 represents as another landmark in theoretical physics. He showed, unlike $1D$, Ising model in $2D$ did exhibit spontaneous order below a finite temperature comparable to the value of exchange interaction parameter J. While analytic solutions of low dimensional systems are very appealing, however, except for a few cases, it is difficult to find the exact solution of an interacting many-body system (MBS) [12, 53]. Therefore, to provide a better understanding of main features of MBS, computational approaches are constantly developed.

Numerical approaches are often limited to the finite number of particles and in many cases they are not sufficient to allow inference of thermodynamic limit behavior, which plays a central role in the development of collective phenomena. One of the most frequently adopted method to study MBS is Monte Carlo [54]. They have been proven successful in the classical limit, i.e. when spins are large enough to be considered as classical vectors. They can also provide correct solutions in higher dimensions for which analytical solutions are not available. For instance, numerical solutions based on Monte-Carlo simulations for 3D Ising model are available but the analytical solution for the same doesn't exist. For accurate description of physics of low spin at low temperatures,

the most promising technique is Quantum Monte Carlo method. It uses the mapping of D-dimensional quantum system to its $(D+1)$ dimensional classical counterpart [55, 56]. However, it fails for many frustrated systems of interest, due to the infamous "sign-problem" [57, 58]. The most powerful tool available to study the ground state physics of low dimensional systems is the Density Matrix Renormalization Group (DMRG)[59, 60]. The method is applicable for frustrated systems however, it is limited to low lying excitations above ground state physics. Various other theoretical techniques like matrix product states [61], cluster variational method [62], projected entangled pair states [63] and series expansion method [64] are developed to extract finite temperature correlations. While sophisticate mathematical and computational methods are constantly developed, mean field theory (MFT) has been frequently adopted as a starting point for the investigations of MBS [65, 66, 67]. MFT is capable of describing the qualitative behavior of macroscopically large systems despite its limitations. In the following sections, a detailed introduction to the mean field approach and some recent developments aimed at improving the treatment of quantum correlations will be discussed.

2.1 Exact Diagonalization

A complete knowledge of a quantum system can be obtained by exactly diagonalizing the full Hamiltonian. In principle, all eigenstates can be computed exactly for a finite system by numerically diagonalizing the Hamiltonian. However, in practice such studies are limited to small system sizes consisting of few tens of spins. This limitation is due to large Hilbert space of quantum many-body systems. For spin Hamiltonians, the dimension of Hilbert space scales exponentially with the number of particles, for e.g., Hilbert space dimension for N spin-1/2 is 2^N. For a quantitative idea, consider $N \sim 10^{23}$ (of the order of the Avogadro number) spins, then the number of basis states in the Hilbert space is $((2S+1)^{10^{23}})$. Therefore, the brute force exact diagonalization (ED) is computationally limited and not enough to fully understand long range orders. Drawing conclusions about thermodynamic limit from ED on small clusters is rather tricky. However, insights gained from ED are useful to complement other calculations.

For a given Hamiltonian, the first step for exact diagonalization is to chose the basis states. Basis for spin-1/2 system consist of single spin state $\uparrow_i$ and $\downarrow_i$ with the quantization axes assumed to be z direction. For computational generation of the basis of spin-1/2 Hamiltonian matrix ($2^N \times 2^N$), bit values (0 or 1) of numbers a = 0,1,... $2^N - 1$ corresponds to the spin states. This can be understood as a decimal to binary (base 2) number system

conversion. Similarly for higher spin state, decimal to general base conversion can be used to construct the basis. Bit operations are implemented to construct the Hamiltonian and other operator matrix [68].

Symmetries of the Hamiltonian are utilized to reduce the dimension of Hilbert space. One of the symmetries that can be easily taken advantage of is conservation of magnetization. Other symmetries like transnational invariance, spin rotational invariance, parity symmetry, spin-inversion symmetry, etc. may lead to complicated basis state. With total spin conserved ($[\mathcal{H}, S^z] = 0$), the Hamiltonian breaks into blocks labelled by quantum numbers (S, m_z) where $m_z \in \{-S, -S+1, ...S\}$ is the total magnetization in the direction of quantization axis. Block Hamiltonians are created by sorting the original Hilbert space with given $m_z = (n_\uparrow - n_\downarrow)/2$ with dimension $M = N!/(n_\uparrow! n_\downarrow!)$. The block diagonalization method, reduces the dimension of matrix to be diagonalized considerably. Blocks can be further block diagonalized by utilizing other symmetries. Even the block diagonalization of the Hamiltonian is restricted to $\approx$ 20 spins for S=1/2, which is lesser for higher S. Problems where only low lying excitations above ground state are of relevance, Lanczos diagonalization techniques can be implemented which can access to larger system sizes.

2.2 Mean Field Theory

Mean field theory (MFT) is an approximate treatment, which reduces the problem of macroscopically large number of interacting particles to an an effective one-body problem. The system is divided into an environment and a subsystem, where the environment is then replaced by an effective field representing the average interaction between subsystem and the environment. Molecular mean field approach was originally utilized by Pierre Weiss, he showed a transition to magnetically ordered state for Heisenberg and Ising models at non zero temperature [69]. The mean-field approximation is at the heart of understanding of many complex systems, for instance, it is the basis of the Hartree-Fock approximation in electronic structure calculations and the BCS theory of superconductivity [70].

Following the treatment of Weiss MFT, phase transition in Ising model is discussed to illustrate the effectiveness of the MFT [71]. To distinguish between magnetically ordered state from a non-magnetic disordered phase, local magnetization, $m_i = \langle \sigma_i \rangle$, is considered as the order parameter for Ising model. Within MFT, all the spins are considered identical therefore, $m_i \equiv m$. Now, spin value at each site, σ_i can be written as the sum of the mean

value, m and fluctuations around it. Using this approximation, the interaction term of the Hamiltonian 1.12 becomes,

$$\begin{aligned} \sigma_i\sigma_j &= (m+\delta\sigma_i)(m+\delta\sigma_j) && (2.1)\\ &= m^2 + m(\delta\sigma_i + \delta\sigma_j) + \delta\sigma_i\delta\sigma_j && (2.2) \end{aligned}$$

The fundamental idea in mean-field approximation is to replace the fluctuating fields from the inter- and intra-particle interactions by a non-fluctuating mean field. Since *fluctuations around the order parameter are considered small*, $\delta\sigma_i\delta\sigma_j$ which is quadratic in fluctuations can be ignored.

$$\begin{aligned} \sigma_i\sigma_j &= m^2 + m(\delta\sigma_i + \delta\sigma_j) && (2.3)\\ &= m^2 + m[(\sigma_i - m) + (\sigma_j - m)] \\ &= -m^2 + m(\sigma_i + \sigma_j) && (2.4) \end{aligned}$$

Within mean-field approximation, the Hamiltonian 1.12 becomes

$$\mathcal{H}_{MF} = J\sum_{\langle ij\rangle} m^2 - Jm\sum_{\langle ij\rangle}(\sigma_i + \sigma_j) - h\sum_i \sigma_i \tag{2.5}$$

Total number of bonds in a lattice consisting of N spins with coordination number z are $Nz/2$.

$$\mathcal{H}_{MF} = J\frac{Nz}{2}m^2 - (h + zJm)\sum_i \sigma_i \tag{2.6}$$

Hamiltonian for N interacting spins in Ising model is now reduced to a non-interacting spin interacting with an *"effective magnetic field"*, $h_{eff} = zJm + h$. Using $\mathcal{H}_{MF}$, the partition function can be simply written as:

$$Z = e^{-\beta Jm^2 Nz/2}\big\{2\cosh[\beta(h + Jmz)]\big\}^N \tag{2.7}$$

Calculating magnetization of Ising model from partition function results in a transcendental equation:

$$m = \tanh\beta(h + zJm), \tag{2.8}$$

known as **Curie-Weiss equation**. The equation is solved self-consistently for m. For $h = 0$, in the limit when m is very small,

$$m \simeq \beta zJm - \frac{(\beta Jzm)^3}{3}. \tag{2.9}$$

Real solutions for this equation are $m = 0$ and

$$k_B T_C = zJ \tag{2.10}$$

From 2.10, it can be inferred that the critical temperature increases with interaction constant J, which can be understood as stronger interaction leads to higher resistance to thermal fluctuations. Result obtained via MFT overlooks the geometry of lattice as T_C is only dependent on coordination number and it increases with the dimension of system. The two point correlation function is

$$\langle \sigma_i \sigma_{i+r} \rangle = \langle (m + \sigma_i)(m + \sigma_{i+r}) \rangle \simeq m^2 \tag{2.11}$$

which shows that correlation between spins is independent of distance and are completely ignored.

Single spin interacting with an average field generated by the system, completely neglects the correlations between its elementary constituents. Consequently, MFT breaks down in presence of strong fluctuations such as, critical points. Moreover, exact solution of Ising model in one $1D$ exhibits no phase transitions at a non zero temperature, while MFT predicts a phase transition at finite temperature. Remarkably, even though the predictions of MFT are quantitatively incorrect, it correctly predicts the Ising model's qualitative behaviour for $2D$ and higher. This is because fluctuations are more important in lower dimensions, so the MFT approximation is less accurate in lower dimensions. Furthermore, it is expected to be exact for $D > 4$ and in presence of strong long-range interactions . Despite its limitations, the MFT is often adopted as the starting point to get insights into properties and behaviour of enormous class of problems. They are capable of predicting behaviour of the system over a wide range of parameters (e.g. temperature, field) at relatively low cost.

2.3 Bethe-Peierls-Weiss approximation

Original MFT completely ignores any fluctuations among strongly interacting spins. Hans Bethe improved it qualitatively and quantitatively by systematically including local correlations [72]. The method was originally developed for an order-disorder model, it was later applied to the Ising model by Peierls and the Heisenberg model by Weiss. The Bethe-Peierls-Weiss (BPW) approach treats all the interactions of a central spin with its neighboring spin exactly, while the subsequent interactions of neighboring spins is ap-

proximated via mean field. This method includes local spin correlations and fluctuations, it also takes into account the effect of lattice geometry beyond coordination number, z.

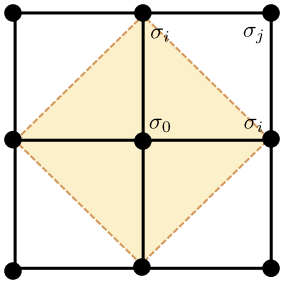

Figure 2.1: Schematic representation of a cluster (shaded region) used for a square lattice where σ_0 is the central site and σ_i (σ_j) is the nearest (next nearest) neighbor.

In the lowest approximation, spin σ_0 together with its z nearest neighbors σ_j are considered, hence a cluster of $z+1$ spins. For instance a cluster of 5 spins on a square lattice (see Fig. 2.1). The Hamiltonian for the cluster can be written as:

$$\mathcal{H}_c = -J\sigma_0 \sum_{i=1}^{z} \sigma_i - h\sigma_0 - h' \sum_{i=1}^{z} \sigma_i \tag{2.12}$$

where the first sum considers the interaction of σ_0 with its nearest neighbors coupled by interaction strength J and h is the external field applied. The last term contains the effective field h' acting on the neighbor spins of σ_0. It consists of the external field h, and the effective field of the surrounding spins. It can be noted that interaction of σ_0 (central spin) with its neighbors is treated exactly in comparison to the interaction of its neighboring spins with their corresponding neighbors. The correlations will be strongest between spins that are within each others immediate vicinity. However, due to translational invariance of system all spins must be identical and a self consistent condition can be imposed,

$$\langle \sigma_0 \rangle = \langle \sigma_i \rangle \tag{2.13}$$

To calculate the magnetization,

$$\begin{aligned} Z_c &= \sum_{\{\sigma_i\}} \sum_{\sigma_0=\pm 1} e^{\beta h \sigma_0} e^{\beta J \sigma_0 \sum_i \sigma_i} e^{\beta h' \sum_i \sigma_i} \\ &= e^{\beta h} (2\cosh \beta(J+h'))^z + e^{-\beta h} (2\cosh \beta(J-h'))^z \end{aligned} \tag{2.14}$$

Calculating $\langle \sigma_0 \rangle$ and $\langle \sigma_i \rangle$ results in

$$\coth \beta_C J = z - 1. \tag{2.15}$$

For a $1D$ chain ($z = 2$), unlike simple MFT, this approximation correctly predicts absence of phase transition at a finite temperature, $T_c = 0$. For $2D$ square lattice ($z = 4$ in 2.15) , $k_B T_c/J = 2.885$, which is an improvement over to MF result, $k_B T_c/J = 4$ (2.10). However, it is still far from the exact result 2.269 given by Onsager's equation $\sinh 2\beta_c = 1$ [73]. It suggests that certain features of mean-field theory are independent of the precise details of approximation.

2.4 Cluster Mean Field Theory

A natural improvement over standard MFT, as suggested by Bethe, was systematic inclusion of interactions. Similar to the treatment in BPW approximation, in cluster mean field theory (CMFT), lattice is divided into small clusters within which interactions between the spins are treated exactly. Oguchi's method [74] is another simple way to extend the MFT to clusters. He studied ferromagnetism and antiferromagnetism of the low-dimensional Heisenberg model by using a cluster of up to three spins to include the short-range correlations between the spins. CMF approach studied in this thesis is an extension of Oguchi's method to larger-size clusters.

The model is approximated by dividing the lattice into identical clusters consisting of N_c spins. The shape of the cluster is selected such that the symmetry of the original lattice is preserved. CMFT can be thought of as an ED of a finite cluster with periodic boundary conditions (PBC), where across the boundary, interactions are replaced by mean fields. In contrast to ED analysis with PBC, the existence of mean fields, whose values are self-consistently determined, approximates the effect of spontaneous symmetry breaking expected to take place in thermodynamic limit. Decoupling of a random bond within a cluster instead of the edge boundaries are also other ways to implement CMFT [75]. Similar treatments with the same key concepts are utilized to study weakly coupled chains keeping interchain interactions at level of mean field [76, 77].

Using this approximation, Hamiltonian for the Ising model can be written as :

$$\mathcal{H}_c = -J \sum_{\langle i,j \rangle}^{N_c} \sigma_i \sigma_j - \sum_{i}^{N_c} h_{eff} \sigma_i \tag{2.16}$$

The first sum represents intra-cluster interactions where the sum runs over all nearest-neighbor pairs within the cluster C. Inter-cluster interactions are included in the second sum where interactions are approximated by effective fields, h_{eff} acting on the boundary

spins of the cluster (see Fig. 2.2). This method reduces to the conventional MF (Weiss's molecular-field) theory for $N_c = 1$, and becomes exact in the limit $N_c \to \infty$.

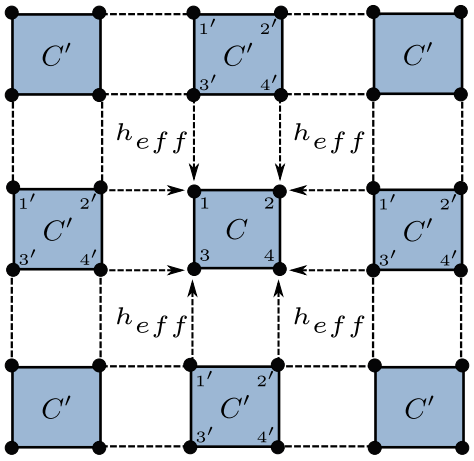

Figure 2.2: A schematic representation of cluster mean field theory (CMFT) for the square lattice. The arrows indicate the effective fields acting on the boundary sites of cluster C.

For self-consistency, a randomly chosen mean field values are selected and $\langle \sigma_i \rangle$ is computed at every site i using 2.17, which are then fed back to $\mathcal{H}_c$ until all the field values are converged.

$$m = \langle \sigma_i \rangle = \frac{Tr(\sigma_i e^{-\beta H_C})}{Tr(e^{-\beta H_C})} \tag{2.17}$$

This method can be extended to other spin models like Heisenberg model where mean fields will have three components. For computation of higher cluster sizes, block diagonalization can be implemented isotropic spin Hamiltonians. However, in case of anisotropic Hamiltonians or in presence of magnetic field, block diagonalization cannot be implemented in order to incorporate mean fields in transverse directions.

The technique is useful in distinctly characterizing the ground states at the level of finite-size calculations. Similar to BPW, CMFT includes the effects of geometry of the lattice. The approximate error caused by finite size effects and mean-field decoupling can in principle be reduced by performing cluster size scaling $N_c \to \infty$. However, there is a practical limitation on cluster size that can be numerically diagonalized. Another shortcoming of the method is the system looses equivalence of all sites or periodicity of the system as it gets divided into finite sized clusters.

2.5 Self Consistent Correlated Mean-Field Theory

Motivated by Onsager reaction field idea [78], a simpler improvement over the standard MFT for Ising model was suggested in [79], where the central spin directly influences the mean-value of nearest neighbors. In this approach, the correlated MF Hamiltonian is written as an effective field h_{eff} acting on the central spin, σ_i,

$$\begin{aligned} H_{MF} &= -\sigma_i h_{eff} \\ h_{eff} &= zJ(\delta_{\sigma_i,1}m^+ + \delta_{\sigma_i,-1}m^-). \end{aligned} \tag{2.18}$$

Two different mean-field values are introduced in effective field (h_{eff}) m^+ and m^-, depending on whether the state of central site (σ_i) has value $+1$ or -1, respectively. Using this average σ_i can be written as,

$$m \equiv \langle \sigma_i \rangle = \frac{e^{\beta z m^+} - e^{-\beta z m^-}}{e^{\beta z m^+} + e^{-\beta z m^-}} \tag{2.19}$$

Now the average value of the neighboring spin, σ_j depends on the state of σ_i. Similarly, the $(z-1)$ neighbors of the site j (next nearest neighbor to site i), assumes m^+ or m^- based on the state of σ_j. Therefore, $\langle \sigma_j \rangle$ can be written as:

$$m^+ = \langle \sigma_j \rangle|_{\sigma_i=+1} = \frac{e^{\beta(z-1)m^+ + 1} - e^{-\beta(z-1)m^- + 1}}{e^{\beta(z-1)m^+ + 1} + e^{-\beta(z-1)m^- + 1}} \tag{2.20}$$

$$m^- = \langle \sigma_j \rangle|_{\sigma_i=-1} = \frac{e^{\beta(z-1)m^+ - 1} - e^{-\beta(z-1)m^- - 1}}{e^{\beta(z-1)m^+ - 1} + e^{-\beta(z-1)m^- - 1}} \tag{2.21}$$

As $T \to T_c$, mean magnetization m in 2.19 goes to zero, while local fields m^+ and m^- are non-zero. However, algebraic average Δ must go zero at T_c.

$$\Delta \equiv \frac{m^+ + m^-}{2} \tag{2.22}$$

Rewriting m, m^+, m^- in terms of Δ and expanding for $\Delta \ll 1$,

$$m = \tanh z\beta\Delta, \tag{2.23}$$

$$m^\pm = \tanh \beta[(z-1)\Delta \pm 1], \tag{2.24}$$

Using 2.22, 2.24, Δ can be written as:

$$2\Delta = \tanh \beta[1 + (z-1)\Delta] - \tanh \beta[1 - (z-1)\Delta] \tag{2.25}$$

Expanding 2.25 around $\Delta = 0$ and keeping only linear terms leads to

$$\cosh^2 \beta_c = (z-1)\beta_c. \tag{2.26}$$

This self consistent correlated field (SCCF) approximation includes local fluctuations near T_c as the central site and its neighboring sites interacts with a self consistently determined fluctuating molecular field (m^+ & m^-), rather than a single-valued mean field. It is able to provide a more accurate estimates of T_C for the Ising model than obtained from BPW approximation. However, unlike BPW, this method only depends on coordination number, z thus missing out the lattice dependence. Furthermore, this approximation does not predict a phase transition for $z < 4$ (for example, honeycomb lattice).

2.6 Correlated cluster mean-field theory

Correlated cluster mean-field theory (CCMFT) combines the idea of CMFT approximation and SCCF theory. Using the concept of CMFT, this method deals with clusters consisting of N_c number of spins where, inter cluster interactions are approximated using correlated fields which, unlike CMFT, depend on the state of the central cluster.

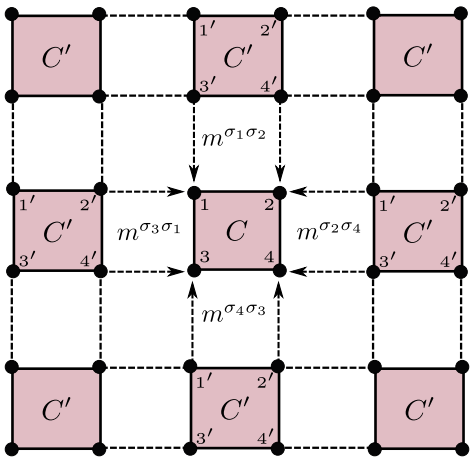

Figure 2.3: A schematic representation of correlated cluster mean field theory (CCMFT) for the square lattice. The arrows indicate the effective fields acting on the boundary sites of cluster C, which depend on the state of the spin as well as the state of its neighboring spin along the boundary.

Hamiltonian for the Ising model using this approximation is same as CMFT with h_{eff} in 2.16 replaced by a correlated field $h_{eff}^{\{s\}}$ acting on the boundary sites. Effective field

$h_{eff}^{\{s\}} = Jm^{\{s\}}$ acting on σ_i ($\in C$) from neighboring spins, depends on state of spin i and of its neighbors ($\{s\}$) belonging to same cluster boundary (see Fig. 2.3). To calculate $h_{eff}^{\{s\}}$, neighboring cluster C' is considered where all the sites couple to an effective field with an exception to the set of spins connected to the central cluster C. Then the fields are computed self consistently depending on the state of C.

For Honeycomb lattice, $\{s\}$ consist only of one spin σ_i since there is only one bond connecting a spin in the central cluster to neighboring cluster (C') (see Fig. 2.4).

$$m^{\pm} = \langle \sigma_{4'} \rangle|_{\sigma_1 = \pm 1} = \frac{Tr(\sigma_{4'} e^{-\beta H_{C'}^{\pm}})}{Tr(e^{-\beta H_{C'}^{\pm}})} \tag{2.27}$$

$$\mathcal{H}_{C'}^{\pm} = -J \sum_{\langle i,j \rangle \in C'}^{n_c} \sigma_i \sigma_j - \sum_{i'}^{n_c} h_{eff}^{\sigma_i} \sigma_i \mp J \sigma_{4'} \tag{2.28}$$

Whereas for square lattice, $\{s\}$ has two spins including σ_i itself (see Fig. 2.3). Effective mean fields acting on site 1 and site 2 in cluster C, depend on the state of both the sites. For square lattice, there are m^{++}, m^{+-}, m^{-+} and m^{--}

$$m^{ss'} = \langle \sigma_{4'} \rangle|_{\sigma_1 = s, \sigma_2 = s'} = \frac{Tr(\sigma_{4'} e^{-\beta H_{C'}^{ss'}})}{Tr(e^{-\beta H_{C'}^{ss'}})} \tag{2.29}$$

$$\mathcal{H}_{C'}^{ss'} = -J \textstyle\sum_{\langle i,j \rangle \in C'}^{n_c} \sigma_i \sigma_j - \sum_{i,\bar{i} \in C'}^{n_c} h_{eff}^{\sigma_i, \sigma_{\bar{i}}} \sigma_i - Js'\sigma_{3'} - Js\sigma_{4'} \tag{2.30}$$

$$= -J(\sigma_{1'}\sigma_{2'} + \sigma_{2'}\sigma_{3'} + \sigma_{3'}\sigma_{4'} + \sigma_{4'}\sigma_{1'}) - J(m^{\sigma_{1'}\sigma_{2'}} + \sigma_{1'}\sigma_{4'})\sigma_{1'} \tag{2.31}$$

$$-J(m^{\sigma_{2'}\sigma_{3'}} + \sigma_{2'}\sigma_{1'})\sigma_{2'} - J(m^{\sigma_{3'}\sigma_{2'}} + s')\sigma_{3'} - J(m^{\sigma_{4'}\sigma_{1'}} + s)\sigma_{4'} \tag{2.32}$$

The treatment, in principal, can be extended to any lattice geometry. This method is an improvement over both SCCMF and CMFT as unlike SCCMF, this method incorporates the dependence on lattice geometry while also improving T_C. CCMFT has been successfully adopted to analyze several classical spin-1/2 interacting systems with interactions up to the next-nearest neighbors [80], including disordered [81] and geometrically frustrated lattices.

2.7 Quantum correlated cluster mean-field theory

CCMFT proved effective for classical spin systems however, it shows inconsistent results in presence of quantum fluctuations as it restricted the states to classical quantization

axes. In order to make CCMFT useful for quantum models, a more general state is allowed in quantum version of the CCMFT (QCCMFT) [82]. Following the approach of CCMFT, spins at boundary of central cluster interacts with expected value of the magnetic moment of neighboring site for two general orthogonal states:

$$|\Phi^{\pm}\rangle = \cos(\theta/2)|\uparrow\rangle \pm e^{i\phi} sin(\theta/2)|\downarrow\rangle, \tag{2.33}$$

where the angles $\theta \in [0, \pi]$ and $\phi \in [0, 2\pi]$ have to determined self-consistently. For transverse field Ising model, there exists an easy axis for exchange interaction therefore, only z component of the magnetic moment is relevant.

$$\langle \Phi^{\pm}|\sigma_i^z|\Phi^{\pm}\rangle = \pm \cos\theta \tag{2.34}$$

Where ϕ is set to zero. Using the approximation, Hamiltonian can be written as:

$$\mathcal{H}^{\pm}_{C'} = -J \sum_{\langle i,j\rangle \in C'}^{n_c} \sigma_i \sigma_j - \sum_{i'}^{n_c} h_{eff}^{\sigma_i} \sigma_i - J\sigma_{4'} s \cos\theta \tag{2.35}$$

which is similar to 2.28 with an additional parameter θ. Notice for $\theta = 0$, QCCMFT reduces to CCMFT. Imaginary time spin self-interaction, $\overline{q}$ is evaluated to find the value of θ,

$$\overline{q} \;=\; \left\langle \frac{1}{\beta}\int_0^{\beta} d\tau \sigma_i^z \sigma_i^z(\tau) \right\rangle_{\rho_B(\mathcal{H})} = Tr\left(\frac{1}{\beta}\int_0^{\beta} d\tau \sigma_i^z \sigma_i^z(\tau)\rho_B(\mathcal{H})\right) \tag{2.36}$$

τ is the imaginary time evolution operator leading to $\sigma_i^z(\tau) = e^{-\tau\mathcal{H}}\sigma_i^z e^{-\tau\mathcal{H}}$. Considering eigenstates $|n\rangle$ with associated eigenvalues E_n,

$$\overline{q} \;=\; \frac{\sum_{n,m}\int_0^{\beta} d\tau \langle n|\sigma_i^z|m\rangle\langle m|\sigma_i^z|n\rangle e^{\tau(E_n - E_m)} e^{-\beta En}}{\beta \sum_n e^{-\beta E_n}} \tag{2.37}$$

$$\;=\; \frac{\sum_n e^{-\beta E_n}|\langle n|\sigma_i^z|n\rangle|^2}{\sum_n e^{-\beta E_n}} - \frac{\sum_{n\neq m} \frac{e^{-\beta E_m} - e^{-\beta E_n}}{E_m - E_n}|\langle m|\sigma_i^z|n\rangle|^2}{\beta \sum_n e^{-\beta E_n}} \tag{2.38}$$

Spin self-interaction for eigenstates $\langle \Phi^{\pm}\rangle$ with eigenvalues $E_{\pm}$ is,

$$\overline{q} = \cos^2\theta + \sin^2\theta \frac{\tanh \beta\Delta E/2}{\beta\Delta E/2} \tag{2.39}$$

where $\Delta E = E_+ - E_-$. In the limit where thermal fluctuations are small compared to energy gaps, $\theta = \cos^{-1}\sqrt{\overline{q}}$. Using this in 2.35, magnetization is computed self-consistently in the manner exactly similar to CCMFT.

2.8 Comparing different mean field approximations

Having discussed the details of various mean field approximations, in this section comparisons of the methods for Ising, transverse-field Ising and Heisenberg models for different lattices namely, square and honeycomb will be discussed. The honeycomb lattice is divided into topologically equivalent clusters of the shape of smallest honeycomb unit (see Fig 2.4), which consist of six sites each ($n_s = 6$). In this scenario, there is only one spin in the cluster which interacts with another spin in neighboring cluster. Similarly, the square lattice is divided into clusters with ($n_s = 4$) sites where each spin in the cluster has two spin interactions in the neighboring cluster (see Fig 2.3).

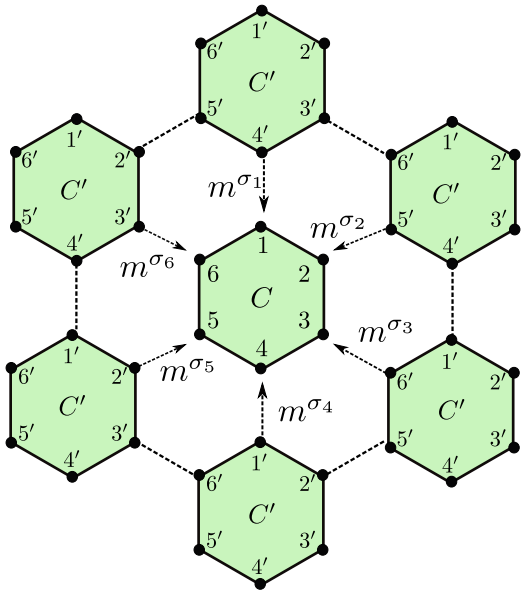

Figure 2.4: A schematic representation of correlated cluster mean field theory (CCMFT) for honeycomb lattice. The arrows indicate the effective fields acting on the boundary sites of cluster C which depends on the state of the spin itself.

For Ising model on honeycomb lattice, when the temperature decreases, the system presents spontaneous magnetization m^z below the critical temperature T_c. In Fig. 2.5, we show a comparison of magnetization as obtained from all the methods. CMFT over estimates the transition temperature in comparison to CCMFT. Variation in m^z is sharper in CCMFT as it includes more accurate correlation effects compared to CMFT. It should be noted that for a classical Ising model ($\Gamma = 0$), QCCMFT reduces to CCMFT due to absence of quantum fluctuations which consequently sets $\overline{q} = 1$. Transition temperatures obtained from simple MFT (red square in Fig 2.5) and BPW (blue circle in Fig 2.5) approximation over estimates the transition temperature in comparison to CCMFT. Unfortunately, SCCMF does not have a solution for $z = 3$ (2.26). Cluster considered in

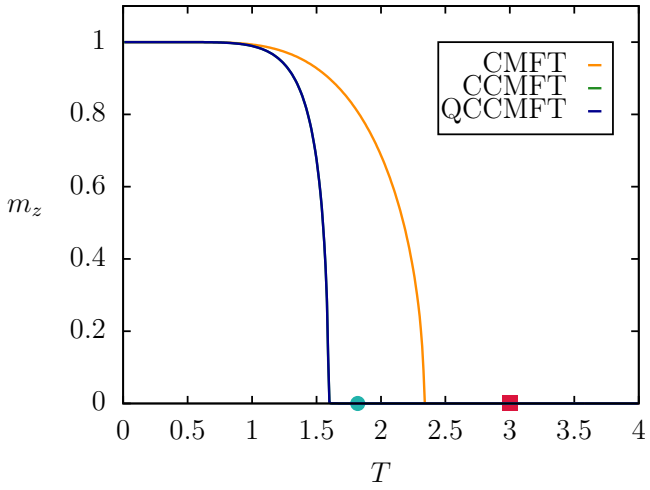

Figure 2.5: Temperature dependence of magnetization of Ising model on honeycomb lattice using various approximation schemes. Blue circle (red square) is the transition temperature obtained from BPW (MFT) approximation.

this analysis consists of $n_s = 6$, in principle estimates can be improved by considering larger cluster size for cluster analysis.

The idea of cluster mean field models is to incorporate quantum fluctuations near transition points to give a more accurate description. The effectiveness of all the models in capturing quantum fluctuations can be put to test by utilizing the methods for the simplest model describing quantum phase transition, transverse field Ising model (TFIM) (discussed in previous chapter 1.13). Fig. 2.6 depicts the quantum phase transition driven by transverse field (Γ) in TFIM on honeycomb lattice computed using various mean field methods. When $\Gamma > 0$, m^z gradually decreases as quantum fluctuations increase. On further increasing Γ, the system leads to a quantum critical point (QCP) Γ_c where m^z becomes zero. In contrast to QCCMFT and CMFT, CCMFT leads to a discontinuity in magnetization close to QCP.

QCCMFT seems to capture the most accurate description of thermal as well as quantum fluctuations. Using the details of correlation functions, a comparison between QCCMFT and CMFT is discussed for TFIM on a square lattice. Fig. 2.7 shows the longitudinal correlation functions, C_{zz} and the corrected one $C_{zz} - (m^z)^2$, between nearest neighbor spin pairs for a 4 spin square plaquette, therefore all the bonds are equivalent. For $\Gamma = 0$, TFIM becomes a classical Ising model, where correlation between its constituents are maximum in the ordered phase. As thermal fluctuations in the system increase, C_{zz} reduce, becoming totally uncorrelated at higher temperatures. At the critical point, thermal fluctuations diverge in the thermodynamic limit, resulting as peak in

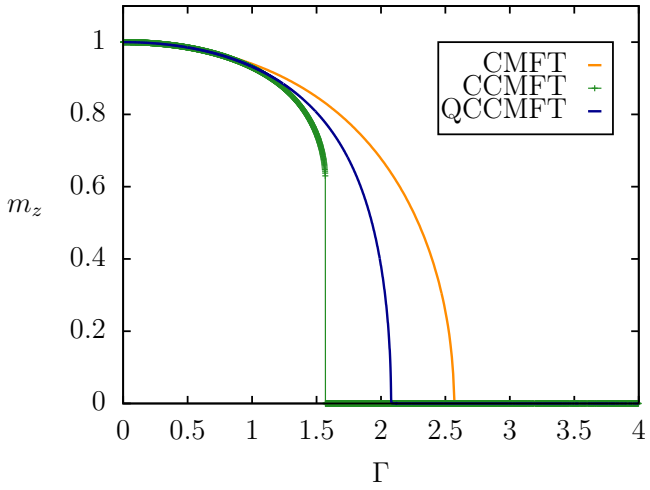

Figure 2.6: Variation of magnetization (m^z) as function transverse field (Γ) of transverse field Ising model on honeycomb lattice for different mean field approximations.

corrected correlations. Since CMFT and QCCMFT are approximations to finite lattices aiming to capture this effect, the expected divergence is related to the peak shown in (2.7 (a)). For a quatum phase transition driven by quantum fluctuations at $T = 0$, the corrected correlation function shows a maximum at Γ_c. Maximum obtained in quantum fluctuations is lower than thermal fluctuations (2.7 (b)).

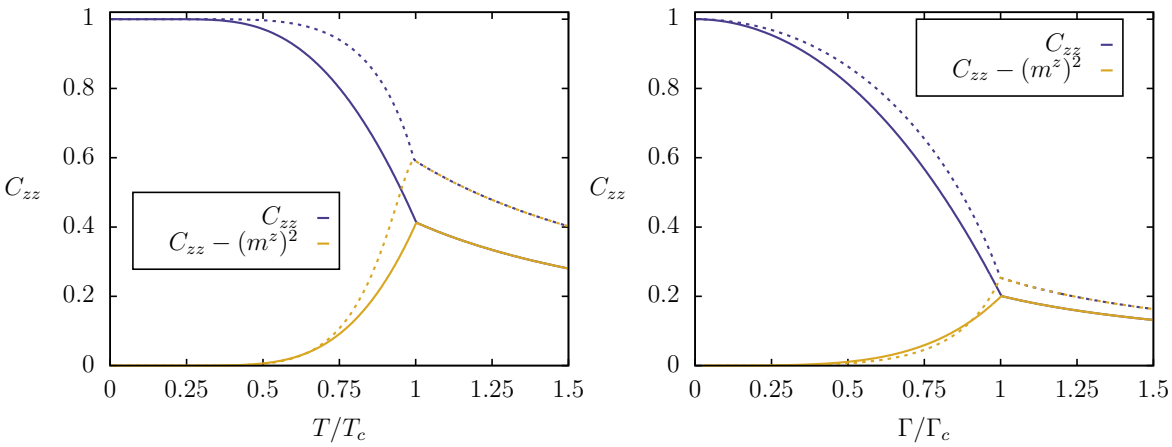

(a) (b)

Figure 2.7: Correlation as a function of (a) reduced temperature at $\Gamma = 0$ and (b) reduced transverse field T = 0 for TFIM on the square lattice obtained using CMFT (solid lines) and QCCMFT (dashed lines).

This peak can be made sharper with larger cluster size, however the exponents would still remain classical like due to the semi-classical nature of the method. As QCCMFT

(dashed lines) incorporates more details of correlations among spins in comparison to CMFT (solid lines), the peak of corrected correlations is higher in both quantum and thermal fluctuations. Another interesting feature is the correlations are finite in the classical or quantum paramagnetic regime unlike simple MFT. It is interesting to note that CMFT being simpler in comparison to other correlated methods yields qualitatively correct physics.

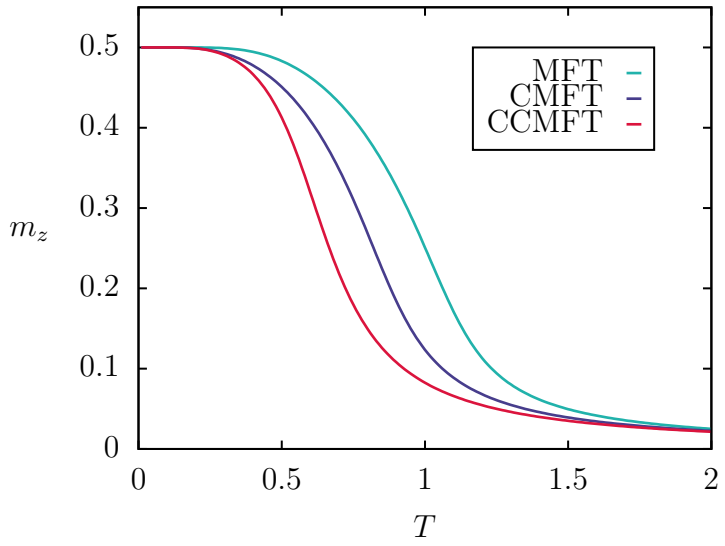

Figure 2.8: Temperature dependence of magnetization (m^z) of an isotropic Heisenberg ferromagnet on a square lattice at $h/J = 0.1$. Comparison of results obtained from MFT, CMFT and CCMFT approach are illustrated.

Ising model discussed above posses a discrete symmetry, Heisenberg model on other hand obeys rotational symmetry. Isotropic Heisenberg model in $2D$ is known to not show a finite temperature phase transition due to Mermin-Wagner theorem. However, a presence of a small magnetic field destroys the symmetry of the Hamiltonian, therefore the system can spontaneously order which can be continuously destroyed with increase in temperature. Fig. 2.8 shows the results for Heisenberg ferromagnetic system, on a square lattice in presence of a finite magnetic field ($h/J = 0.1$), as obtained from MFT, CMFT and CCMFT. Due to presence of applied field, m^z does not vanish completely even after transition temperature. Remarkably, MFT is also able to capture the phase transition qualitatively. Since CCMFT incorporates more local quantum correlations, it shows faster convergence when compared to other methods.

2.9 Cluster size scaling

As suggested by Bethe, critical points can be further improved quantitatively with increasing the number of interactions that are treated exactly. In this section, a series of clusters are used upto $N_c = 16$ (for which the Hamiltonian is block diagonalized) to illustrate the scaling of transition temperatures for a ferromagnetic Heisenberg model on a square lattice via CMFT (see Fig. 5.4). A scaling parameter [83] is defined for quantitative dependence,

$$\lambda = \frac{N_B}{N_c * z/2} \tag{2.40}$$

where N_B is the number of bonds with in the cluster, the denominator means the number of bonds of the original lattice (with coordination number, z) for N_c number of spins in the cluster. The scaling parameter λ provides a quantitative measure of the amount of correlation effects are account using the cluster. For $\lambda = 0$, CMFT reduces to simple Weiss MFT, where as $\lambda = 1$ is the infinite size limit with exact result. Note for two different clusters, 2X2 and 1X4, λ is different even though number of spins considered is same. λ is higher of 2X2 since the number of bonds that are treated exactly is higher. It is also interesting to note that T_c obtained from $1D$ clusters are higher than for ones where cluster respects the symmetry of the lattice. Fit to the data shows that T_c in the infinite limit is still finite owing to the mean-field nature of calculation.

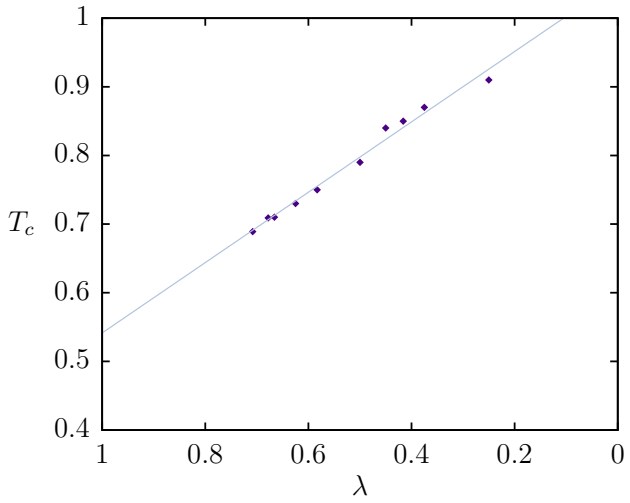

Figure 2.9: Cluster size scaling of transition temperature of ferromagnetic Heisenberg model on a square lattice with the scaling parameter λ. Straight line is a fit to the data points obtained from different cluster.

2.10 Dependence on cluster shape

Previous section emphasize on the dependence of critical points on lattice geometry and cluster size. Fig. 5.4 points out the difference in the T_c when the shape of cluster is different even though the number of interacting spins remain same. Magnetic phases obtained within CMFT also depends on the shape of the cluster considered as a consequence of finite size. To illustrate this, Heisenberg Hamiltonian on a honeycomb lattice is considered,

$$H = J_1 \sum_{\langle ij \rangle} \mathbf{S}_i \cdot \mathbf{S}_j + J_2 \sum_{\langle\langle ij \rangle\rangle} \mathbf{S}_i \cdot \mathbf{S}_j + J_3 \sum_{\langle\langle\langle ij \rangle\rangle\rangle} \mathbf{S}_i \cdot \mathbf{S}_j \tag{2.41}$$

where J_1, J_2 , J_3 ($J_a \geq 0$) are first, second and third nearest neighbor interactions. This frustrated spin model has been explored previously using various techniques like spin-wave theory [84], Schwinger boson approaches [85] and exact diagonalization [86]. Competition between various spin pairs gives rise to a rich phase diagram shown in [86] using exact diagonalization up to 42 spins. The spin model hosts various phases like, a Néel ordered phase (I), a collinear magnetically ordered phase (II, IV), short ranged spiral state (III) (which is also connected to a state which decoupled into two triangular lattices exhibiting 120 deg order) and a magnetically disordered state forming valence bond crystal (V). The article also compliments its extensive ED results with CMFT using two different cluster shapes. The two clusters selected vary in the number of spins considered as well as symmetry, 6-site cluster is a honeycomb plaquette which respects the lattice properties completely. Where as the other cluster considered was a slightly non-trivial 8-site cluster (see Fig 3(a) in [86]). It was shown that not all the phases are compatible with the two cluster shapes selected, phase III was not obtained for 8-site cluster where as phases II and IV were missing from the computation of 6-site cluster. In an attempt to obtain all the phases within CMF another 8-site cluster is proposed here, and the obtained phase diagram is compared with 6-site cluster.

Phase diagram obtained from a 6-site cluster (Fig 2.10 (a)) shows are broad range of disordered phase with Néel order and spiral order. However other collinear orders are not obtained in this calculations. In addition, a collinear phase (III') is also obtained in the region, however it seems to be a meta-stable state which would eventually lead to a proper spiral state with proper scaling. Region supporting Néel order is reduced in 6-site cluster and the parameter space resulting in a disordered region is increased compared to the 8-site cluster considered in the said article. With the 8-site cluster (Fig 2.10 (b)), Néel state is stabilized in a larger parameter space, disordered phase (V) is stable in a reduced parameter region reduced giving rise to other collinear phase III'. Phase III' is

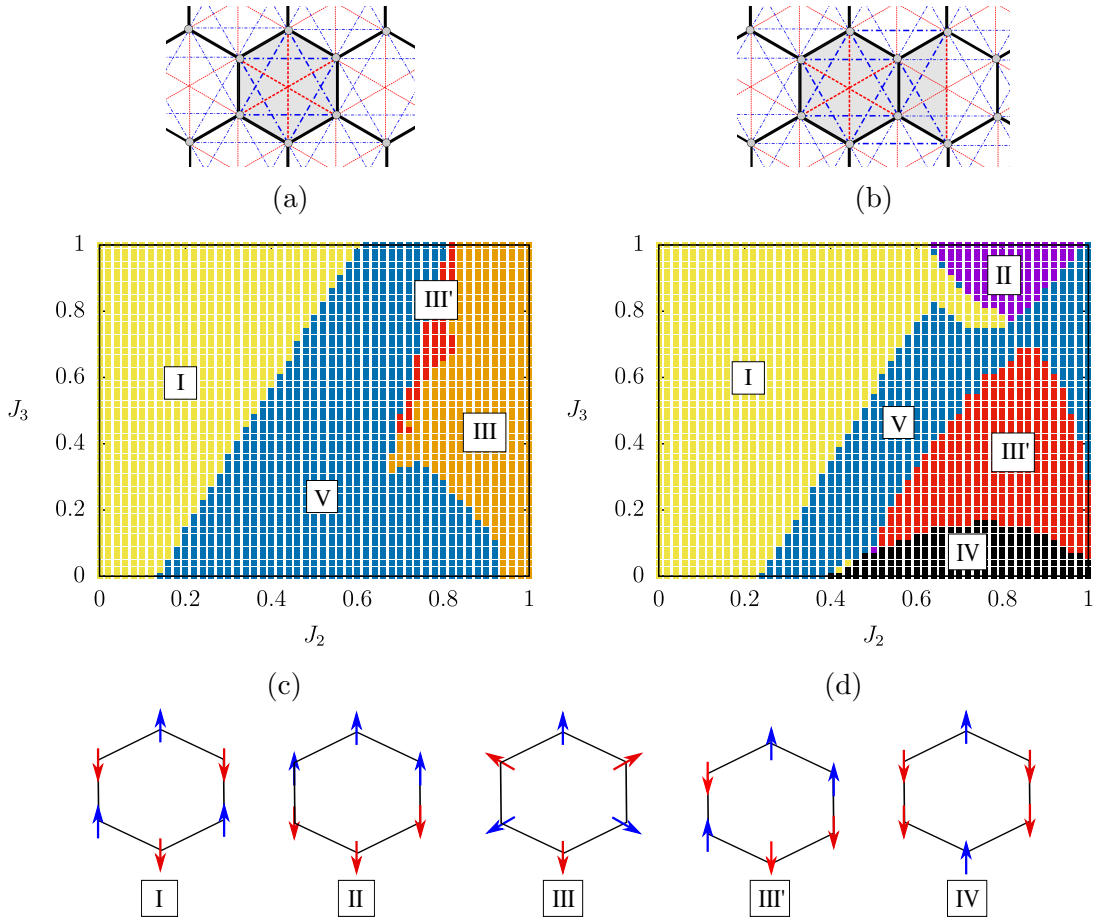

Figure 2.10: Clusters (a), (b) employed for CMFT calculations consisting of $N = 6$ and $N = 8$ spins. Thick(thin) lines connecting the circles in the shaded area are intra-cluster (inter-cluster) couplings, J_1 (black), J_2 (blue) and J_3 (red). Phase diagrams (c)((d)) obtained from CMFT as applied to the N=6 cluster (a) (N= 8 cluster (b)).

a meta-stable state which will be replaced by the spiral phase obtained in 42 spin ED if larger clusters were considered. It should be noted that unlike cluster (a), all the sites are not equivalent in this cluster, due to this in-equivalence, Néel order is obtained for larger J_2 and J_3. With this analysis it is safe to conclude the shape of the cluster considered for the calculation controls the resulting phase diagram obtained. It is very important to find a cluster which is compatible with most of the magnetic phases.

2.11 Effective in Frustrated systems

Frustration in magnetic systems has attracted much attention in last few decades as it results in non-trivial phases by weakening conventional magnetic order. However, it adds enormous complexity in determining the properties of such exotic physics. Various sophis-

ticated numerical approaches like quantum Monte Carlo fail in correctly understanding such systems. In this context, approximate approaches like CMFT are valuable as it goes beyond a single site mean field classical theory and results in the symmetry-broken states partially accounting for local quantum fluctuations. This treatment may allow for disordered states in cases when frustration of interactions dominates, such as highly frustrating models like Kitaev-Heisenberg model. Kitaev Heisenberg model on honeycomb lattice holds a lot of importance as it is motivated by the family of iridates, candidate material to host Kitaev physics. CMFT has been employed for KH model on honeycomb [87] as well as Kagome lattice [88] with large clusters using Lanczos diagonalization. It correctly predicts all the phases with qualitatively accurate phase boundaries. It has also been utilized as a starting point to understand ground states of various frustrating models like, $J_1 - J_2 - J_3$ Heisenberg model on a honeycomb lattice as discussed in previous section [86]. It gives surprisingly accurate ground state phase boundaries for the frustrated quantum magnetic model, spin-1/2 $J_1 - J_2$ Heisenberg model in a two-dimensional square lattice [89]. CMFT with proper scaling analysis quantitatively reproduced the magnetization curve, including the stabilization of the one-third magnetization plateau in antiferromagnetic model on triangular lattice in magnetic field [90, 91]. The effects of inter-chain/layer coupling, which are unavoidable in real low-D materials can also be demonstrated using the method. This technique has been shown to improve upon conventional mean-field approaches for the case of hard-core bosons on the triangular lattice [92] and when applied to an effective model for a frustrated antiferromagnet bilayer square lattice [93, 83]. Recently, CMFT has also been applied to study electron-hole pair (or excitonic) condensation in the extended Falicov-Kimball model at finite temperatures [94]. The method has been proven effective to study Kugel-Khomskii type superexchange interactions with finite spin-orbit couplings [95, 96] as well as to study spin crossover in strongly correlated electron systems[97]. It has also been used to study magnetic effects of electron doping in molecular magnets [98]. In this thesis, CMFT will be utilized to understand not only ground state, but also the temperature and field dependent experimental results of real materials possessing frustrating interactions.

2.12 Ground state of AF spin chain

Antiferromagnetic spin-1/2 chains are model systems for realizing a wide range of interesting quantum many-body ground states. For a classical antiferromagnetic system the ground state for any dimensional lattice will be a state with alternating spin on adjacent lattice site but when quantum nature of the spins is included, ideally the spins would like

form valence bond states where nearest neighbor spins form a singlet pair. However, it is well known that AFM Heisenberg magnet on a 2D and 3D lattice results is a Néel AFM and not a valence bond state. The ground state of spin-1/2 Heisenberg antiferromagnetic chain (HAFC) model is characterized as a quantum critical spin liquid in which the spin correlations decay as a power law [4]. However, despite the absence of static long-range order, the model exhibits well-defined spin-1/2 excitations called spinons. The spinons are created in pairs leading to a quantum continuum of gapless two-spinons states [30]. In systems where the spin-1/2 HAFC model can be realized, the presence of interchain coupling, disorder, spin frustration, or applied magnetic field brings about novel and unexpected changes to the low-energy properties [50]. The question addressed here is what will be the ground state of an antiferromagnetic spin chain using CMFT?

Fig. 2.11 shows the variation staggered magnetization with increasing length of spin chain. The value of staggered magnetization obtained is less than 10% of the spin magnitude. Its reduction with increasing chain length suggests that Néel order induced in the system is the artefact of mean field character. CMFT is an iterative method where the self-consistency loop runs until the mean field values are converged. Mean fields considered converged when the difference between mean fields in each iteration is less than the a fixed value, known as tolerance factor.

Here we show that staggered magnetization is further reduced with stronger tolerance factor. Within CMFT, ground state of antiferromagnet Heisenberg model on a chain is a mixed stated forming valence bonds on alternate sites. However, the true valence bond with ($C_{rr'} = -0.75$) is disturbed due to mean fields at the edge of the spin chain which leads to the appearance of a Néel type order with very small staggered magnetization.

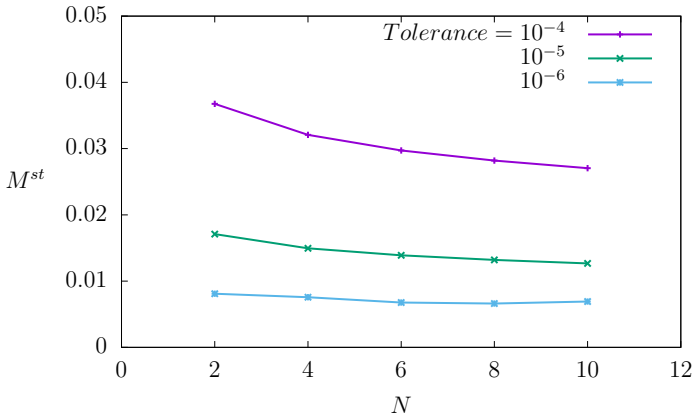

Figure 2.11: Variation of staggered magnetization with different chain lengths and tolerance error for an antiferromagnetic Heisenberg chain calculated using CMFT.

In conclusion, we have demonstrated that CMFT is capable of qualitatively describing classical and quantum phase transitions in an important class of spin Hamiltonians by considering thermal and quantum effects within the same framework. Despite the shortcomings related to estimations of ordering temperatures, etc. the method holds a great promise as it provides a qualitative picture of thermodynamic behaviour owing to an accurate treatment of short range spatial correlations. In the rest of the thesis, CMFT will be utilized as the main tool to capture the subtle competition between different possibilities of magnetic ordering in complex Hamiltonians motivated by real magnetic materials.

Chapter 3

Cluster mean-field study of the Heisenberg model for $CuInVO_5$

Adapted from the work :

Singhania, A., Kumar, S., "Cluster mean-field study of the Heisenberg model for $CuInVO_5$", ***Phys. Rev. B*** 98, (2018) 104429

3.1 Introduction

Spin-1/2 quasi-one-dimensional (Q1D) magnets are ideal candidates for observing fundamental quantum phenomena as the combination of low dimensionality and small spin-magnitude maximizes quantum fluctuations [3, 48]. This has motivated experimentalists for many decades to realize one dimensional quantum magnets [99, 100]. These efforts have led to the discovery of many Q1D magnets and to the experimental verifications of various quantum phenomena [101]. Indeed, quantum phase transitions driven by magnetic field or external pressure have been reported in low dimensional magnets such as $TlCuCl_3$, $KCuCl_3$, $LiCuVO_4$, $CoNb_2O_6$, etc. [102, 103, 104, 105, 106, 107, 108, 109]. Certain low-dimensional magnets have also been identified as being close to a quantum critical point [110, 111]. Presence of extended quantum critical region has been inferred from the magnetic field dependence of excitations in copper pyrazine dinitrate [112]. Due to enhanced quantum fluctuations, Q1D magnets are also considered strong candidates for hosting quantum spin liquid states [113, 106, 114, 115]. Another aspect that makes low-dimensional magnets very interesting is the possibility of qualitatively new type of excitations [116, 117, 118]. A classic example is that of spinon excitations in one-dimensional antiferromagnets [119, 120]. More recently a realization of longitudinal spin excitations, the so called Higgs mode, in certain Q1D magnets has been proposed [121, 122, 123, 124, 125, 126, 127].

Recent experimental studies on spin-1/2 tetramer compound $CuInVO_5$ show unusual magnetism at low temperatures [126]. Thermodynamic measurements, such as specific heat and magnetic susceptibility, show that a long-range ordered antiferromagnetic state exists below 2.7K. There are two inequivalent Cu sites and the size of the ordered moment strongly differs at these two sites. This leads to a magnetization plateau in the magnetic field dependence at nearly half the saturation magnetization. While some of the features observed in $CuInVO_5$ can be explained within a simple mean-field approach, the presence of two peaks in the low-temperature specific heat and the presence of a cusp in the magnetic susceptibility remain as two of the unexplained features in the data [126]. Furthermore, a microscopic picture of the ordered state and its evolution with magnetic field and temperature has been lacking.

Motivated by these puzzles in the experimental data on $CuInVO_5$, we present a comprehensive analysis of a four-sublattice one-dimensional Heisenberg model with three different nn exchange couplings. We make use of cluster mean-field (CMF) approach where intra-cluster interactions are treated exactly while inter-cluster interactions are treated at

the mean-field level. The approach is well justified in the context of $CuInVO_5$ due to the existence of a hierarchy of coupling strengths as inferred from the experimental results [126]. We find that treating inter-tetramer coupling beyond mean-field, which requires a minimum of 8 sites in the cluster for the CMF study, brings out a subtle competition between two different spin-spin correlations. This emphasizes the presence of two distinct limiting phases in the model, and the ground state in $CuInVO_5$ is best understood as a compromise of these two competing tendencies. Interestingly, the temperature dependence of the correlations is non-monotonic with certain spin-spin correlations strengthening with increasing temperature. Such effects are typically encountered in frustrated magnets where entropic effects at higher temperatures can help in enhancement of order [128, 129, 130]. We also identify multiple spin-flop transitions in the presence of external field which highlight the inequivalence of spins within a tetramer. Most importantly, the subtle interplay between different spin-spin correlations accounts for the presence of an extra peak in the magnetic specific heat and a cusp in the magnetic susceptibility at low temperatures, in excellent agreement with the experimental data on $CuInVO_5$ [126].

The remainder of the paper is organized as follows. In Section 3.2 we define the model and discuss the CMF approach used for the study. Results are discussed in Section 3.3 where we begin by discussing the phase diagrams for the general choice of model parameters. This is followed by a discussion of various observables calculated for the parameters specific to $CuInVO_5$. For a clear understanding of the microscopic details we analyse the longitudinal and transverse spin-spin correlations between different pairs of spins. Summary and conclusions are presented in Section 3.4.

3.2 Model

We begin with a Heisenberg model on a 1D chain of spin-1/2 tetramers in the presence of an external magnetic field. The model is described by the Hamiltonian,

$$\begin{aligned}\mathcal{H} &= \sum_{i=1}^{N_t}[J_2(\mathbf{S}_{4i-3}\cdot\mathbf{S}_{4i-2}+\mathbf{S}_{4i-1}\cdot\mathbf{S}_{4i})+J_1\mathbf{S}_{4i-2}\cdot\mathbf{S}_{4i-1} \\ &\quad +J_3\mathbf{S}_{4i}\cdot\mathbf{S}_{4i+1}]-h_z\sum_{i=1}^{N_t}\sum_{j=0}^{3}S^z_{4i-j}. \qquad (3.1)\end{aligned}$$

Here, $\mathbf{S}_{4i-j}$ with $j = 0, 1, 2, 3$ are the Heisenberg spin operators belonging to the i^{th} tetramer. $J_1 > 0$, $J_2 < 0$, $J_3 > 0$ are the Heisenberg exchange constants and h_z is the

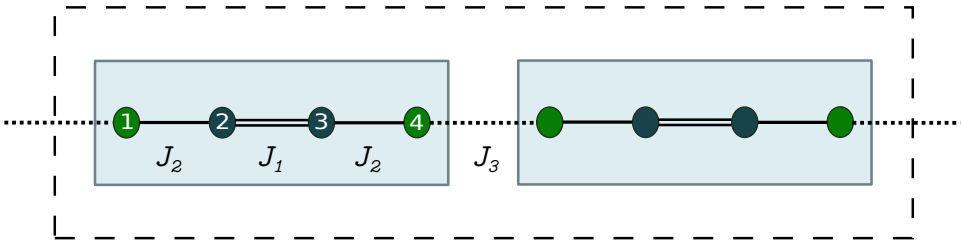

Figure 3.1: A schematic picture of the coupled tetramer model. Each dot represents a spin-1/2 and the nearest-neighbor couplings are indicated by double (J_1), solid (J_2) and dotted (J_3) lines.

magnitude of the applied magnetic field. N_t is the total number of tetramers, and periodic boundary condition is imposed via the identification $\mathbf{S}_{4N_t+1} \equiv \mathbf{S}_1$. For the analysis of the model Hamiltonian we will use $J_1 = 1$ as the elementary energy scale. This leaves us with J_2, J_3 and h_z as free model parameters. The inter-tetramer exchange J_3 is inferred to be much smaller than the intra-tetramer couplings J_1 and J_2 in $CuInVO_5$.

In order to understand the nature of long-range magnetic order in the model Hamiltonian Eq. (3.1), we employ the CMF approach. CMF method is an extension of the single-site Weiss mean-field approximation, and has been very successful in studying the competition between different ordered states even in low dimensions [89, 131, 87]. It is well know that the Mermin-Wagner theorem prohibits the presence of any long range order at non-zero temperatures for isotropic spin Hamiltonians in dimensions $d \leq 2$ [46]. However, most low-dimensional magnets exhibit long-range order at small but finite temperatures [100, 132, 41]. $CuInVO_5$ is no exception to this trend as a long-range order sets in at 2.7K. This apparent violation of Mermin-Wagner theorem can be understood in terms of the presence of magnetic anisotropies and/or the role of weaker inter-chain or inter-layer coupling. The importance of quantum effects in low-dimensional ordered magnets is typically reflected in the suppression of the ordered moment [133]. The existence of long-range magnetic order in $CuInVO_5$ further justifies the use of CMF approach for describing low-temperature magnetism. One can argue that the mean-field aspect of the method is taking into account the three dimensional character of the magnetic system. Hence, the feature that CMF calculations lead to an ordered state at low enough temperatures is consistent with the experimental results. Although the CMF approach has been extensively discussed in literature [131, 87], for completeness, we briefly introduce the method here. Specifically, let us consider a one-dimensional system which can be thought of as repeated structure of clusters containing linear segments of N_c spins. We want to treat the interactions within the cluster exactly while inter-cluster interactions will be treated approximately. In a one dimensional system there are two edge spins, $\mathbf{S}_1$

and $\mathbf{S}_{N_c}$ that couple the central cluster to two adjacent clusters (see Fig 3.1). These two inter-cluster coupling terms can be approximated via the standard mean-field decoupling where $\mathbf{S}_i \cdot \mathbf{S}_{i+1}$ is replaced by $\langle \mathbf{S}_i \rangle \cdot \mathbf{S}_{i+1} + \mathbf{S}_i \cdot \langle \mathbf{S}_{i+1} \rangle - \langle \mathbf{S}_i \rangle \cdot \langle \mathbf{S}_{i+1} \rangle$ by ignoring the higher order fluctuation terms. Therefore, the original Hamiltonian reduces to a cluster Hamiltonian in the presence of mean-fields that are experienced by the edge spins. The mean fields acting on spins $\mathbf{S}_1$ and $\mathbf{S}_{N_c}$ are then calculated self-consistently. For a cluster with N_c spins of magnitude 1/2, the size of the Hilbert space for the cluster Hamiltonian is 2^{N_c}, and therefore the cluster Hamiltonian can be easily diagonalized exactly for $N_c \leq 12$. Note that in the general case where the mean fields are allowed to have components along x and y directions, the resulting mean-field Hamiltonian does not possess many of the symmetries of the full interacting Hamiltonian. Therefore, it is not generally possible to make use of symmetries to achieve diagonalizations of larger clusters. The quantum expectation values of the spin operators $\langle S_i^\alpha \rangle$ where i denotes the site and α the spin component, can be computed following the standard quantum statistical mechanics. The angular bracket denotes the quantum statistical average of the operator, and is defined for any operator O as

$$\langle O \rangle \;\; = \;\; \frac{1}{\mathcal{Z}} Tr\ [O\ e^{-\beta H_c}], \tag{3.2}$$

where β is the inverse temperature, H_c is the cluster Hamiltonian, and $\mathcal{Z} = Tr\ e^{-\beta H_c}$ is the partition function. The process is repeated until a self-consistent solution is obtained upto a desired tolerance factor. In our calculations we take 10^{-5} as tolerance factor for convergence. As with all self-consistent approaches, we begin with a variety of initial mean-field configurations to ensure that the resulting self-consistent solution corresponds to a global minimum.

3.3 Results and Discussions

Before we consider the model parameters relevant to $CuInVO_5$, it is useful to explore the ground state phase diagram of the model in the parameter space $|J_2|/J_1$, J_3/J_1 and h_z/J_1. To obtain these CMF phase diagrams we work with an 8-site cluster containing two tetramers. The justification for this choice will become clear in Sections 3.3.2 and 3.3.3. where we will present a comparison between results obtained using 4-site and 8-site clusters.

3.3.1 Spin-spin correlations in the ground state

In order to characterize the ordered states at low temperature, we compute the transverse and longitudinal components of the spin-spin correlations defined by,

$$\begin{aligned} C_{ij}^{\perp} &= \frac{1}{2}\langle S_i^+ S_j^- + S_i^- S_j^+ \rangle, \\ C_{ij}^{zz} &= \langle S_i^z S_j^z \rangle. \end{aligned} \tag{3.3}$$

The total spin-spin correlations C_{ij} can be obtained by adding the transverse and longitudinal components, $C_{ij} = C_{ij}^{\perp} + C_{ij}^{zz}$. In the absence of external magnetic field, we present the evolution of total spin-spin correlations as a function of $|J_2|$ and J_3, keeping $J_1 = 1$ as the strongest exchange parameter. As expected, we find that C_{23} retains its singlet-like character across the entire parameter regime covered in Fig. 3.12 (see Appendix 3.5.1). Similarly, C_{12} and C_{34} (see Fig. 3.2(c)) remain ferromagnetic in nature, except in the vicinity of the $J_2 = 0$ line where these correlations become vanishingly small. The behavior of $C_{23}(C_{12}/C_{34})$ is not at all surprising since these spins are directly coupled via antiferromagnetic (ferromagnetic) interactions. Most interesting variation is noticed in C_{14} and C_{45}. C_{45} begins with a perfect singlet nature ($C_{45} \approx -0.75$) along $J_2 = 0$ line and the correlations diminish gradually as we move towards $J_3 = 0$ line. The behavior of C_{14} is complementary to that of C_{45}. This can be easily understood as $\mathbf{S}_4$ can participate in only one perfect singlet, either with $\mathbf{S}_1$ or with $\mathbf{S}_5$. The tendency for singlet formation between $\mathbf{S}_4$ and $\mathbf{S}_5$ is easy to understand as these two spins are directly coupled via J_3. On the other hand, the singlet between $\mathbf{S}_1$ and $\mathbf{S}_4$ is mediated via an antiferromagnetic exchange J_1 and a ferromagnetic exchange J_2. The perfect singlet character for either pairs is disturbed when all the interaction strengths are finite. Instead, a compromise state with AFM correlations between both $\mathbf{S}_1$-$\mathbf{S}_4$ and $\mathbf{S}_4$-$\mathbf{S}_5$ pairs is preferred. It is important to note that this subtle competition is not captured in calculations that limit the cluster size to 4-sites (single tetramer), as in that case C_{45} cannot be distinguished from C_{14}. The correlation C_{18} originates from the inter-cluster couplings where $\mathbf{S}_1$ and $\mathbf{S}_8$ belonging to the central cluster are coupled to mean-fields of $\mathbf{S}_8$ and $\mathbf{S}_1$, respectively. As expected, we find that this mean-field treatment restricts the correlation strengths to classical value of -0.25 (see Fig. 3.2(b)). The behavior of correlations between different spin pairs in the cluster points to the following three distinct ground states: (i) The simplest limit corresponds to $J_3 \to 0$ and $J_2 \to 0$ where the system is a collection of $\mathbf{S}_2$-$\mathbf{S}_3$ singlets and isolated spins $\mathbf{S}_1$ and $\mathbf{S}_4$. (ii) If J_3 dominates over J_2, then the system can be considered close to a valance bond solid limit where two different type of singlets, one due to J_1 coupling and other due to J_3 coupling, are formed (see schematic picture

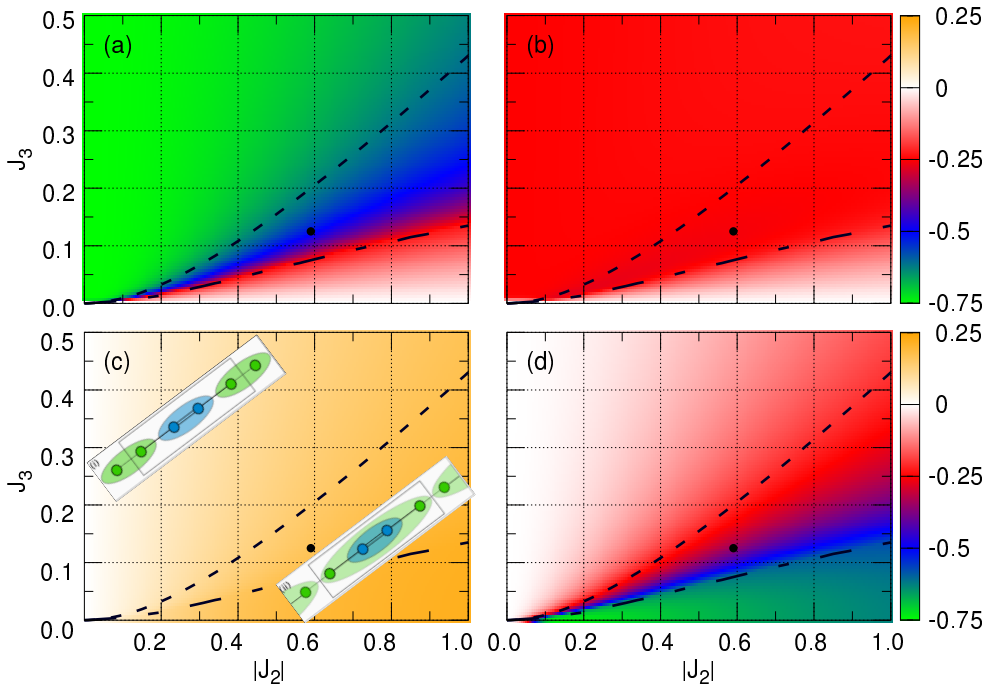

Figure 3.2: Variation of different spin-spin correlations with $|J_2|/J_1$ and J_3/J_1 for $h_z = 0$: (a) C_{45}, (b) C_{18}, (c) C_{12} and (d) C_{14}. C_{ij} are computed within CMF approach using 8-site cluster. The dot indicates the location of the magnetic model for $CuInVO_5$ in the $|J_2|$-J_3 plane. The dashed line is an estimate for the path in parameter space where two different tendencies for singlet formation strongly compete (see text). In panel (c) we show the schematic picture of two limiting states. The long-dashed line marks the separation between Néel-type long-range ordered state and the state consisting of non-interacting tetramers.

near top-left corner in Fig. 3.2(c)). Of course, the exact singlet correlations are spoiled by the presence of the ferromagnetic J_2 coupling and also by the CMF treatment. As a consequence, an $\uparrow\uparrow\downarrow\downarrow$ type antiferromagnetic ordering with reduced magnetic moments emerges. Finally, (iii) in the case of $|J_2|$ dominating over J_3, the C_{14} correlation achieve values close to that of perfect singlet, *i.e.*, -0.75, while C_{45} is almost uncorrelated (compare Figs. 3.2(a),(d), and see schematic picture near bottom-right corner in Fig. 3.2(c)). By plotting the change in the self-consistent mean fields $\langle S_1^z \rangle$ and $\langle S_8^z \rangle$ as a function of $|J_2|$ for fixed values of J_3 (see Appendix 3.5.2), we identify this limit in terms of the inequality $|J_2| > 8J_3$, marked as long-dashed line in Fig. 3.2. The ground state in the region $|J_2| > 8J_3$ corresponds to that of an isolated 4-site cluster. The magnetic phase diagram as inferred from the C_{ij}, therefore, consists of three qualitatively distinct regimes discussed above which are connected to each other continuously.

It is instructive to quantify the competition between different limiting cases. Fig. 3.2(a), (d) suggest that the key competition is between the singlet correlations C_{14} and

C_{45}. Solving the isolated 8-site cluster with open boundary conditions, we find that the ground state energy is given by,

$$E_1 = -\frac{1}{4}(J_1 + 2J_2 + 2\sqrt{J_1^2 - 2J_1J_2 + 4J_2^2}). \tag{3.4}$$

On the other hand, the state in the limit $J_2 = 0$ is a collection of alternating singlets having energy per tetramer,

$$E_2 = -\frac{3}{4}(J_1 + J_3). \tag{3.5}$$

Therefore, the competition between these two tendencies is strongest when the two energy contributions are equal. This gives us a relation between J_2 and J_3 which is obtained by numerically solving equations (3.4) and (3.5). The result is plotted as a dashed line in Fig. 3.2(a) and 3.2(d). Exchange parameters obtained by fitting susceptibility and magnetization data for $CuInVO_5$ are $J_1 = 240K$, $J_2 = -142K$ and $J_3 = 30K$ [126]. The dot in Fig. 3.2 represents the location of the magnetic model for $CuInVO_5$ in the parameter space of the model Eq. (3.1). We note that $CuInVO_5$ is not far from this strongly competing regime, therefore, treating the C_{45} correlations exactly is very important to capture the important aspects of magnetism in $CuInVO_5$.

Next, we took at the dependence of spin-spin correlations on external magnetic field. In this case we discuss both the longitudinal and the transverse components of the correlations. For this purpose we fix the value of the inter-tetramer exchange $J_3 = 0.125$ and explore the phases in $h_z - J_2$ plane. The specific choice of the J_3 value is relevant to $CuInVO_5$ where J_1 and J_3 are estimated to be 240K and 30K, respectively [126]. For small values of J_2, the longitudinal and transverse components of C_{23} are close to -0.25 and -0.50, respectively. These singlet-like correlations for C_{23} remain unaffected by the external magnetic field in the regime $|J_2| < 1$. Interesting conclusions can be drawn by comparing the field dependence of component resolved C_{18} and C_{45}. For small J_2, C_{18} starts off with AFM correlations in the z-component and no correlations in the transverse direction, *i.e.*, $C_{18}^{zz} = -0.25$ and $C_{18}^{\perp} = 0$ (See Figs. 3.3(c) and 3.4(c)). A sharp change in these correlations is found near $h_z = 0.01$ where the longitudinal component becomes close to zero and transverse component rises to -0.25. This is a clear signature of the spin-flop state involving a flopping of $\mathbf{S}_1$ and $\mathbf{S}_8$. The longitudinal component then gradually increases to positive values at the cost of reduction in transverse correlations in accordance with the standard picture of a spin-flop state evolving towards a canted state. Following the change in components of C_{45} (say, at $J_2 = -0.58$ which is relevant for $CuInVO_5$) upon varying magnetic field highlights a similar effect for $\mathbf{S}_4$-$\mathbf{S}_5$

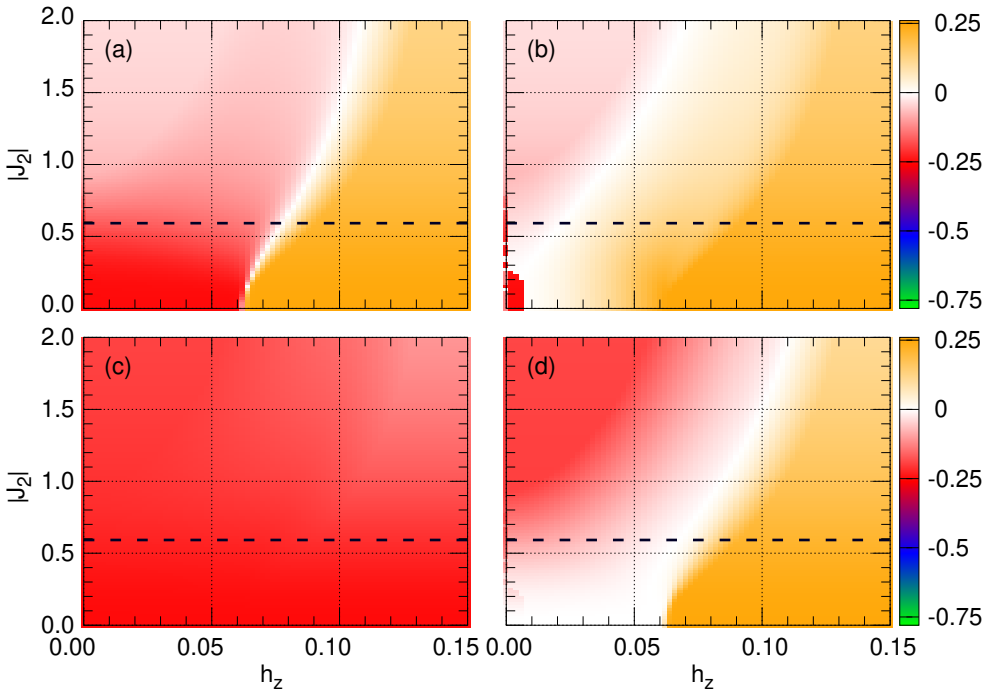

Figure 3.3: Variation of longitudinal component of spin-spin correlations with $|J_2|/J_1$ and h_z/J_1 for $J_3/J_1 = 0.125$: (a) C^{zz}_{45}, (b) C^{zz}_{18}, (c) C^{zz}_{23} and (d) C^{zz}_{14}. Dashed horizontal lines correspond to the $|J_2|/J_1$ ratio estimated for $CuInVO_5$.

pair. The transverse correlations reduce sharply near $h_z = 0.08$, and the longitudinal correlations vanish and then rapidly rise to positive values. Thus a clear picture emerges for the presence of two spin-flop transitions in this spin-1/2 tetramer model – the first one corresponding to a flopping of edge spins and the second one to that of the central pair of spins. For still larger values of h_z, another spin-flop corresponding to $\mathbf{S}_2$-$\mathbf{S}_3$ pair is present. Note that the anti-correlation between C_{14} and C_{45} is also present for finite magnetic fields (see panels (a) and (d) in Fig. 3.3 and Fig. 3.4). Having discussed the broad picture for different spin-spin correlations and their component resolved evolution with magnetic field, we now focus on the parameter values considered relevant for $CuInVO_5$. We begin by discussing results for a 4-site cluster.

3.3.2 Single-tetramer cluster

In this section, we will discuss results obtained via the CMF approach using a 4-site cluster. We begin by comparing the temperature dependence of spin-spin correlations obtained for an isolated tetramer and those via CMF with a 4-site cluster. In the case of isolated tetramer, cluster is treated exactly with open boundary conditions where as in

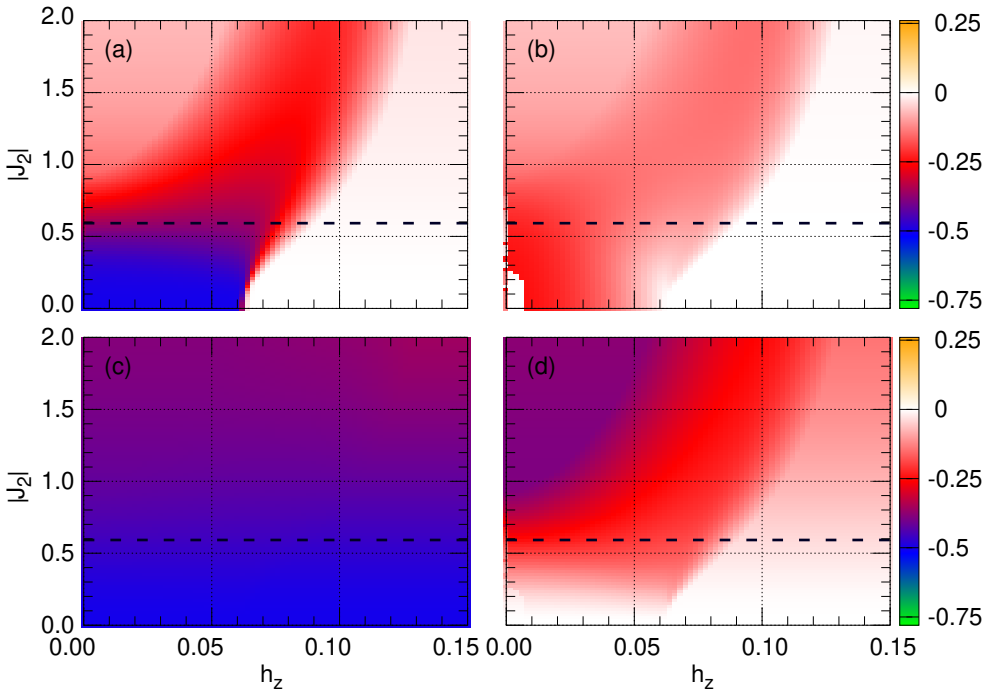

Figure 3.4: Variation of transverse component of spin-spin correlations with $|J_2|/J_1$ and h_z/J_1 for $J_3/J_1 = 0.125$: (a) $C^{\perp}_{45}$, (b) $C^{\perp}_{18}$, (c) $C^{\perp}_{23}$ and (d) $C^{\perp}_{14}$. Dashed horizontal lines correspond to the $|J_2|/J_1$ ratio estimated for $CuInVO_5$.

case of CMF, edge spins $\mathbf{S_1}$ and $\mathbf{S_4}$ couple to average fields $\langle \mathbf{S_4} \rangle$, $\langle \mathbf{S_1} \rangle$ respectively, via J_3. Difference in the two sets of correlation functions vanish above $\sim$ 8K. This indicates that the self-consistent mean-fields vanish above 8K and the long-range order, which can be captured via CMF approach, is present below 8K. Indeed, the main advantage of using a mean-field approach is to obtain results in thermodynamic limit. However, we point out a crucial shortcoming of the CMF approach applied to this system. The correlation C_{14} for the two edge spins of a tetramer are treated better in an isolated tetramer. These correlation have a value, $C_{14} \approx -0.68$, close to that of a perfect singlet. In the mean-field approach the edge-spins are coupled to average fields due to finite $\langle \mathbf{S}_1 \rangle$ and $\langle \mathbf{S}_4 \rangle$, and therefore the correlations are strongly reduced. This can be observed for all the correlations involving the edge spins (see Fig. 3.5). The correlation of the central spin-pair C_{23} is identical in the two calculations, as expected. In addition to computing spin-spin correlation functions defined in Eq. (3.3), we also compute quantities that can be compared directly with the experiments. To this end, we compute the specific heat and the magnetic susceptibility using the standard definitions,

$$C_V(T) = \frac{d\langle H \rangle}{dT}, \qquad \chi(T) = \frac{d\langle M_z \rangle}{dh}. \tag{3.6}$$

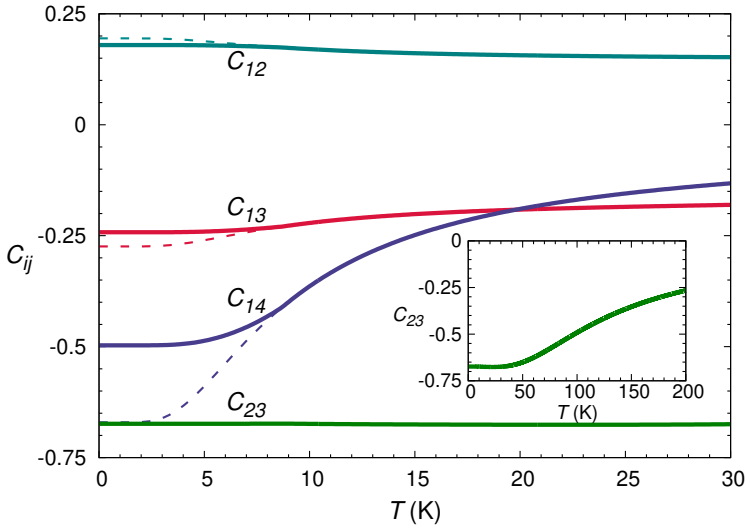

Figure 3.5: Spin-spin correlations C_{ij} as a function of temperature for an isolated tetramer (dashed lines) and within CMF approach using a 4-site cluster (solid lines). Variation of C_{23} over larger T scale is shown in the inset.

We now present the comparison of specific heat calculations for isolated cluster and for the 4-site CMF approximation. For an isolated cluster the ground state belongs to the $S_T = 0$ sector and is characterized by singlet correlations between spin pairs $\mathbf{S}_1$-$\mathbf{S}_4$ and $\mathbf{S}_2$-$\mathbf{S}_3$. This is indeed reflected in Fig. 3.5 where the pair correlations C_{23} and C_{14} are found to be close to perfect singlet type. Treating the inter-tetramer interactions at the mean-field level spoils the singlet correlation C_{14} as the edge spins now experience classical mean fields. The specific heat for an isolated cluster shows two broad peaks which can be naively associated with the loss of correlations C_{14} at around 10K, and the breaking of the stronger singlet between the central Cu spins at around 100K. The CMF results lead to a sharp peak in C_V, signifying the on-set of long-range order below $\sim$ 8K. In order to confirm the simple picture proposed from the spin-spin correlation and the specific heat calculations, we now show the magnetic susceptibility results. If the simple picture of two-step loss of correlations is indeed true then it should have specific consequences for the behavior of magnetic susceptibility. To verify this, we plot the inverse magnetic susceptibility obtained for an isolated cluster in Fig. 3.7. Given the tendency for singlet formation at low temperatures, we fit the magnetic susceptibility differently in three temperature regimes. In the range 0K $< T <$ 40K, we fit the susceptibility via the following behavior for singlets [134] (see Appendix 3.5.3),

$$\chi(T) = \frac{a_1}{T} \frac{e^{(-b_1/T)}}{1 + 3e^{(-b_1/T)}}. \tag{3.7}$$

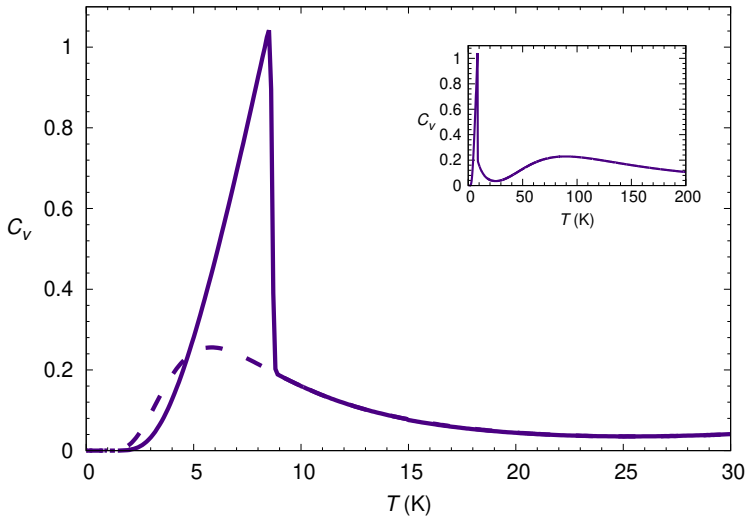

Figure 3.6: Specific heat as a function of temperature for isolated tetramer (dashed line) and for CMF approximation with 4-site cluster (solid line). The inset shows the behavior over wider temperature scale for the CMF approximation.

In the above, the fitting parameter a_1 contains information about number of singlets, and b_1 is related to the excitation gap. In the regime 40K $< T <$ 300K, the system should display a mixed behavior since the weaker singlets cease to exit and the participating spins will now contribute as free paramagnetic moments. Therefore, we fit the susceptibility via,

$$\chi(T) = \frac{a_2}{T}\frac{e^{(-b_2/T)}}{1+3e^{(-b_2/T)}} + \frac{c_2}{T-d_2}. \tag{3.8}$$

The second term is simply Curie-Weiss behavior and the two fitting parameters contain information regarding the total number of paramagnetic moments and the Curie-Weiss temperature. In the high-temperature regime, one expects a total Curie-Weiss behavior for all the constituent spins. Therefore, a Curie-Weiss fit, $\chi(T) = \frac{c_3}{T-d_3}$, is used in the range 300K $< T <$ 600K. The actual $\chi^{-1}(T)$ and the three fits discussed above are shown in Fig. 3.7. From the quality of the fit the following simple picture is reconfirmed. At low temperature, the magnetic susceptibility fits very well to a singlet behavior. At intermediate temperatures, two of the spins get free and contribute to Curie-Weiss susceptibility. Finally a paramagnetic behavior emerges at high temperatures. The obtained fit parameters differ slightly from the above picture in terms of number of spins contributing to susceptibility as singlets or paramagnetic moments at different temperatures (see Appendix 3.5.3). We find that while the tendency for singlet formation below 100K between $\mathbf{S}_2$ and $\mathbf{S}_3$ and the long-range order to a Néel state with $\uparrow\uparrow\downarrow\downarrow$ pattern below about 10K is obtained within the 4-site CMF approach, the experimental observation of a second peak in the specific heat at about 2.7K is not consistent with the CMF results.

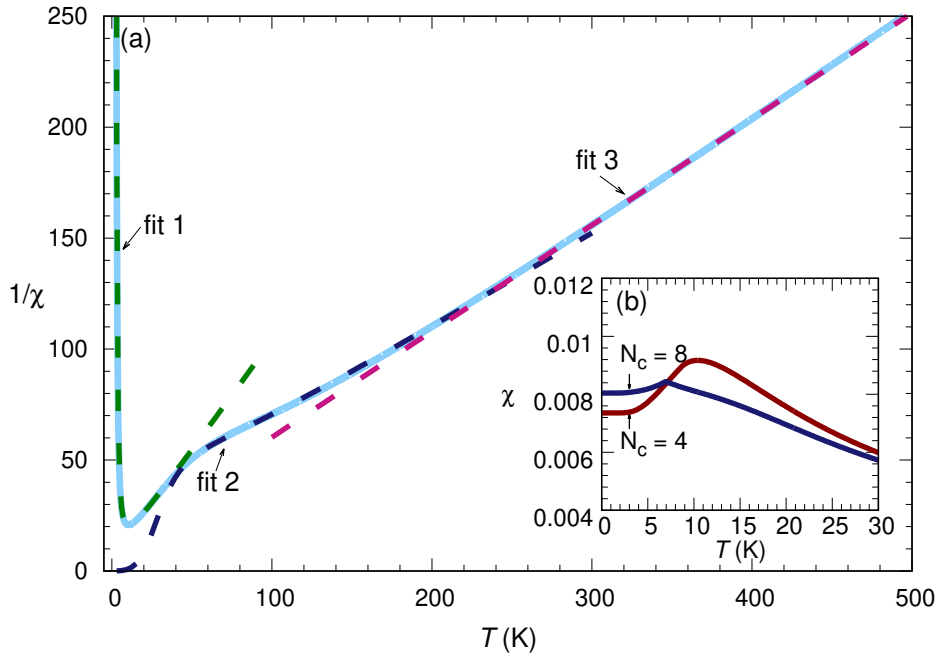

Figure 3.7: Inverse magnetic susceptibility, χ^{-1}, as a function of temperature for an isolated tetramer. The dashed lines are the best fits corresponding to three different temperature regimes (see text). Inset shows the result for $\chi(T)$ within CMF approximation using 4-site and 8-site clusters.

We argue that treating inter-tetramer interactions beyond mean-field is the key to understanding the magnetism of $CuInVO_5$. We discuss the 8-site CMF results in the next section. Nevertheless, we already find that 8-site CMF results for magnetic susceptibility are qualitatively different from those obtained for 4-site CMF (see inset in Fig. 3.7). A cusp-like feature followed by a broad hump is reported in the experiments which seems to be captured within 8-site CMF calculations. Clearly, if the interaction J_3 happens to be stronger than the ferromagnetic interaction J_2 then the system would prefer to form singlets between $\mathbf{S}_2$ and $\mathbf{S}_3$ and $\mathbf{S}_4$ and $\mathbf{S}_5$ instead of a pair of singlets within a tetramer. In fact, even if J_3 is much smaller than J_2, since J_3 is antiferromagnetic in nature it may be important to retain the correlations in the inter-tetramer interaction. The simplest way to achieve this is to increase the cluster size to 8-spins (two-tetramers) where one central inter-tetramer exchange term will be treated exactly. Next, we present results on CMF using two- and three-tetramer units as the cluster.

3.3.3 Beyond single-tetramer cluster

We begin by presenting the spin-spin correlation functions for different pairs as a function of temperature. Note that the most important correlation that was missing in the 4-site cluster treatment is C_{45}. Exact solution of the isolated 8-site cluster shows that at $T = 0$, C_{14} is antiferromagnetic in nature and larger in magnitude than C_{45}. With increasing temperature $|C_{14}|$ reduces rapidly (see Fig. 3.8). Interestingly, this decrease of $|C_{14}|$ is accompanied by an increase of $|C_{45}|$. Note that it is rather unusual to find an increase in the magnitude of correlations as a function of temperature. This hints towards competing tendencies for order in the ground state. We can comprehend this finding as follows. Spin $\mathbf{S}_4$ can have singlet type correlations with $\mathbf{S}_5$ due to the antiferromagnetic exchange constant J_3. However, it can also have quantum antiferromagnetic correlations with spin $\mathbf{S}_1$ due to combined effect of an antiferromagnetic J_1 and ferromagnetic J_2. These two tendencies for singlet correlations are competing in the ground state, and for the material-specific values of the exchange parameters a dominant antiferromagnetic correlations with spin $\mathbf{S}_1$ is energetically favoured With increasing temperature, a weakening of longer-range correlations (C_{14}) allows for strengthening of C_{45}. This intriguing interplay of two competing tendencies for singlet formation is apparent in our discussion of the model for generic parameter values (compare Fig. 3.2(a) and Fig. 3.2(d)). Interestingly, this competition between different singlet choices is also at play when temperature varies, and has consequences for physical observables. The fact that different spin-spin correlations are being affected at different temperatures should be reflected in specific heat results. To verify this we plot in Fig. 3.9 the specific heat calculated within the CMF approach using 4, 8, 12 and 16 site clusters. In contrast to the results for 4 site cluster, two peaks at low temperatures are found in the 8, 12 and 16 site CMF calculations.

The results suggest that the most important improvement to the 4-site CMF results already occurs when we use 8 site cluster and hence treat inter-tetramer interaction exactly. The relative strength and position of the two low-temperature peaks in C_V change as we increase the cluster size (see Fig. 3.10). The first peak which is related to the long-range order reduces with increasing system size. Although, the scaling based on 3 data points is not conclusive, the estimates for the peak locations T_p obtained from the extrapolated data are in very good agreement with the experiments with an overestimations of about 1.5K.

More importantly, it is ruled out that any new peaks in the specific heat arise with adding more tetramers to the cluster used in the CMF approach. Note that the experimental plot for C_V also contains contribution from phonons which needs to be subtracted

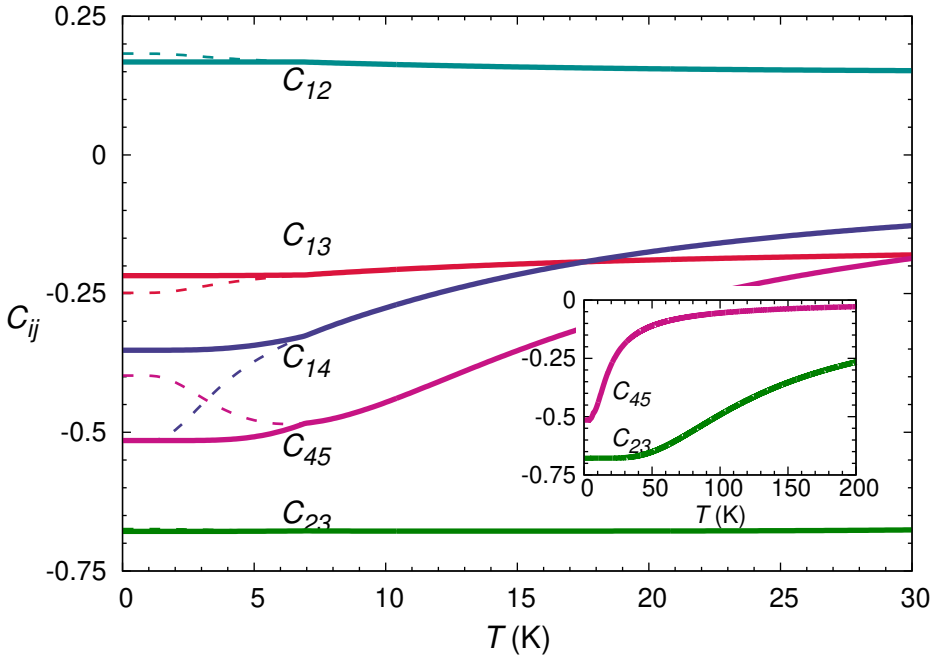

Figure 3.8: Spin-spin correlations, C_{ij}, as a function of temperature for an isolated 8-site cluster (dashed lines) and within the CMF approach using an 8-site cluster (solid lines). Variations in C_{23} and C_{45} over a wider T range is shown in the inset.

in order to identify the pure magnetic contribution. While the phonon contribution will mask the high temperature peak around 90K (see inset in Fig. 3.9), the two lower temperature peaks are easily identified in the experimental data [126]. The magnetic field dependence of the spin-spin correlations is already discussed in Figs. 3.3 and 3.4 for generic choice of model parameters. In order to obtain the results specific to $CuInVO_5$ we simply need to find the appropriate values of model parameters. These results were obtained for $J_3/J_1 = 0.125$, a ratio motivated from the estimated values of J_1 and J_3 in $CuInVO_5$. In the material, $|J_2|/J_1$ is estimated to be 0.58 and we can focus on the $|J_2| = 0.58$ line to discuss the field dependence of correlations in $CuInVO_5$. A partial spin-flop is present at low magnetic fields which leads to a magnetization plateau at $h_z = 0.08J_1$ which turns out to be around 30T when appropriate conversion factors are included. This coincides very well with the presence of the plateau in the field dependence of magnetization (see Fig. 5 in [126]). If the simple picture of partial spin-flop transition is valid, then we should see further increase in magnetization at yet higher magnetic fields. Indeed, we obtain saturation magnetization at about 145T (see supplemental material).

Combining the results on temperature and magnetic field dependence of mean-field parameters and spin-spin correlations, we present a $h_z - T$ phase diagram in Fig. 3.11. The dot product of mean fields $\langle \mathbf{S}_1 \rangle \cdot \langle \mathbf{S}_8 \rangle$ is a measure of the long-range order in the

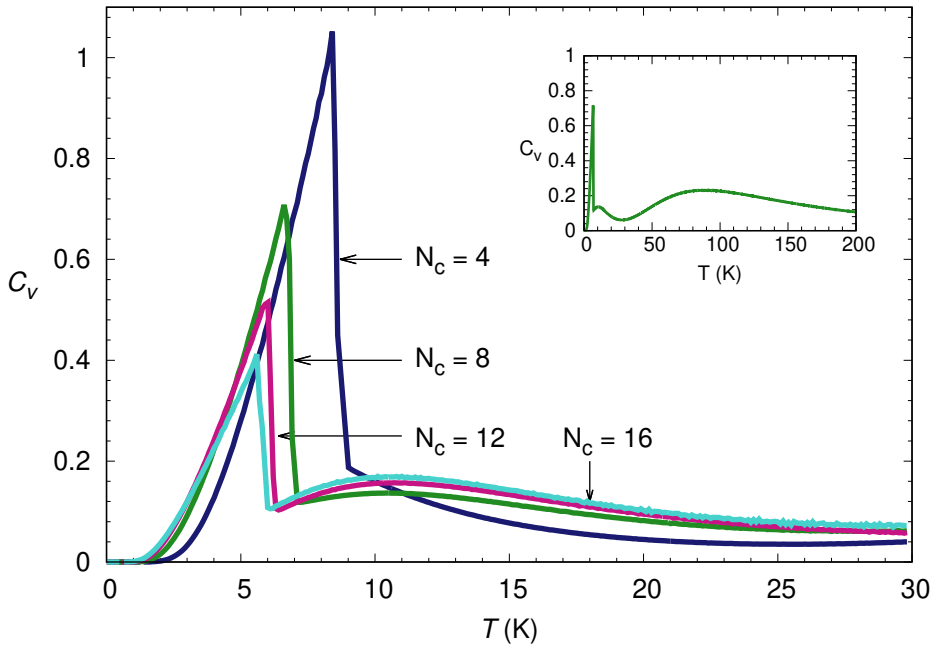

Figure 3.9: Specific heat as a function of temperature within the CMF approximation for 4-site, 8-site, 12-site and 16-site clusters. The behavior across a broader temperature scale is displayed in the inset.

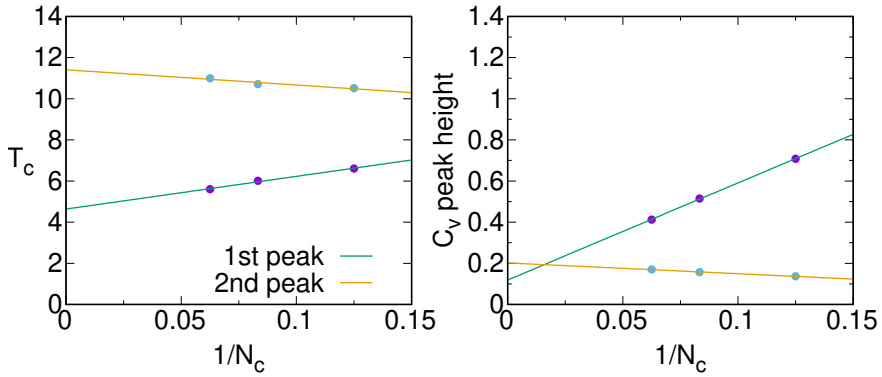

Figure 3.10: Scaling of peak locations, T_p, and peak values, $C_V(T_p)$, in the specific heat shown in Fig. 3.9 with inverse cluster size.

.

system. As we can clearly see in Fig. 3.11(b), for small values of field there is a transition close to 5K from a long-range ordered to disordered state. However, even in the disordered state there are certain short-range correlations that remain finite. The most important of these is C_{45} which is shown in Fig. 3.10(a). These correlations remain finite upto larger temperatures and show a significant variation near $T = 10$K. This variation is the underlying reason for a broad peak in the specific heat near 10K. The evolution of mean-field variables with magnetic field shows that the edge spins gradually approach an aligned

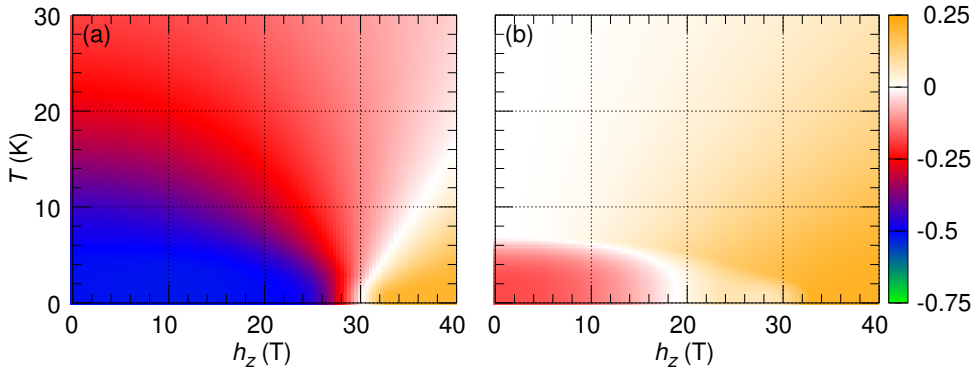

Figure 3.11: Temperature and field dependence of, (a) spin-spin correlations C_{45} and (b) product of mean-field variables, $\langle \mathbf{S}_1 \rangle \cdot \langle \mathbf{S}_8 \rangle$, for the parameter values specific to $CuInVO_5$. Temperature (magnetic field) axis is in the physical unit Kelvin (Tesla). Note that the quantity plotted in (b) is finite for a long-range ordered magnetic state.

state starting with an anti-aligned state. The saturation alignment is achieved at about 30T. Note that while the edge spins are aligned, the central spins still retain considerable singlet correlations and therefore the contribution to magnetization is from these edge spins leading to the magnetization plateau in the experimental data [126]. It is possible to further improve the mean-field description of the model by using different extensions of CMF approach. Two such extensions are correlated CMFT and quantum correlated CMFT [135, 136, 137]. However, the most important aspect of the magnetic model for $CuInVO_5$ is already captured by our minimal description where the inter-tetramer interaction is included in exact manner. While some of the quantitative details, such as the relative magnitude of the low-temperature peaks, the exact location in temperature of the peaks, etc., are likely to change in a more accurate treatment of the model, the qualitative character is well described in our CMF approach.

3.4 Summary and Conclusion

We have performed cluster mean field analysis of a one-dimensional Heisenberg model with alternating signs of exchange constants. The choice of the model is motivated by the unusual low-temperature magnetism in $CuInVO_5$ [126]. We map out the nature of spin-spin correlations as a function of different model parameters. The results are obtained via CMF approach with an 8-site cluster which, in contrast to the 4-site cluster study [126], captures the effect of the inter-tetramer coupling beyond mean-field. It turns out to be an essential ingredient for understanding some of the experimental observations, in

particular, multiple peaks in the low-temperature specific heat. Due to a better treatment of quantum correlations of the inter-tetramer coupling, an interesting competition between two qualitatively different ground states is uncovered. These ground states are best understood in the limiting cases $J_3 \to 0$, and $J_2 \to 0$. In the limit $J_3 \to 0$ the system is a collection of isolated tetramers and the ground state for an isolated tetramer is characterized in terms of quantum antiferromagnetic correlations between spins $\mathbf{S}_2$ and $\mathbf{S}_3$ and those between $\mathbf{S}_1$ and $\mathbf{S}_4$. The latter of these relies on the ferromagnetic exchange J_2 as a mediator. On the other hand, in the limit $J_2 \to 0$ the ground state becomes a collection of alternating singlets, one mediated by exchange J_1 and other by J_3. However, this state is only accessible when quantum correlations of the inter-tetramer interactions are retained. When J_2 and J_3 are both finite, a competition between these qualitatively distinct states is realized. Our study shows that the ground state of the $CuInVO_5$ emerges out of this competition. The above description of the low-temperature magnetism in $CuInVO_5$ is inferred from our analysis of the model for material-specific values of the parameters. We show that an interesting evolution of the competition between different spin-spin correlations exists not only with variation of model parameters but also with increasing temperature. Correlations for certain pair of spins even increase with increasing temperature which is contrary to the general expectations that thermal effects reduce the correlations. Magnetic susceptibility calculations further allow us to identify three distinct regimes in temperature corresponding to a complete paramagnetic behavior at high temperature, a singlet-like behavior at low-temperatures, and a mixed behavior at intermediate temperatures. At intermediate temperatures some of the spins get free from singlets while other retain strong singlet correlations. This is consistent with the experimental finding of the magnetization plateau at nearly half the saturation magnetization. By tracking transverse and longitudinal spin-spin correlations, we observe a two-step spin-flop transition in the model. The most important implication of this competition of correlations captured in our CMF study is the existence of multiple peaks in the specific heat – a puzzling feature reported in the experimental data on $CuInVO_5$ [126].

3.5 Appendix

3.5.1 Spin-spin correlations

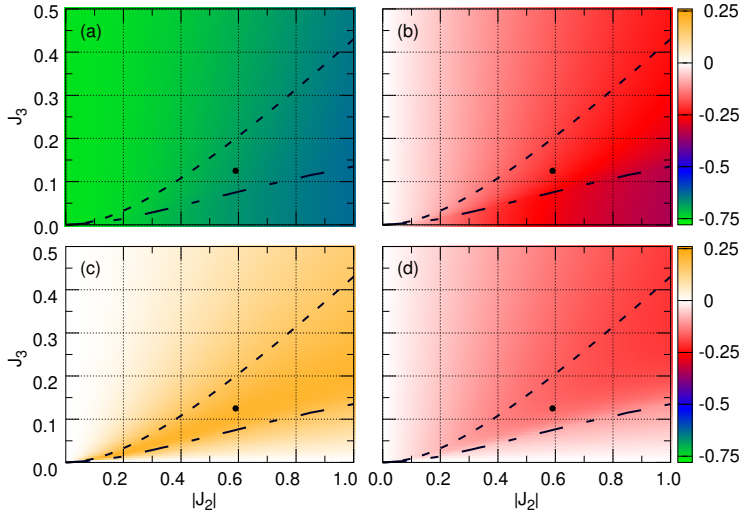

Figure 3.12: Variation of different spin pair correlations (C_{ij}) with $|J_2|/J_1$ and J_3/J_1 for $h_z = 0$ computed within CMF for 8-site cluster: (a) C_{23}, (b) C_{13}, (c) C_{15} and (d) C_{35}. The dashed and long-dashed lines are identical to those shown in Fig. 3.2. The dot represents the location on $CuInVO_5$ in the parameter space.

In continuation of the discussion in Section 3.3.1 about three different limiting states in $J_2 - J_3$ parameter space, we present other relevant spin pair correlations in Fig. S1. J_1 being the strongest exchange parameter, S_2-S_3 pair retains its strong-singlet character throughout the parameter space (see Fig. 3.12 (a)). However, as expected, the correlation begins to weaken as $|J_2|/J_1$ approaches 1. Correlation between S_1 and S_3 increases with increasing $|J_2|$ (see Fig. 3.12 (b)), which is also related to the weakening of $S_2 - S_3$ singlet. This is where J_2 starts competing with J_1. Ordering of spins is largely controlled by C_{45} correlation (see Fig. 3.2), its affect can also be seen in C_{15} and C_{35} (see Fig. 3.12 (c)-(d)). Correlation between S_1 and S_5 cease to exist in $J_3 \Rightarrow 0$ and $J_2 \Rightarrow 0$, however it changes continuously in the intervening region. This correlation is mediated via J_3, as singlet strength begins to increase C_{35} decreases. A strong crossover is observed around $J_3 \sim 0.2|J_2|$ for C_{35}, this is the region when C_{45} varies from classical anti-parallel correlation to quantum mechanical singlet-like bond characterized by values less than -0.25. We also show the evolution of correlation functions and self-consistent mean field m_1^z in the limit $|J_2| >> J_3$ in Fig. 3.13. The mean field vanishes beyond $|J_2| \sim 0.8$, where the 8-site cluster behaves like two weakly coupled tetramers (see C_{45} in Fig. 3.13).

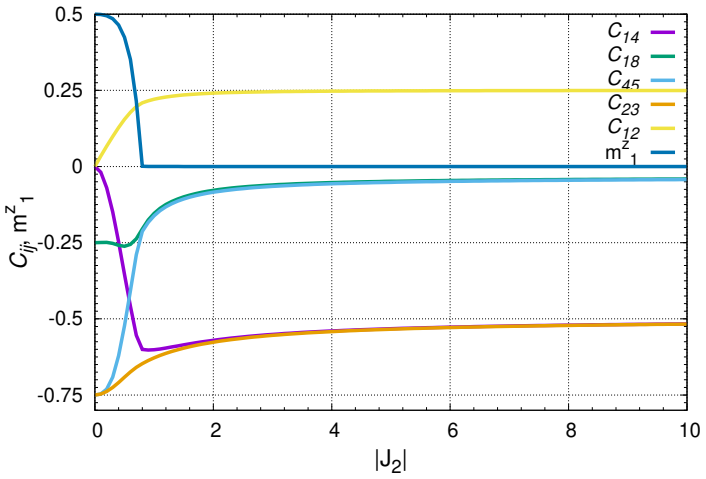

Figure 3.13: Variation of spin-spin correlations and mean fields m_1^z as a function of $|J_2|$ for $J_3 = 0.1$.

For $|J_2| < 0.8$, $\mathbf{S_4}$ continuously forms strong antiferromagnetic correlation with $\mathbf{S_1}$ at the cost of the singlet bond with $\mathbf{S_5}$. Similar calculations for other values of J_3 show that one can define $|J_2| = 8J_3$ as the line separating the Neel-type long-range ordered states from that consisting of weakly coupled tetramers schematically shown in Fig. 3.2

3.5.2 Response to magnetic field

Multiple spin flops are inferred from $h_z - J_2$ phase diagram of 8-site cluster, as discussed Figs. . For the material specific value of J_2, we observe a spin flop at around $h_z \sim 0.08$ and a final re-orientation of spins at higher fields. Figs. S3(a), S3(b) show a component resolved magnetic moment variation with applied field. For CMF results using a single tetramer cluster, we find a two step saturation of magnetic moments. A spin flop transition to a direction perpendicular to applied field is observed, which is followed by the first magnetization ($M = g\mu_B\langle S\rangle$) plateau around $\sim 30T$ (follow the black dashed lines Fig. S3). The first plateau is related to the loss of C_{14} correlation whereas the full saturation of magnetic moments takes place when the singlet between $\mathbf{S_2}$ and $\mathbf{S_3}$ breaks, which is clearly visible in the correlation plot. Two-step saturation of magnetization is also consistent in 8-site (two tetramer) cluster calculations. However, the details of the field dependence are slightly different. In Fig. S3(b), average moments show a non-linear increase below the first magnetization plateau. This is different from single tetramer results where average magnetic moment in the direction of field shows a linear increase. The non-linear increase in directly related to the loss of C_{14} and C_{18} correla-

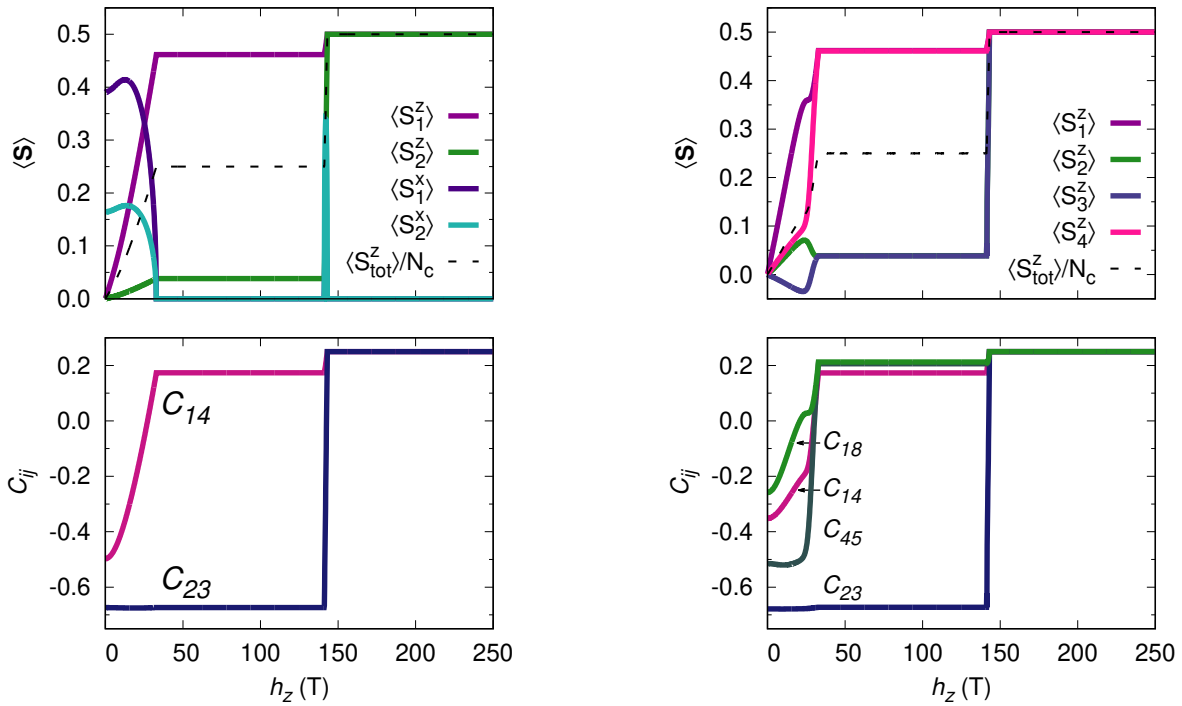

(a) (b)

Figure 3.14: Average spin magnetic moment (upper panels) as a function of applied magnetic field and corresponding behaviour of correlations (lower panels) computed using CMF at $T = 0.01$K for (a) single tetramer and (b) two-tetramer cluster.

tions. The experimentally observed behavior is indeed non-linear and is consistent with the results obtained using two-tetramer CMF. This further highlights the importance of treating the inter-tetramer coupling beyond mean-field for an improved description of the experimental data.

3.5.3 Fitting details of susceptibility for single-cluster

Susceptibility of a dimer spin system is give by [134],

$$\chi_D(T) = \frac{N_D g^2 \mu_B^2}{k_B T} \frac{e^{-J/K_B T}}{1 + 3e^{-J/k_B T}}. \tag{3.9}$$

Susceptibility for antiferromagnetically or ferromagnetically correlated spins is given by the standard Curie-Weiss formula:

$$\chi_{CW}(T) = \frac{N_{CW} g^2 \mu_B^2 S(S+1)}{3k_B} \frac{1}{T - T_{CW}}. \tag{3.10}$$

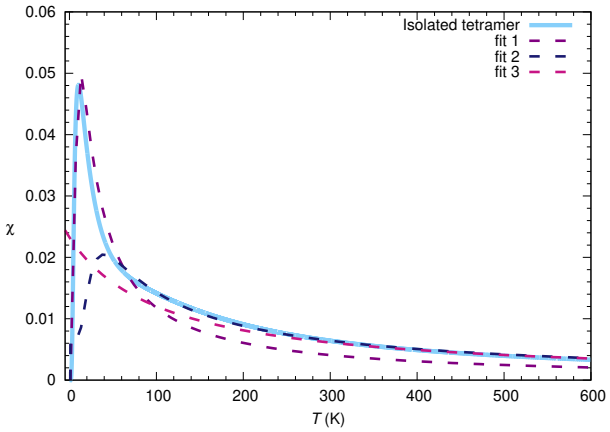

Figure 3.15: Magnetic susceptibility for a isolated tetramer. The dashed lines are best fits when number of spins are fixed in different regimes.

In the above, N_D is the number of spins forming singlets and N_{CW} is the number of spins, g is Lande g factor , k_B is Boltzmann constant, μ_B is Bohr magneton and J is singlet-triplet energy gap.

Susceptibility of an isolated tetramer is fitted using a combination of above two susceptibilities in different temperature regimes (see Table 1). Fitting parameters being $a_i = \frac{N_D g^2 \mu_B^2}{k_B}$, $b_i = \frac{J}{k_B}$, $c_i = \frac{N_{CW} g^2 \mu_B^2 S(S+1)}{3k_B}$ and $d_i = T_{CW}$. For temperature region 1 ($0K < T < 40K$), where the spins are expected to form a singlet. Fitting parameters reveal $N_D \sim 1.61$ and $\frac{J}{k_B} \sim 16.79$. It is interesting to note that even though the system contains 4 spins the fit suggests the presence of a single dimer. This is because edge spins are strongly ferromagnetically coupled to the central spins that form a singlet, and hence the tetramer effectively behaves like a singlet. Energy gap J/k_B found from the fit also matches very well with first energy gap obtained from exact diagonalization. Fig. S4 (fit 1) highlights that the nature of system qualitatively remains same even if we set $N_D = 2$ for temperature range $0K < T < 40K$.
A combination of dimer and Curie-Weiss susceptibility was used in region 2 ($40K < T < 300K$), with an expectation that the ferromagnetic coupling reduces, leaving a pure $\mathbf{S_2} - \mathbf{S_3}$ singlet and two free spins. Number of free spins and spins involved in a dimer obtained from the fit confirms this picture. In Fig. S4, we illustrate that the fit is also reasonably good if we use $N_D = 2$ and $N_{CW} = 2$. For the higher temperature region $300K < T < 600K$ fit to Curie -Weiss susceptibility affirms the presence of free spins. Note the number of spins don't perfectly match due to the presence of finite but small coupling between all the spins, description in terms of these regions is only a simplified picture. Once again, if we use the simplified picture that all 4 spins in a tetramer contribute to Curie-Weiss behavior, the quality of the fit does not detriate much. Therefore,

	Fit Formula	Fitting parameters	Inferences
fit 1 T=[0:40]	$\chi(T) = \frac{a_1}{T}\frac{e^{-b_1/T}}{1+3e^{-b_1/T}}$	$a_1 = 4.02$ $b_1 = 16.79$	$N_D = 1.61$ $J/k_B = 16.79$
fit 2 T=[40:300]	$\chi(T) = \frac{a_2}{T}\frac{e^{-b_2/T}}{1+3e^{-b_2/T}} + \frac{c_2}{T-d_2}$	$a_2 = 5.24$ $b_2 = 188.60$ $c_2 = 0.86$ $d_2 = 0.32$	$N_D = 2.1$ $J/k_B = 188.60$ $N_{CW} = 1.38$ $T_{CW} = 0.32$
fit 3 T=[300:600]	$\chi(T) = \frac{c_3}{T-d_3}$	$c_3 = 2.06$ $d_3 = -21.19$	$N_{CW} = 3.31$ $T_{CW} = -21.19$

Table 3.1: Fitting parameters of susceptibility for isolated tetramer.

although in the main text we discuss an accurate fitting of the susceptibility data to a mixed dimer and Curie-Weiss behavior and identify three distinct regimes in temperature, here we show that even fixing N_D and N_{CW} to the naively expected values leads to good fits.

3.5.4 Details of calculations for $N_c = 16$

The size of the Hilbert space for cluster Hamiltonian of a 16 spin cluster (four tetramers) is $2^N \sim 65000$. A brute force diagonalization of such large matrix multiple times to reach self consistency requires enormous computational time. Moreover, it turns out that if we allow for an unrestricted self-consistency approach wherein the mean-field vectors can point in any direction then the cluster Hamiltonian lacks many of the symmetries that are present in the full interacting Hamiltonian. For example, the bulk spins are not equivalent to edge spins and hence the translation symmetry is lost. The mean fields are not restricted to point along z axis, leading to coupling terms of the form $S_1^+ B_{N_c}^- + S_1^- B_{N_c}^+$ where B_{N_c} contain x and y components of mean fields. The presence of these terms spoil conservation of total S^z. Therefore, the conservation of z-component of total spin does not hold in the general case. For $h_z = 0$, to apply conservation of total spin (S_{tot}^z) we restrict mean fields to be in z direction. We divide the matrix into block diagonals with $S_{tot}^z = 0, 1, 2...8$ sectors. To further speed up calculation we only compute lowest 500 eigenstates in every sector. In order to justify this cut-off we show the comparison between the full eigen-spectrum and the truncated low-energy spectrum. The low energy eigen-spectrum is unaffected by the truncation (see Figure 3.16).

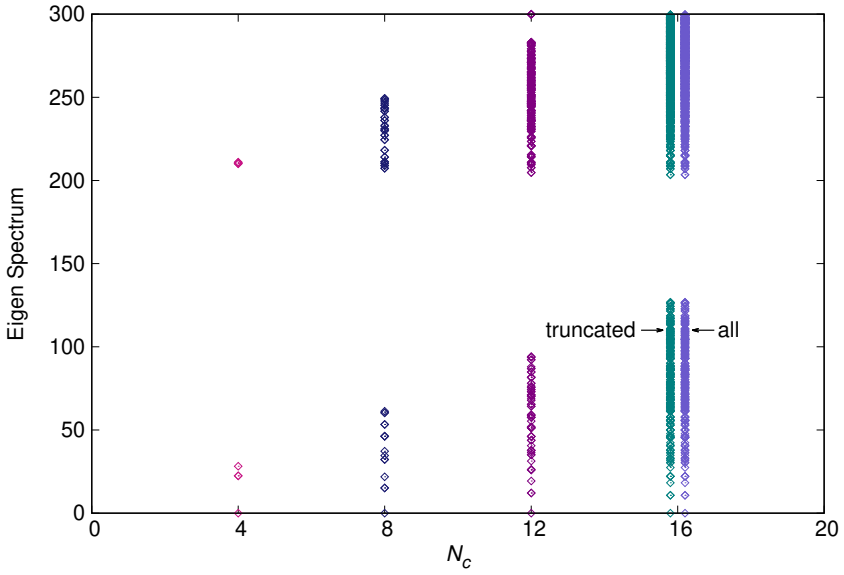

Figure 3.16: Eigen-spectrum for different values of N_c shown as a tower of energies measured w.r.t. the ground state energy in each case. For $N_c = 16$ we show the comparison of the full spectrum with that of the low-energy spectrum consisting of 4500 states.

3.5.5 Dynamical structure factor

Dynamic structure factor is the Fourier transform of the time dependent pair correlation function [138]. It is analogous to the cross section for scattering measured in neutron scattering experiments. Dynamical structure factor can be calculated if the full eigen-spectrum corresponding to the Hamiltonian is known. Then the Fourier transform of the two spin correlation function reads as,

$$\begin{aligned} S^{\alpha\beta}(q,\omega) &= \frac{1}{N}\sum_{l,R} e^{iqR}\int_{-\infty}^{+\infty} dt\, e^{i\omega t}\,\langle s_l^{\alpha}(t) s_{l+R}^{\beta}\rangle \\ &= \frac{2\pi}{Z}\sum_{n,m} e^{-\beta E_n}\,\langle n|S_q^{\alpha}|m\rangle\,\langle m|S_{-q}^{\beta}|n\rangle\,\delta(\omega+E_n-E_m) \end{aligned} \tag{3.11}$$

where Z is the partition function, E_n are the eigenvalues corresponding to eigenvectors $|n\rangle$ and

$$S_q^{\alpha} = \frac{1}{\sqrt{N}}\sum_l e^{-iql} S_l^{\alpha} \tag{3.12}$$

Using symmetry properties of Hamiltonian, dynamical structure factor at $T = 0$ is reduced to

$$S^{\alpha\alpha}(q,\omega) = \sum_n 2\pi\,|\langle G|S_q^{\alpha}|n\rangle|^2\,\delta(\omega+E_G-E_n) \tag{3.13}$$

where E_G is the energy of the ground state $|G\rangle$.

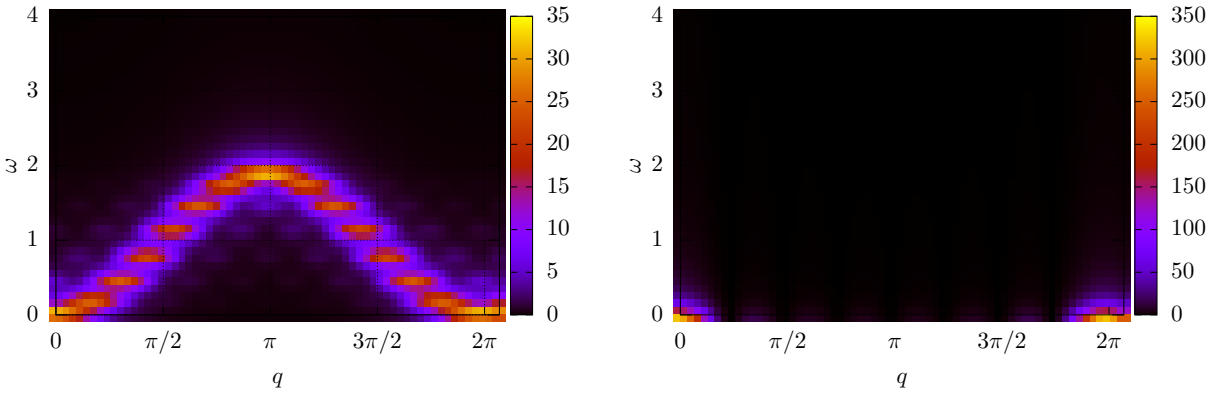

(a) (b)

Figure 3.17: Dynamical structure factor (a) $S^{xx}(q,\omega)$, (b) $S^{zz}(q,\omega)$ at $T = 0$ and $h = 0$ for 1D Heisenberg ferromagnetic chain calculated using CMFT for a cluster of $N_c = 8$.

We calculate component dependent dynamical structure factor (3.13) from the eigenspectrum obtained using CMFT. In order to understand the results in more detail, we also compute the results for a system of ferromagnetic and antiferromagnet Heisenberg chain. The disturbances or excitations of the ferromagnetic order are spin waves, these low energy excitations are quantized and known as magnons [139]. The ground state of the Hamiltonian for ferromagnetic Heisenberg chain obtained using CMFT is an ordered state, where all the spins point in same direction. This is reflected as the sharp peaks at $q = 0, 2\pi$ in $S^{zz}(q,\omega)$ (see Fig. 3.17(b)). However, the transverse component, $S^{xx}(q,\omega)$ shows the spectrum expected from the linear spin wave theory.

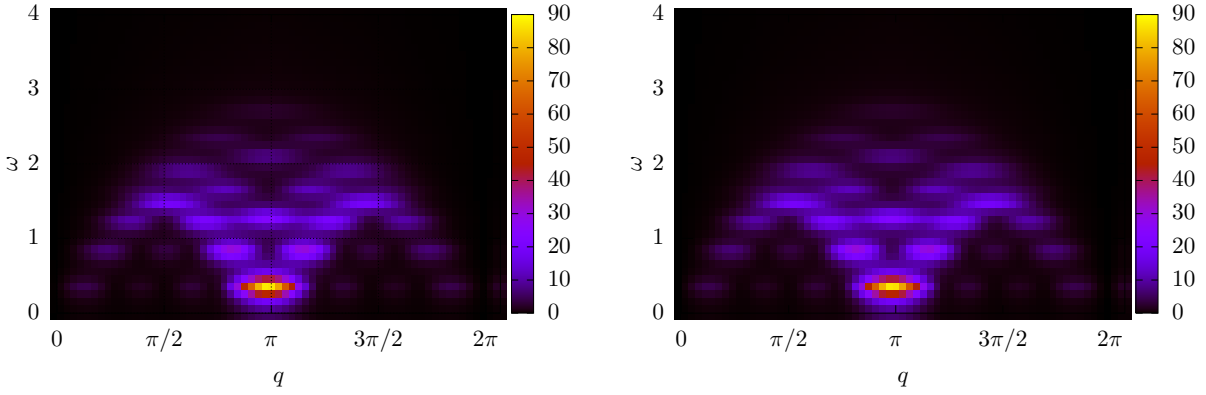

(a) (b)

Figure 3.18: Dynamical structure factor (a) $S^{xx}(q,\omega)$ (b) $S^{zz}(q,\omega)$ at $T=0$ and $h=0$ for 1D Heisenberg antiferromagnetic chain calculated using CMFT for a cluster of $N_c=8$.

The ground state of the antiferromagnetic Heisenberg spin chain obtained using CMFT is a Néel type antiferromagnetic order with staggered magnetization of the order of 10^{-2}. The anti-ferromagnetic nature is reflected as very sharp peak in dynamical structure factor at $q=\pi$ (see Fig. 3.18). Excitations in spin-1/2 AFM chain are fractionalized each of them carrying $S=1/2$, known as spinons [140]. It is interesting to note that the spinon spectrum is obtained in the eigenspectrum obtained by CMFT. The discrete points in the dynamical structure factor is consequence of finiteness of the cluster.

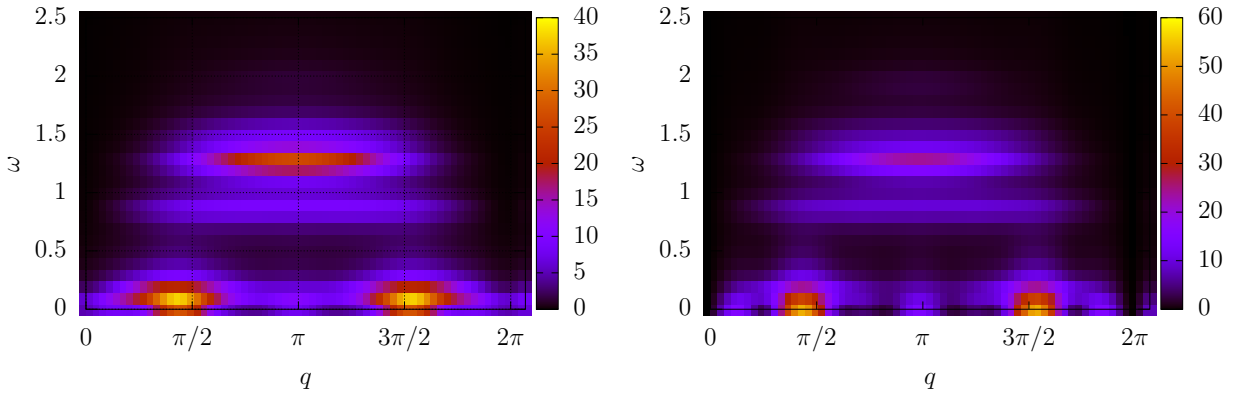

(a) (b)

Figure 3.19: Dynamical structure factor (a) $S^{xx}(q,\omega)$ (b) $S^{zz}(q,\omega)$ at $T=0$ and $h=0$ for 1D Heisenberg model for tetramer compound, $CuInVO_5$ calculated using CMFT for a cluster $N_c=8$.

In Fig. 3.19, we show the component dependent dynamical structure factor obtained from the CMFT results for two-tetramer cluster. For the present calculation we have used $J_1 = 1, J_2 = -(142.0/240.0), J_3 = (30.0/240.0)$. We find a gap above the ground state, which is understood as the order with $q \sim \pi/2$. This closing of gap may be reflected in the peak observed in low temperature specific heat. However, computation of larger cluster is required for conclusive result on the gap above ground state.

Chapter 4

Multiple phase transitions and high-field quadrupolar order in a model for β-$TeVO_4$

Adapted from the work published in :

Singhania, A., Kumar, S., "Multiple phase transitions and high-field quadrupolar order in a model for β-$TeVO_4$", ***Phys. Rev. B*** 101, (2020) 064403

4.1 Introduction

Interacting spin systems realized in condensed matter are well known for manifesting the surprises of quantum physics [141, 142]. A microscopic understanding of quantum spin systems not only enriches us with new fundamental concepts useful across disciplines, but also opens up possibilities for next-generation technologies [143, 144, 145]. Quantum effects come to the fore at low temperatures in low-spin systems. Lower dimensionality and frustrating interactions further reduce the tendency of spin systems to acquire conventional magnetic order, thereby promoting exotic quantum phenomena [143, 146, 147, 148, 149, 150]. Often, the interplay among frustrating interactions, lower dimensionality and the intrinsic quantum nature of the degrees of freedom results in unexpected states and complex magnetic phase diagrams [3, 5].

Weakly coupled frustrated spin-1/2 chains represent a class of systems possessing all of the above ingredients. These are realized in various quasi-one-dimensional magnets, such as, linarite [151, 152], $NaCuMoO_4(OH)$ [153], and $LiCuVO_4$ [154, 155]. In recent years, β-$TeVO_4$ (βTVO) has emerged as another model magnetic material for studying coupled frustrated spin chains. Low-temperature magnetic phases and phase transitions in βTVO are uncovered via a combination of thermodynamic measurements, as well as neutron scattering and NMR experiments [156, 157, 158, 159, 160]. Three magnetic transitions upon cooling, (i) paramagnet to spin density wave (SDW) at $T_{N1} = 4.65$ K, (ii) SDW to spin-stripe at $T_{N2} = 3.28$ K, and (iii) spin-stripe to an elliptical-spiral or vector chiral (VC) order at $T_{N3} = 2.28$ K, are reported. Applied field versus temperature phase diagrams were obtained via a combination of specific heat, magnetization and magnetostriction measurements [159]. Discontinuous changes in magnetization with applied field close to saturation were reported [159, 157]. These discontinuities have been proposed as a realization of theoretically predicted spin-nematic or quadrupolar phase. Recent investigations report that the high-field phase is magnetically ordered with nematic order possibly present in a very narrow range of applied field [161]. Experiments have reported that the intermediate spin-stripe phase hosts unusual elementary excitations called *wigglons* [162] whereas at lower temperatures a coexistence of spinons and magnons is expected [160].

Motivated by the rich magnetic behavior of βTVO, we study a minimal anisotropic Heisenberg model for coupled zigzag chains in two dimensions. In order to capture magnetic field and temperature dependence of various thermodynamic quantities, we make use of the cluster mean field (CMF) approach for our investigations. Using model

parameters reported in ab-initio study of the material, we find: (i) a partially ordered state with zero ordered moments on alternate sites, (ii) a collinear antiferromagnet, (iii) an elliptical spiral state with finite vector chirality, and (iv) unusual metamagnetic behavior close to saturation magnetization. Some of these features, e.g., the VC ground state, the SDW order and the metamagnetic jumps in magnetization are consistent with the experimental data.

In order to place our results in a proper context, we summarize the existing theoretical work that aims to understand the frustrated spin-1/2 chain magnets in general, and βTVO in particular. Isolated zig-zag spin chains with nearest neighbor (nn) FM and next nn (nnn) AFM interactions have been studied using DMRG, exact diagonalization, effective field theories, and coupled cluster methods [163, 164, 165, 166, 167, 168, 169, 170]. Transition from helical to SDW state driven by applied magnetic field in linarite has also been accurately described via a purely classical spin model [151]. Most of these studies focus on ground state phase diagrams in the plane of interaction strength ratio and applied field. Spiral phases and nematic states close to saturation field have been reported in these theoretical investigations [168, 169, 171]. The temperature dependence in the two dimensional model has remained unexplored due to the lack of suitable methods. Classical approximation for spin operators can be invoked with the argument that thermal effects take over at finite temperatures [172]. This approach can work, with the understanding that the transition temperatures and the size of ordered moments will be overestimated, in systems that show a single phase transition. However, for a system that displays multiple transitions with changing temperature a careful treatment of quantum effects becomes most important. Since the CMF approach retains quantum correlations while allowing for thermodynamic-limit calculations of various order parameters in the mean field spirit, the method is well suited for describing temperature and magnetic field dependence within a single framework.

4.2 Model and Method

We begin with anisotropic Heisenberg model on coupled zigzag spin-1/2 chains in the presence of an external magnetic field. The model is described by the Hamiltonian,

$$\begin{aligned}\mathcal{H} &= \sum_{n,j}[J_1(\mathbf{S}_{j,n}\cdot\mathbf{S}_{j+1,n}) + J_2(\mathbf{S}_{j,n}\cdot\mathbf{S}_{j+2,n} + \delta_2 S^z_{j,n}S^z_{j+2,n}) \\ &\quad + J_{2b}(\mathbf{S}_{j,n}\cdot\mathbf{S}_{j-1,n+1}) - h_z S^z_{j,n}]. \end{aligned} \tag{4.1}$$

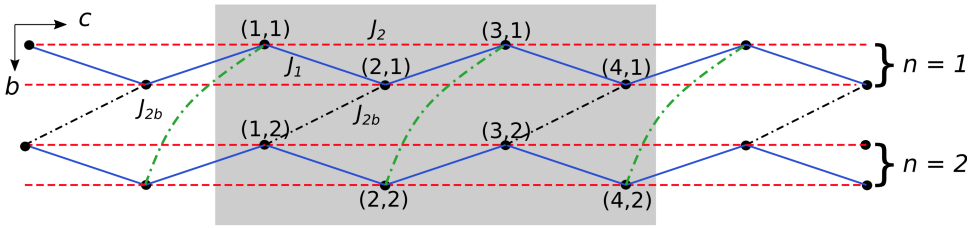

Figure 4.1: A schematic picture of the magnetic model for $\beta-TeVO_4$. The shaded area highlights the cluster within which interactions are treated exactly. The chain and site indices for each spin inside the cluster are specified. The dot-dashed lines represent connectivity due to periodic boundary condition in the b direction.

Here, $\mathbf{S}_{j,n}$ represents the spin-1/2 operator located at n^{th} chain and j^{th} site. J_1 is the nn ferromagnetic (FM) interaction, J_2 is the nnn antiferromagnetic (AFM) interaction and J_{2b} is the AFM interchain coupling. Strength of anisotropy and applied magnetic field are denoted by δ_2 and h_z, respectively. The parameters used in our work, following a Density Functional Theory study for $\beta-TeVO_4$, are: $J_1 = -26.2$K, $J_2 = 24.6$K, and $J_{2b} = 7.3$K [173, 159]. The anisotropy value is fixed to $\delta_2 = -0.2$ throughout the study, except for results discussed in Fig. 4.4. We show in Section 4.3.1. that exact diagonalization (ED) calculations on small clusters miss out on most features related to conventional magnetic order. Therefore, in this work, CMF is used as the main method to understand the nature of magnetic order and the magnetic transitions. The CMF has proven extremely useful for investigating spin models possessing magnetic frustrations of geometrical or Kitaev nature [136, 89, 137, 87, 174]. The key idea of the method is to treat all interaction links located within the cluster exactly, and to make use of the conventional mean field decoupling, $\mathbf{S}_i \cdot \mathbf{S}_j \approx \langle \mathbf{S}_i \rangle \cdot \mathbf{S}_j + \mathbf{S}_i \cdot \langle \mathbf{S}_j \rangle - \langle \mathbf{S}_i \rangle \cdot \langle \mathbf{S}_j \rangle$, for interaction links connecting the cluster and the environment. Applying this approximation to the Hamiltonian Eq. (4.1) leads to the cluster Hamiltonian,

$$\begin{aligned} \mathcal{H}_c &= \sum_{n,j}{}' [J_1(\mathbf{S}_{j,n} \cdot \mathbf{S}_{j+1,n}) + J_2(\mathbf{S}_{j,n} \cdot \mathbf{S}_{j+2,n} \\ &\quad + \delta_2 S^z_{j,n} S^z_{j+2,n}) + J_{2b}(\mathbf{S}_{j,n} \cdot \mathbf{S}_{j-1,n+1}) - h_z S^z_{j,n}] \\ &\quad + \sum_{n,j}{}'' \mathbf{M}^{j,n} \cdot \mathbf{S}_{j,n}, \end{aligned} \tag{4.2}$$

where the prime over the summation sign refers to all the links contained inside the cluster, and the double-primed sum is over all those spins that have at least one interaction link outside the cluster. For our choice of cluster shown in Fig. 4.1, all eight spins contribute to the double-primed summation. $\mathbf{M}^{j,n}$ denotes the effective mean field vector

that couples to the spin $\mathbf{S}_{j,n}$. The mean field vector is defined as an appropriate vector sum $\mathbf{M}^{j,n} = \sum J_p \langle \mathbf{S}_{j',n'} \rangle$, where the sum is over all spins $\mathbf{S}_{j',n'}$ that are located outside the cluster and are coupled to spin $\mathbf{S}_{j,n}$ via coupling parameter J_p, with $p = 1, 2, 2b$. Setting up the equivalence between environment and cluster sites, in the spirit of a mean field theory, enables the closing of a self-consistency loop. We impose periodic boundary conditions perpendicular to the chain direction (b-direction in Fig. 4.1), and couple the spins to mean fields along the chain (c-direction in Fig. 4.1). Note that the intra-cluster interaction between $\mathbf{S}_{3,1}$ and $\mathbf{S}_{2,2}$ is a consequence of periodic boundary condition along the b direction. Average of a general operator $\hat{O}$ is computed, following the standard quantum statistical approach, as,

$$\langle \hat{O} \rangle = \frac{Tr\ \hat{O}\ e^{-\beta H_c}}{Tr\ e^{-\beta H_c}}, \tag{4.3}$$

where H_c is the cluster Hamiltonian defined in Eq. (4.2), and the trace is over all states of the H_c with converged values of the mean field parameters. Further details of the method and its extensions are available in some recent papers [136, 89, 137, 87, 174].

4.3 Results and Discussions

4.3.1 Exact diagonalization

We begin by discussing specific heat and magnetization obtained via ED calculations on finite clusters. We present results of ED for an 8-site cluster where two zigzag chains of 4 spins each are coupled, and a 16-site cluster where four zigzag chains are coupled. Periodic boundary conditions (PBC) in both directions are imposed. Details of the calculations are similar to those presented in a recent study [174]. In Fig. 4.2 (a), we show the temperature dependence of specific heat, $C_V = \frac{1}{N_c} d\langle H \rangle / dT$, where N_c denotes the number of spins in the cluster. In the same panel we plot the variations of spin-spin correlations, $C_{pq} = \langle \mathbf{S}_{j,n} \cdot \mathbf{S}_{j',n'} \rangle$ where $p = 4(n-1)+j$ and $q = 4(n'-1)+j'$ for different spin pairs. Within ED a dimer state comprising of perfect singlets on nnn sites, characterized by $C_{13} = -0.75$, emerges as the ground state. These singlet correlations gradually decrease upon increasing temperature leading to a characteristic hump in specific heat [175, 176]. We conclude that for the Hamiltonian under consideration, ED calculations on small clusters do not support the existence of a conventional ordered magnetic state. Consequently, stand alone ED

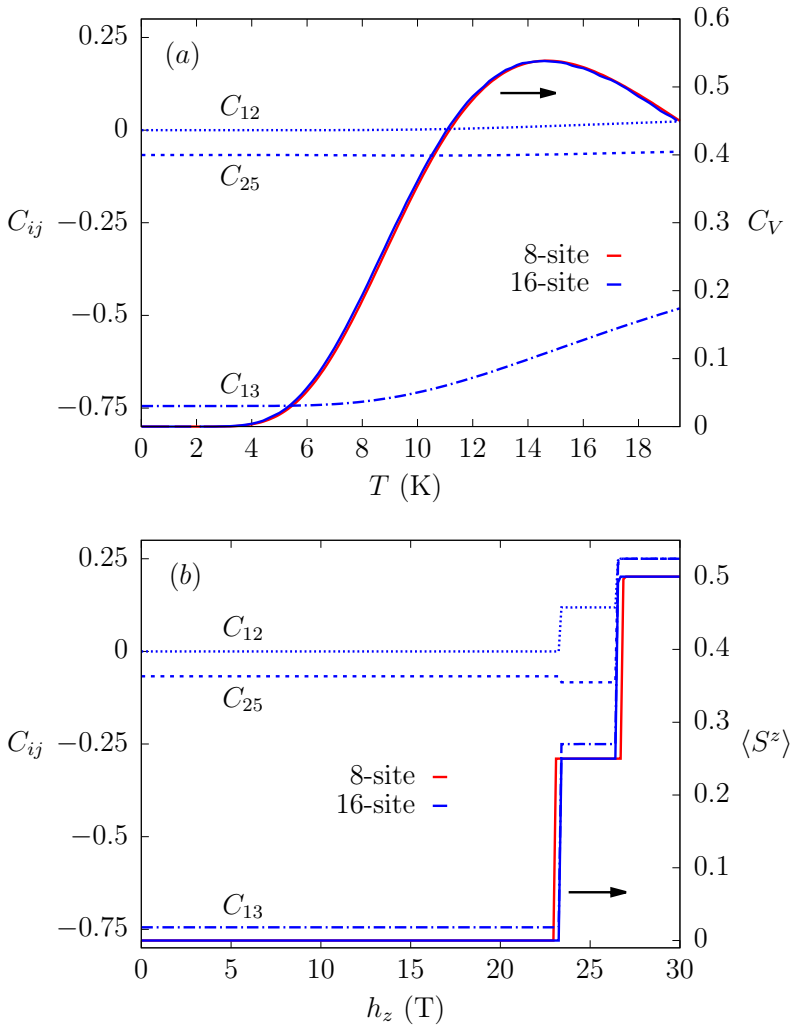

Figure 4.2: Solid lines display the variation of, (a) specific heat with temperature, and (b) magnetization with applied field for 8-site and 16-site clusters with PBC calculated using exact diagonalization. The broken lines represent variations of correlations for different spin pairs with, (a) temperature and (b) applied magnetic field for 16-site cluster. Results in panel (a) are at $h_z = 0$, and those in panel (b) are at $T = 0$. The results for spin-spin correlations for 8-site cluster are almost identical to those for 16-site cluster.

calculations are unable to provide any hint of multiple phase transitions that are observed in the experiments on βTVO. Similarly, the field dependence of magnetization displays large jumps coinciding with discontinuities in the correlation functions (see Fig. 4.2(b)). Such discontinuities associated with level crossings in the spectrum of a finite cluster will not be present in a larger system. Since ED calculations on very large systems are extremely difficult, we take an alternate approach of capturing thermodynamic limit with the help of mean field scheme. In next subsections we discuss the results obtained via CMF approach and present a comparison with available experimental data.

4.3.2 Cluster Mean Field: Temperature Dependence

In Fig. 4.3 we show the temperature dependence of specific heat C_V, the VC order parameter $\langle \kappa^z \rangle$, and the magnitude $\langle S_{1,1} \rangle$ and $\langle S_{1,2} \rangle$ of local spin averages at two inequivalent sites. The VC order parameter is defined as,

$$\begin{aligned} \langle \kappa^z \rangle &= \frac{1}{N_c} {\sum}' (\mathbf{S}_{j,n} \times \mathbf{S}_{j+1,n})^z \\ &= \frac{1}{N_c} {\sum}' (S^x_{j,n} S^y_{j+1,n} - S^y_{j,n} S^x_{j+1,n}) \\ &= \frac{1}{N_c} {\sum}' Im[\langle S^+_{j,n} S^-_{j+1,n} \rangle - \langle S^+_{j,n} \rangle \langle S^-_{j+1,n} \rangle] \end{aligned} \tag{4.4}$$

As we will discuss below in detail, there are three distinct features in $C_V(T)$ which have an associated feature in one of the three order parameters mentioned above. Upon reducing T, one of the mean-fields, $\langle S_{1,1} \rangle$, becomes non-zero at $T = 7.2$ K while the other remains zero. This is an unusual partially ordered state where alternate sites remain quantum-disordered and are unable to develop finite magnetic moments (see Fig. 4.3(b)). Such partially ordered states have also been reported in Kondo systems where they can be understood as arising out of the competing tendencies of Kondo screening and ordering of magnetic moments [177]. PO state can be viewed as an extreme case of a SDW order where difference between magnitude of ordered local moments on neighboring sites is maximum. Indeed, the magnetic order reported in experiments on βTVO below 4.65 K is SDW with weaker moment-size modulation and larger wavelength. The onset of the PO state is accompanied by a 'shoulder' feature in C_V exactly at $T = 7.2$ K. The second mean field parameter, $\langle S_{1,2} \rangle$, becomes finite at $T = 6.8$ K leading to a conventional magnetic order. Indeed, this is accompanied by a sharp peak in specific heat signifying a conventional long-range order (see Fig. 4.3(c)). Upon further lowering the temperature these mean-fields approach towards their saturation values. However, a discontinuous change in both $\langle S_{1,1} \rangle$ and $\langle S_{1,2} \rangle$ occurs at 4 K, exactly at the temperature at which vector-chiral order parameter becomes finite confirming a change in the nature of the magnetic order. This first order phase transition manifest itself in the specific heat through a discontinuity exactly at $T = 4$ K. The ground state is therefore characterized by a finite vector chirality and unequal magnitude of magnetic moments on alternate sites (see Fig. 4.3(d)), describing an elliptical spiral state similar to the ground state reported in experimental studies on βTVO [159]. While the magnitude and locations of the specific-heat anomalies discussed above are likely to depend on the cluster size, the

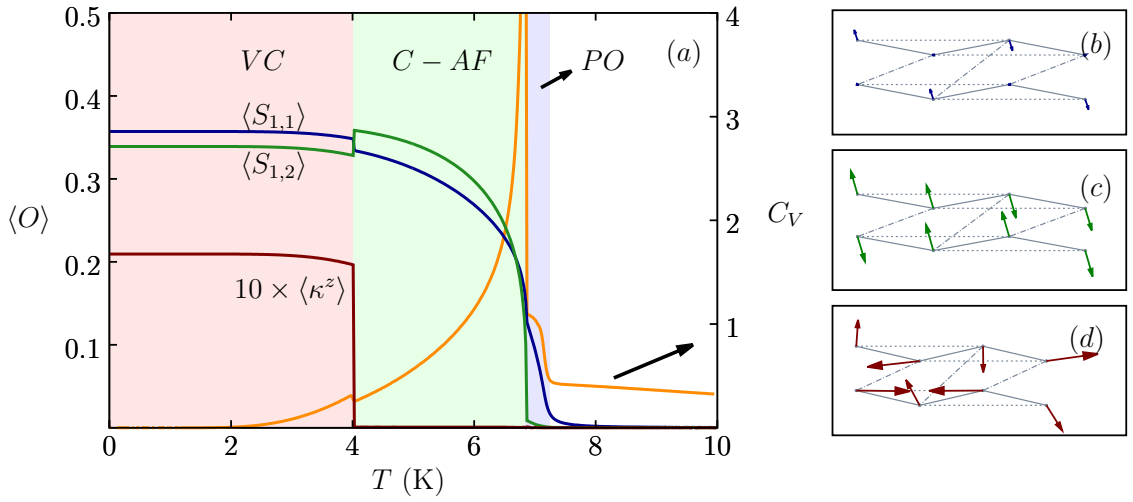

Figure 4.3: (a) Specific heat, C_V, vector chiral order parameter $\langle \kappa^z \rangle$, and magnitudes of self-consistent mean fields $\langle S_{1,1} \rangle$ and $\langle S_{1,2} \rangle$ as a function of temperature. The right y-axis is for specific heat and the left y-axis is for all other quantities. The vector chiral order parameter is scaled up by a factor of 10 for clarity. Three distinct magnetically ordered states can be clearly identified with the help of these thermodynamic observables. (b)-(d) Real-space patterns of mean-field spin vectors in the three phases.

number of such anomalies remain independent of N_c [174].

While the similarities with the experimental data [157, 159] in terms of multiple phase transitions and the VC ground state become clear from the above discussion, it is important to point out the key experimental features of βTVO that are not captured in our study. We find that the ordered phase between the PO and the VC is a collinear antiferromagnet with varying moment size on alternate sites. Experiments, on the other hand, report a peculiar stripe phase with two orthogonally oriented sublattices in this regime [158]. Stabilizing such a phase may require inclusion of Dzyaloshinskii-Moriya interactions as well as the inter-layer coupling which we have not included in our present model Hamiltonian study. The appearance of VC phase as the ground state of the Hamiltonian considered in this work strongly depends on anisotropy parameter δ_2. In Fig. 4.4 we show specific heat as a function of temperature for different values of δ_2. The discontinuity in the specific heat at low temperatures is absent for a fully isotropic, $\delta_2 = 0$, model, and becomes prominent only for $|\delta_2| \geq 0.2$. A further increase in the strength of anisotropy parameter leads to an increase in the size of the discontinuity, as well as the value of the temperature at which the discontinuity occurs. We simultaneously track the VC order parameter. Indeed, the location of discontinuity in specific heat is correlated perfectly with the on-set of vector chirality. Therefore, we conclude that anisotropy is crucial not only to obtain the vector chiral ground state but also for the correct ordering

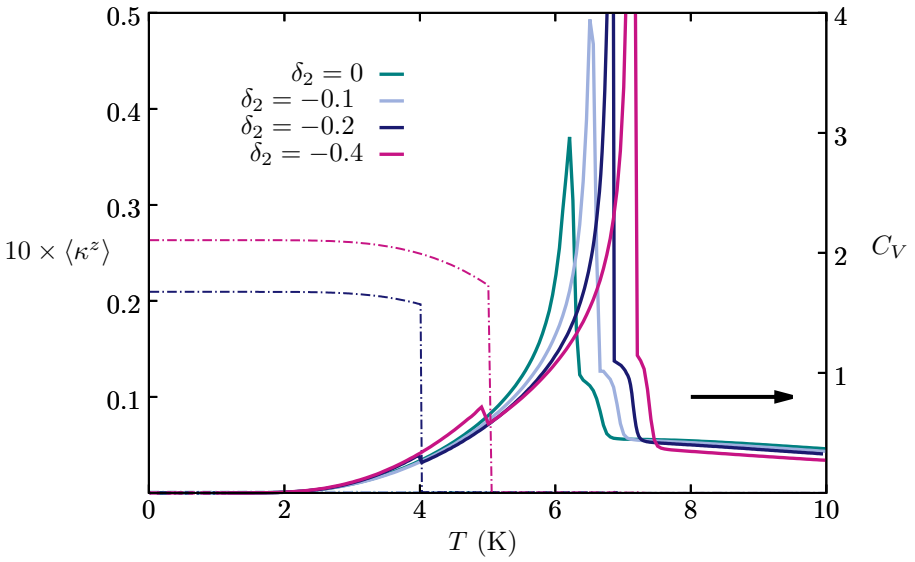

Figure 4.4: Specific heat (solid lines) and vector chiral order parameter (dotted lines) as a function of temperature for different values of the anisotropy parameter δ_2. Note that a significant amplitude for vector chirality appears only for $|\delta_2| \geq 0.2$.

temperature. Note that in general anisotropy in other interactions may also be present in the real material [158].

We also note that for the choice of parameters used for calculations, the range of stability for the partially ordered state was found to be rather narrow. To show that this state is not a result of fine tuning of parameters of the Hamiltonian, we check if the range of stability can be increased by at least one of the model parameters. In Fig. 4.5, we plot specific heat as a function of temperature for different values of the inter-chain coupling parameter J_{2b}. The presence of partially ordered phase is indicated by the difference between the size of local moments on two inequivalent sites. Therefore, we also show in Fig. 4.5 the temperature dependence of $\langle S_{1,1} \rangle - \langle S_{1,2} \rangle$. Increasing the value of J_{2b} leads to an increase in the window over which the specific heat displays the unusual shoulder feature. This is also followed by the large values of the moment difference $\langle S_{1,1} \rangle - \langle S_{1,2} \rangle$. However, for large values of inter-chain coupling, partially ordered state destabilizes the vector chiral ground state. Therefore, only a suitable combination of J_{2b} and δ_2 allows for the appearance of both the vector chiral and the partially ordered phases.

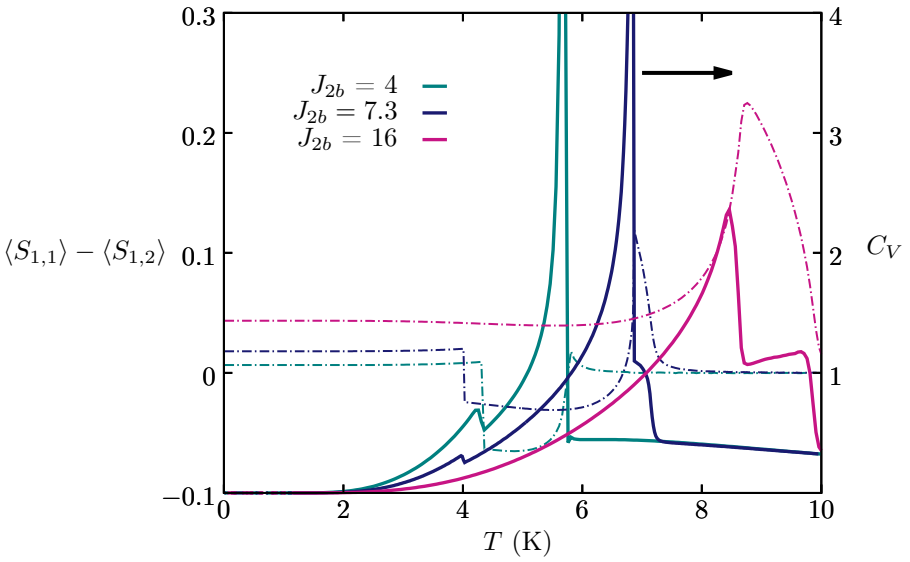

Figure 4.5: Specific heat (solid lines) and the difference in the magnitude of two ordered moments (dotted lines) as a function of temperature for different values of the inter-chain coupling parameter J_{2b}.

4.3.3 CMF: Magnetic Field Dependence

Having discussed the temperature dependence of various physical quantities in the absence of external magnetic field, we now focus on the magnetic field dependence in the low-T regime. The component along external field of local magnetizations on two inequivalent sites, $\langle S^z_{1,1}\rangle$ and $\langle S^z_{2,1}\rangle$, are plotted in Fig. 4.6. Note that conversion factor of $k_{\rm B}/\mu_{\rm B} \approx 1.5$ T/K is used throughout to represent the applied magnetic field values in units of Tesla. We find a metamagnetic response in terms of discontinuities in magnetization close to saturation. We also show the field dependence of vector chiral order parameter $\langle \kappa^z \rangle$, with appropriate scale factor, in the same figure. The first jump in magnetization coincided with abrupt vanishing of VC order parameter, and the second jump takes the system to the fully saturated FM state(Fig 6.). Therefore, we infer the existence of a new magnetic phase bounded between a fully saturated FM and the vector chiral state. These results match remarkably well with those reported in the experiments. Recent theoretical studies based on spin-wave approach about the fully saturated FM state have suggested the presence of quadrupolar order in the metamagnetic regime. In order to verify these predictions, we explicitly calculate quadrupolar order parameter (QOP), $Q_{x^2-y^2} = \frac{1}{N_c}\sum' Re[\langle S^+_{j,n}S^+_{j+1,n}\rangle - \langle S^+_{j,n}\rangle\langle S^+_{j+1,n}\rangle]$, as a function of applied field. The outcome of these calculations at different temperatures are plotted in Fig. 4.6. Indeed, the QOP becomes finite in the metamagnetic regime (see Fig. 4.6(a)-(b)). Therefore, our explicit calculations support the existing theoretical proposals regarding the presence of

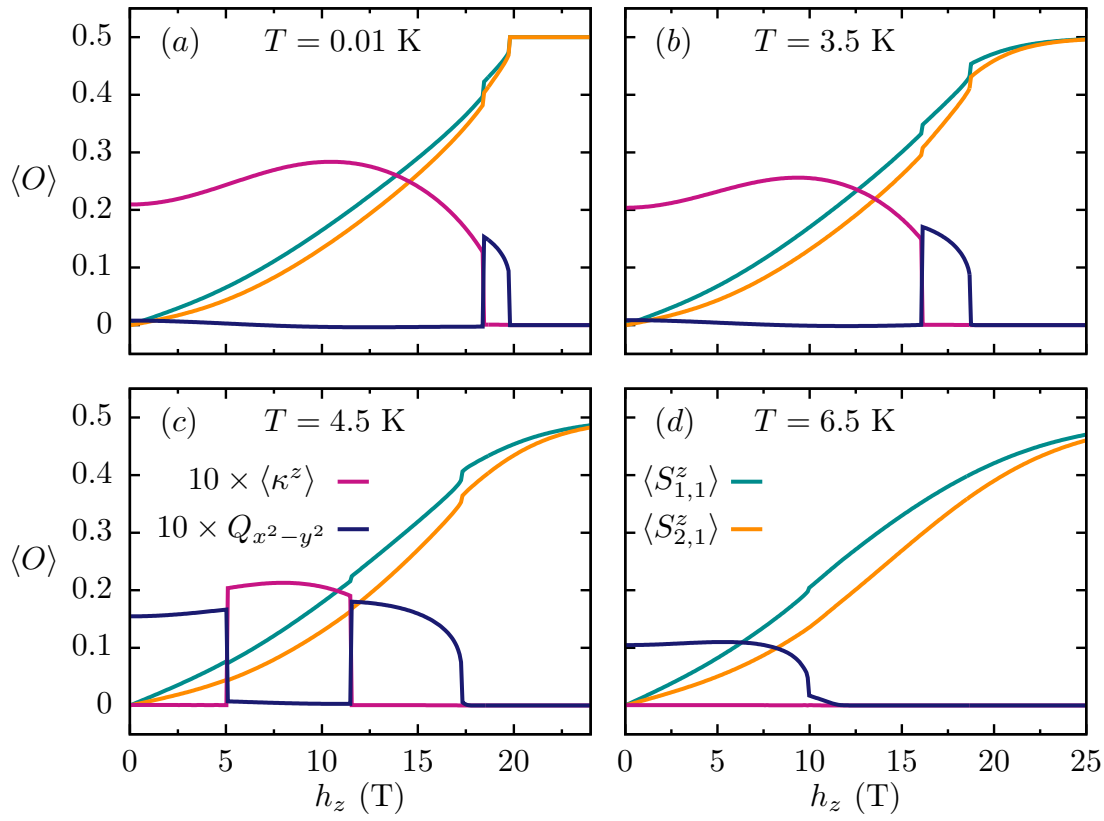

Figure 4.6: Component along applied field of local magnetizations, $\langle S^z_{1,1} \rangle$ and $\langle S^z_{2,1} \rangle$, on two inequivalent sites as a function of applied magnetic field for different temperatures. Magnetic field dependence of the vector chiral order parameter, $\langle \kappa^z \rangle$ and quadrupolar order parameter, $Q_{x^2-y^2}$, is also shown. The factor $k_B/\mu_B \approx 1.5$ T/K is used to express h_z in physical units of Tesla.

a quadrupolar order close to saturation magnetization [150, 178, 179]. Upon increasing temperature the discontinuities in magnetization become weaker in magnitude and their locations shift to lower magnetic fields and (see Fig. 4.6 (b)-(d)). The QOP also tracks these evolution of magnetization jumps. However, we also note that the QOP also becomes finite in the low-field regime for larger temperatures (see Fig. 4.6(c)-(d)) For $T = 4.5$ K, an additional discontinuity is obtained at the on-set of the vector chiral order. This is indicative of a re-entrant behavior which becomes more clear as we discuss the complete phase diagram below. Comparing our results with the experimental data, we note that the transition to a PM state occurs at 7.2 K whereas the corresponding experimental value is 4.6 K. On the other hand, the magnetic field required to obtain a fully saturated FM state, h_z^{sat}, is 20 T in our study compared to 22 T reported in experiments [159]. It is interesting to note that while the transition temperature is significantly over-

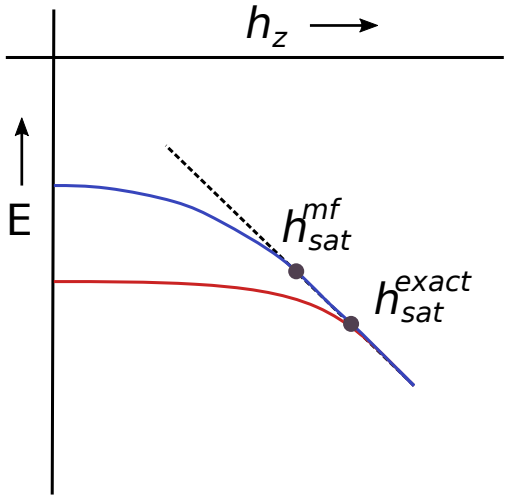

Figure 4.7: A schematic energy versus applied field plot demonstrating how mean field, or any approximate method, always underestimates saturation field. The lower curve is the energy obtained from exact calculations and the upper curve represents the approximate energy. The linear part is the energy of fully saturated state which is accurately captured in the mean field scheme as well. The intersection of the linear part with the exact (mean field) energy defines h_{sat}^{exact} (h_{sat}^{mf}).

estimated in the CMF approach, the saturation field is only slightly underestimated. We present a simple argument to justify these findings. In general, any mean field approximation suppresses thermal as well as quantum fluctuations. While both thermal and quantum fluctuations play an important role in determining the temperature at which the magnetic order is lost, only quantum fluctuations are responsible for transition to a saturated FM state at zero temperature. A more accurate estimate of h_z^{sat} reflects the fact that CMF approach captures quantum fluctuations well. Furthermore, it can be shown that mean field approximations will always underestimate h_z^{sat}. The argument, presented with reference to the schematic Fig. 4.7, is as follows: the energy of a saturated FM state is a linear decreasing function of applied field. This estimate can be accurately obtained in any approximate scheme as well. For non-saturated states, on the other hand, the ground state energy obtained via any approximate method is always higher than the exact energy. By definition, the saturation field, h_z^{sat}, is the value of applied field at which the energy curves for the saturated FM state (linear part in Fig. 4.7) crosses the energy of the non saturated state. Therefore, this crossing will necessarily occur at a lower value of magnetic field for any approximate method. Note that in the schematic Fig. 4.7, $h_{sat}^{mf} < h_{sat}^{exact}$. The magnetic susceptibility is calculated as $\chi(T)|_{h_z} = (dM_z/dh_z)|_{h_z}$ for different values of applied field h_z. Results are shown in Fig. 4.8. We find that the magnetic susceptibility shows a clear indication of the transition to the vector chiral state. However, the presence of two other transitions at higher temper-

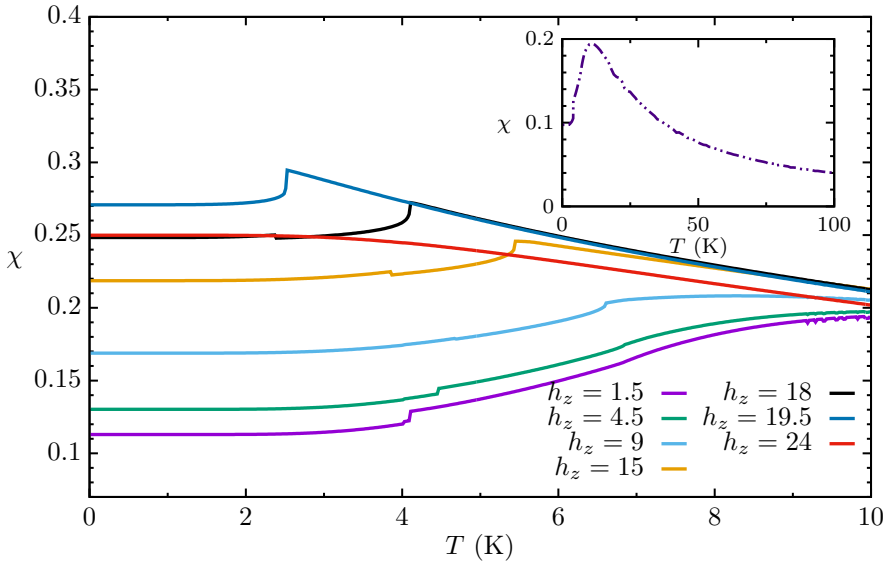

Figure 4.8: Magnetic susceptibility as a function of temperature for various field strengths. Inset shows susceptibility over a wider range of temperature for $h_z = 1.5$T.

atures is not very apparent looking at the magnetic susceptibility results. Interestingly, even this situation is similar to that found in experiments. The experimental susceptibility data does not provide conclusive evidence for the presence of transitions. On the other hand, the specific heat data shows clear anomalies [157]. For the vector chiral order, the non-monotonic evolution of the transition temperature with increasing magnetic field is correctly captured.

4.3.4 $h_z - T$ Phase Diagram

Finally we discuss the complete $h_z - T$ phase diagram obtained in our CMF study of the anisotropic Heisenberg model. As discussed so far, in addition to the trivial paramagnet and fully saturated ferromagnet, we have identified four qualitatively distinct magnetic phases with varying temperature and magnetic field. These are, (i) VC, (ii) collinear-AF, (iii) PO, and (iv) quadrupolar (Q) (see Fig. 4.9(a)). The boundaries between these phases are extracted from the changes in order parameters which also coincide with the anomalies in the specific heat. Intra-chain and inter-chain spin-spin correlations carry important information about the competition between different magnetic phases and provide additional insights regarding the phase boundaries. We show the color map in $h_z - T$ plane for the nn inter-chain correlation C_{36} (Fig. 4.9(b)) and nn intra-chain correlation C_{23} (Fig. 4.9(c)). The definition of the correlation functions as well as the site indices are as given in Section 4.3.1. Qualitative changes in the inter-chain and the intra-

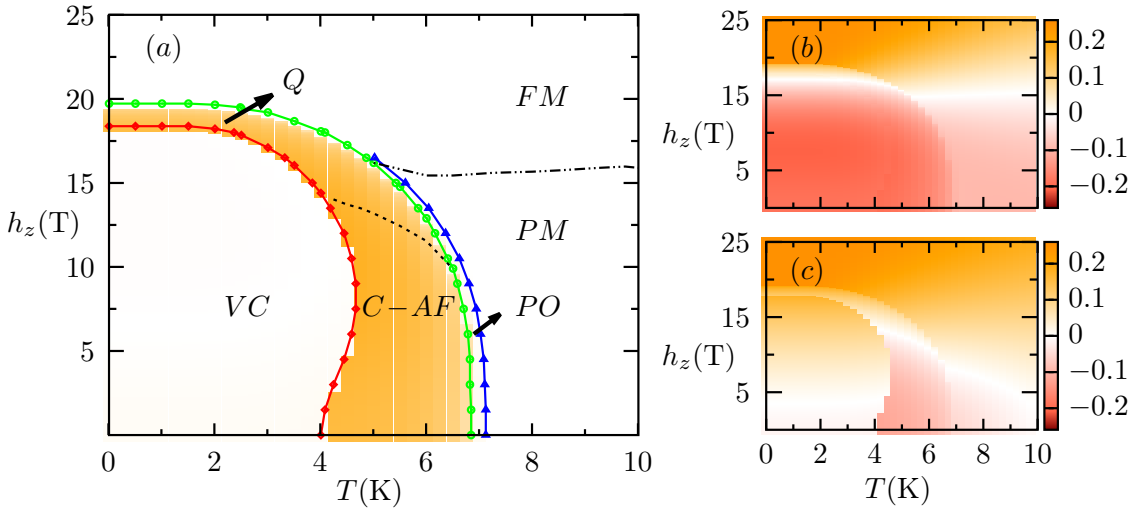

Figure 4.9: (a) The $h_z - T$ phase diagram inferred from the variations in different order parameters and the anomalies in specific heat. The color map in the background represents the value of quadrupolar order parameter $Q_{x^2-y^2}$. (b)-(c) The color map in $h_z - T$ plane of the, (b) inter-chain $\langle \mathbf{S}_{3,1} \cdot \mathbf{S}_{2,2} \rangle$ (C_{36}), and (c) intra-chain $\langle \mathbf{S}_{2,1} \cdot \mathbf{S}_{3,1} \rangle$ (C_{23}), spin-spin correlations. Since dipolar correlations become vanishingly small in the region above the dotted line in (a), a pure quadrupolar order exists.

chain correlations across different phase boundaries are clearly visible from Fig. 4.9(b) and Fig. 4.9(c). In addition, we display the color map corresponding to the value of the QOP, $Q_{x^2-y^2}$. The resulting phase diagram is shown in Fig. 4.9. Interestingly, the region of finite $Q_{x^2-y^2}$ is bounded between two phase boundaries. What still remains puzzling is the finiteness of QOP at low fields for which there is no support in the experimental data. We provide a resolution of this with the help of inter- and intra-chain spin-spin correlation maps. It is interesting to note that the CMF approach allows access to both thermodynamic behavior, in the mean field spirit, as well as short range spatial correlations. This is an advantage of the CMF method over both, a fully microscopic approach such as quantum Monte Carlo, and a simple mean field approach which totally misses out on spatial correlations. It would be interesting to check if the short range spatial correlations can provide us with additional insights regarding the behavior of the system. In particular, one may ask if the information regarding change of magnetic phases is encoded in short-range spin-spin correlations. To this end, we show in Fig. 4.9(b)-(c) the map of correlations in the $h_z - T$ space for selected spin pairs. The intra-cluster spin-spin correlations display significant changes across various phase boundaries. The inter-chain correlations, $\langle \mathbf{S}_{3,1} \cdot \mathbf{S}_{2,2} \rangle$, become vanishingly small in the low-temperature high-field region (see Fig. 4.9(b)). Therefore, this can be seen as an effective decoupling of chains leading to destabilization of the VC order [160]. Furthermore, the effective

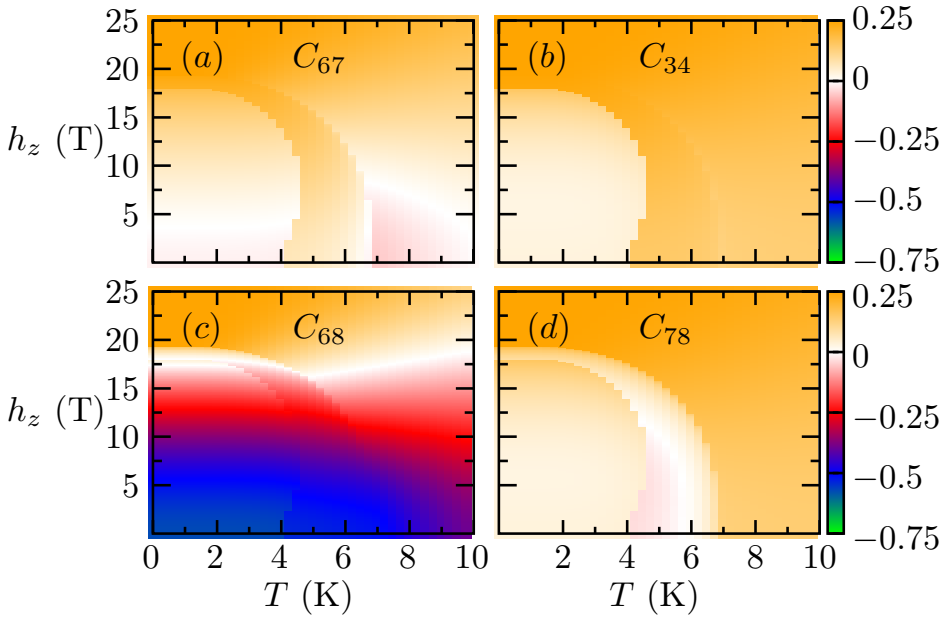

Figure 4.10: (a)-(d) Color map representing the value of spin-spin correlations Cpq for different spin pairs in the $h_z - T$ plane.

reduction in dimensionality also implies a loss of long range dipolar order. Hence, this region of vanishingly small inter-chain correlations should be seen as supporting pure quadrupolar order. Similarly, intra-chain correlation $\langle \mathbf{S}_{2,1} \cdot \mathbf{S}_{3,1} \rangle$ display a change of sign (see Fig. 4.9(c)). If the nn links in a zigzag chain get decoupled then the chain can be viewed as consisting of two inter-twined decoupled sublattices, and does not support long range dipolar order. Therefore, the region of finite QOP can be qualitatively divided into two parts with the help of the discussion above. One with coexisting long-range dipolar order and other with pure quadrupolar order. The boundary between these two regions is the dotted line in Fig. 4.9(a), which is the line of vanishing spin-spin correlations in Fig. 4.9(c). This displays a better correspondence with the experimentally reported phase diagrams where only the high-field phase is marked as quadrupolar. Importantly, this is also consistent with the discontinuities in the magnetization which are thermodynamic signatures for the existence of an unusual, such as quadrupolar, order. It is important to note that experimental phase diagrams show appreciable dependence on the direction of applied field. Our results correspond to field applied along b axis. We believe that the inter-layer couplings become essential for capturing the experimental phase diagram corresponding to the field in $a - c$ plane. We also display the behavior of other spin spin correlation functions in Fig. 4.10. Since $|J_1| \sim J_2$ for $\beta-$ TVO, nnn spin correlations are strongest owing to their antiferromagnetic nature (see Fig. 4.10 (c)). The nnn correlation C_{68} gradually decreases with increasing temperature due to thermal fluctuations. Upon

increasing applied field a region with vanishingly small C_{68} is indicative of complete absence of dipolar order. Finally, $C_{68} = 0.25$ characterizes a field induced saturated FM state. Panels (a), (b) and (d) in Fig. 4.10 display the variations of nn correlations C_{67}, C_{34} and C_{78} in that order. Given that the nn interactions are FM, these correlations have a positive value over most of the parameter regime. The re-entrant behavior as a function of applied magnetic field can also be noticed from the color maps of these nn correlation functions.

4.4 Summary and Conclusion

With the aim to describe complex magnetic phase diagram of β-TVO, we have investigated anisotropic Heisenberg model with nn FM and nnn AFM interactions on weakly coupled zigzag spin-1/2 chains. The CMF approach utilized in our study allows for an accurate treatment of short range spatial correlations, and therefore, captures the subtle competition between different possibilities of magnetic ordering. The results are obtained using realistic values of interaction parameters taken from ab-initio studies for β-TVO. We find, (i) a sequence of three phase transitions upon reducing temperature, (ii) vector chiral ground state, (iii) quadrupolar order close to saturation field accompanied by metamagnetic response, and (iv) re-entrant behavior as a function of applied field. While some of these features are consistent with the experimental data, our analysis does not capture the unusual spin-stripe state existing in the intermediate temperature regime. Additional anisotropic terms, such as Dzyaloshinskii-Moriya interaction, may be important for stabilizing the spin stripe state. Furthermore, the anisotropy of the $h_z - T$ phase diagram may crucially depend on the inter-chain couplings along the a axis which is not included in the present study [159]. We have also shown that the relative locations of the transition temperatures can be tuned by varying the relative strengths of the coupling parameters. Nevertheless, the transition temperatures are overestimated due to the mean field nature of the method. To conclude, in addition to capturing certain general features of the complex magnetic phase diagram for β-TVO, our results highlight how the CMF approach can become a powerful tool in understanding the nature of magnetic order emerging at low temperatures in frustrated magnets.

Chapter 5

Effect of XXZ anisotropies on a spin-1/2 Heisenberg chain

5.1 Introduction

It is well known that the presence of impurities in solids can lead to quantitative changes in their properties. For example, a disordered metal is expected to have higher resistivity compared to a defect-free metal [180], transition temperature to superconducting order can be altered by the presence of impurities [181], etc. However, in some cases the presence of impurities can even modify the qualitative behaviour of the system. For instance, metals can turn into insulators due to the disorder-induced phenomenon known as Anderson localization [182, 183]. Such qualitative change of behaviour can also occur in magnets. A famous example is the disorder-induced change in the order of phase transitions [184]. Defects in magnetic materials can modify, not only the ground state properties but also the excitation spectrum [50]. Substitution of a magnetic ion by a different ion with the same or different spin, or a magnetic ion coupled to random spin in a lattice, corresponds to presence of defects [185]. Low dimensional systems are very sensitive to disorder and often display dramatic effects in presence of impurities due to the interplay between quantum effects, strong correlations and disorder [41].

Some of the observations of impurity-induced effects in spin systems are emergence of $S = 1/2$ degrees of freedom at the edges, when Cu is doped in a Haldane material [186]. A low concentration of non-magnetic impurities induce a long range magnetic order in spin-Peierls material $CuGeO_3$ [187, 188]. Similar observations have been made for a two-leg spin-1/2 ladder compound $SrCu_2O_3$, where doping of as low as 1% Zn ($S_{imp} = 0$) resulted in antiferromagnetic behaviour. Furthermore, it was shown that corresponding Néel temperature can be increased with increase in concentration of impurities [189]. Several experimental studies have been performed on Sr_2CuO_3 and $SrCuO_2$, spin-1/2 materials which are considered good realizations of 1D Heisenberg model [190]. Experimental investigations reveal reduction in T_N, on introduction of non-magnetic impurity ($S_{imp} = 0$) in $SrCuO_2$ (zig-zag chain) and Sr_2CuO_3 (linear chain)[191]. On the other hand, substitution of ($S_{imp} = 1$) impurity in a spin-1/2 Heisenberg chain is known to result in a Kondo-singlet where the impurity spin is Kondo screened by the two neighboring spins of the chain. Similar to non-magnetic substitution, formation of singlets at ($S_{imp} = 1$) impurity site disrupts the translational invariance of the chain breaking it into finite lengths. This leads to confinement of spinons and results in emergence of a spin gap in low-lying excitations. This has been confirmed experimentally for low concentration of Ni ($S_{imp} = 1$) doping in $SrCuO_2$, where sizeable spin pseudogap appears as a consequence of impurities [192]. While experimental results reveal that doping $S_{imp} = 0, 1$ in spin chain materials suppress long range magnetic ordering temperature [193]. Investi-

gations of replacing a spin-1/2 magnetic ion (Cu^{2+}) with another spin-1/2 ion (Co^{2+}) in spin chain material $SrCuO_2$, reveal that the bulk behaviour switches from Heisenberg to Ising-like. Due to this induced Ising-like anisotropy, magnetic ordering temperature is enhanced, however gapless nature of the spin excitations are not disturbed [51]. Similar behaviours of Néel-type ordering appears in Co based spin-1/2 Ising chain compounds $BaCo_2V_2O_8$ [194] and $SrCo_2V_2O_8$ [195].

Theoretical efforts using field theory, renormalization arguments [185, 196] and numerical methods like quantum Monte Carlo [197, 198] have been successfully employed to investigate properties of low dimensional materials when doped with magnetic (specifically $S_{imp} = 1$) and non-magnetic impurities. Field theoretical and numerical studies using DMRG of *isotropic* spin-1/2 impurity coupled to spin-1/2 chain expects the impurity spin to be over-screened in analogy to Kondo effect [196, 199, 200]. However, experimental results with $S_{imp} = 1/2$ embedded in the chain stresses the importance of anisotropic effects. Motivated by this interesting effect, the model system employed in the following investigations are the spin-1/2 Heisenberg antiferromagnetic model with anisotropic impurities. We have shown in previous chapters that CMF approach successfully captures a number of experimentally observed features by a simple inclusion of short-range spatial correlation, we test this method further by applying it to a model of 1D disordered quantum magnet.

5.2 Model and Method

In order to investigate the effect of anisotropic impurities in magnetic materials, we consider a spin model where a fraction n_{imp} of the randomly selected spin-1/2 sites are replaced by impurity sites. The model considers that the presence of an impurity in the chain induces an anisotropy $\delta = \Delta - 1$ in Heisenberg exchange between impurity sites and its nearest neighbors. The resulting disordered Hamiltonian reads,

$$\mathcal{H} = \sum_{i,i+1\notin \text{imp.}} \mathbf{S}_i \cdot \mathbf{S}_{i+1} + \sum_{j\in \text{imp.}} [(S^-_{j-1} + S^-_{j+1})S^+_{\text{imp},j} + \text{H.c.} + \Delta(S^z_{j-1} + S^z_{j+1})S^z_{\text{imp},j}], \quad (5.1)$$

where $\mathbf{S}_i$ is spin-1/2 operator at non-impurity site i and $\mathbf{S}_{\text{imp},j}$ is a spin-S operator at impurity site j. For the present study, spin of the impurity site is restricted to $S_{imp} = 1/2$. Note that in the absence of impurities (either $n_{imp} = 0$ or $\Delta = 1$), the Hamiltonian reduces to an isotropic spin-1/2 Heisenberg chain. The impurity density, n_{imp} is defined as the ratio of (N_{imp}/N_c) where N_{imp} is number of impurities embedded in the chain consisting

of N_c spins.

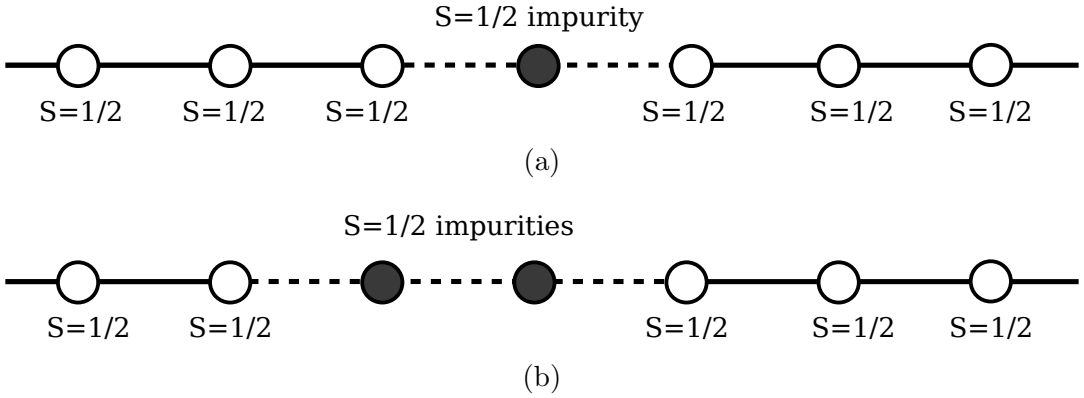

Figure 5.1: A schematic view of spin-1/2 Heisenberg chain with (a) single and (b) two spin-1/2 impurities (filled circle) sitting on adjacent sites. The exchange interaction on the original chain is isotropic (solid line) and that between the magnetic impurity and its neighboring sites is of the XXZ-type.

We utilize cluster mean field approach to study the Hamiltonian with spin-1/2 impurities on one dimensional cluster. As already discussed in previous chapters, CMFT is an extension of a single-site Weiss mean field theory, where instead of a single site we consider a cluster comprising of N_c spins. For one- dimensional system, the edge spins $\mathbf{S_1}$ and $\mathbf{S_{N_c}}$ couple to neighboring cluster via standard mean-field decoupling. Since, there are numerous ways in which impurity sites can be distributed, we average observables over various random configurations N_{av} for a fixed number of impure sites. The edge spins are forced to remain pure in a random configuration to avoid explicit dependence of anisotropy due to the mean field decoupling. As a result the impurity density, n_{imp} can reach a maximum of $(N_c - 2)/N_c$. We present results computed for a cluster of 10 spins (unless specified otherwise). Calculations are also performed for larger cluster sizes for scaling analysis. The nature of interaction is antiferromagnetic therefore, the order parameter, staggered magnetization is defined as:

$$m^z_{st} = \frac{1}{N_{av}} \sum_p \frac{1}{N_c} | \sum_{i=1}^{N_c} (-1)^i \langle S^z_i \rangle_p | \tag{5.2}$$

For the effect in presence of applied field, net magnetization is calculated which is defined as:

$$m^z = \frac{1}{N_{av}} \sum_p \frac{1}{N_c} \sum_{i=1}^{N_c} \langle S^z_i \rangle_p \tag{5.3}$$

For temperature dependent calculations, specific heat and susceptibility are calculated

using:

$$C_v = \frac{1}{N_{av}} \sum_p \frac{1}{N_c} \frac{d\langle H \rangle_p}{dT}; \chi = \frac{1}{N_{av}} \sum_p \frac{d\langle m^z \rangle_p}{dh} \tag{5.4}$$

5.3 Results

We begin by discussing the results obtained via CMFT for XXZ impurity spin chain. Some of the results are compared with DMRG results (not shown here).

5.3.1 Ground state properties

The ground state of an antiferromagnetic spin chain as obtained by CMFT is a mixed state forming valence bonds on alternate sites with presence of very small yet finite (less than 10% of the spin magnitude) staggered magnetization. The presence of an impurity introduces an anisotropy Δ in the bonds connecting the impurity (see Fig. 5.1). In Fig 5.2 (a) we show the variation of m^z_{st} with n_{imp} for N_c=10 (solid lines), 12 (dashed lines) averaged over 20 random configurations. For a particular Δ, increase in number of anisotropic bonds, increases m^z_{st} indicating the formation of stronger Néel order. It is interesting to note that anisotropic strength as low as $\delta = 0.1$ is able induce an ordered state. Since, calculations performed on larger cluster size of $N_c = 12$ (dashed lines), do not show any qualitative difference in the results, most of the analysis will be restricted to a cluster of 10 sites. Fig 5.2 (b) shows the evolution of m^z_{st} for different n_{imp} with increasing the anisotropy strength. It suggests that introducing a single impurity spin ($n_{imp} = 0.1$) in a spin chain of $N_c = 10$ (n_{imp}=0.08 in a spin chain of $N_c = 12$), affects the overall order of the chain. This effect can be further increased by increasing the strength of anisotropy.

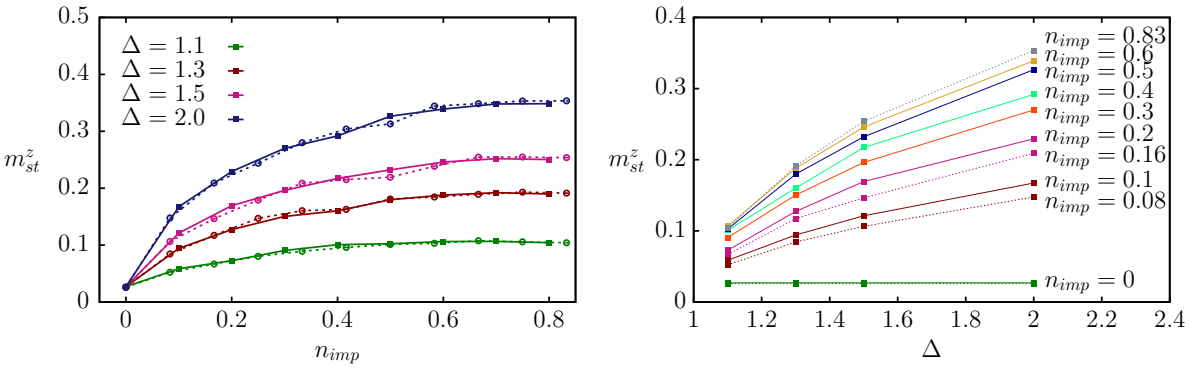

(a) (b)

Figure 5.2: Variation of staggered magnetization m^z_{st} with (a) impurity density n_{imp} for different values of Δ and (b) Δ for fixed n_{imp}. CMFT approach is utilized for a clusters of 10 (solid lines) and 12 (dashed lines) spins where average in each case is taken for 20 random configurations of impurity distribution.

Staggered magnetization is averaged over various random distribution of impure bonds for a fixed number of impurities. Fig. 5.3 shows the dependence of the m^z_{st} with increasing number of random configurations considered for averaging. Due to small cluster sizes, the number of configurations for $n_{imp} = 0.1, 0.8$ cannot be increased. It is evident from Fig. 5.3 (a) that the fluctuations appearing in m^z_{st} can be minimized by increasing the number of configurations. Fig. 5.3 (b) depicts the dependence of number of configurations for different Δ. It suggests that the dependence of m^z_{st} on N_{av} is more significant lower $n_{imp} = 0.2, 0.4$.

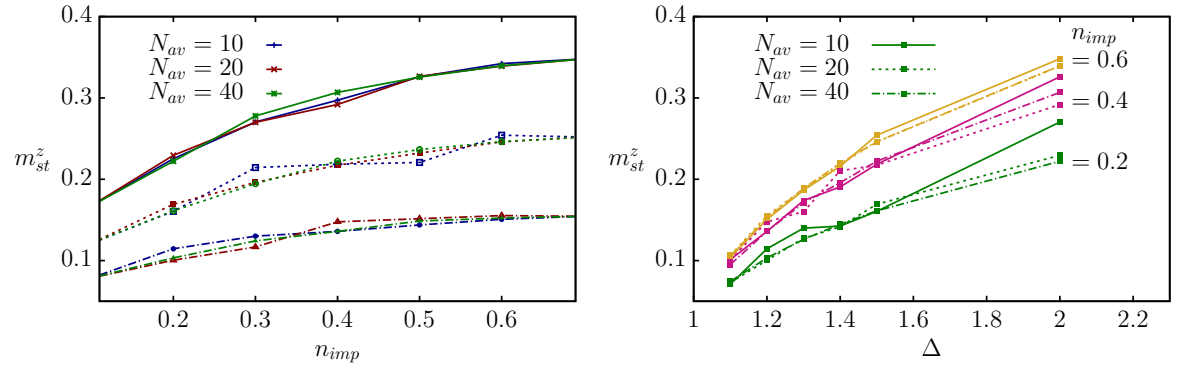

(a) (b)

Figure 5.3: (a) Variation of m^z_{st} with n_{imp} for averaging over different number of random configurations for $\Delta = 1.2$ (dot-dashed lines),$\Delta = 1.5$ (dashed lines), $\Delta = 2.0$ (solid lines). (b) Variation of m^z_{st} with Δ with increasing N_{av} for $n_{imp} = 0.2, 0.4, 0.6$.

While the qualitative behaviour of m^z_{st} calculated using CMFT matches very well with

that obtained via DMRG, results obtained using CMFT suffer from finite size mean field effects. The finite size effect leads to higher m^z_{st} in comparison to DMRG. This effect is more pronounced for small n_{imp}, as for low n_{imp} the number of Heisenberg bonds is larger and CMFT breaks the rotational symmetry of the Hamiltonian. CMFT results can be further improved by increasing the cluster size, Fig. 5.4 shows m^z_{st} for number impurities (N_i) fixed to $N_c/2$ and N_c-2 for respective cluster sizes. Fluctuations for the case of $N_i = N_c/2$ appear as the average is taken for very less number of random configurations ($N_{av} = 10$). We observe that m^z_{st} increases with increasing cluster size upto a certain cluster size, after which it starts to decrease. Power law fits to the data suggests that on further increasing the size, m^z_{st} will reach the value closer to the one obtained by DMRG (solid circles in 5.4). For $N_i = N_c - 2$, finite size scaling analysis show an increase in m^z_{st} with increasing N_c. This is counter-intuitive as for completely Ising($\Delta \to \infty$) or Heisenberg ($\Delta = 1$) spin chain, m^z_{st} decreases with system size. However in our approach, the MF bond remains Heisenberg-like while the impure bonds are XXZ-type or the extreme case Ising type. For $N_c = 4$, the number of impure bonds within the cluster is 3, while there are 2 mean field decoupled Heisenberg bonds. With increasing number of spins in a cluster, the ratio of impure bonds to pure bonds keep on increasing as the number of isotropic MF bonds remain the same. Due to this competition among Heisenberg bonds and Ising-type (XXZ-type) bonds, m^z_{st} increases with system size, eventually saturating towards its maximum value possible value. Solid circles in Fig. 5.4 (b) shows the results obtained by DMRG corresponding to $n_{imp} = 0.8$. Power law fits of CMFT cluster size scaling show that the agreement with DMRG results is higher for larger anisotropy in comparison to $\Delta = 1.1$.

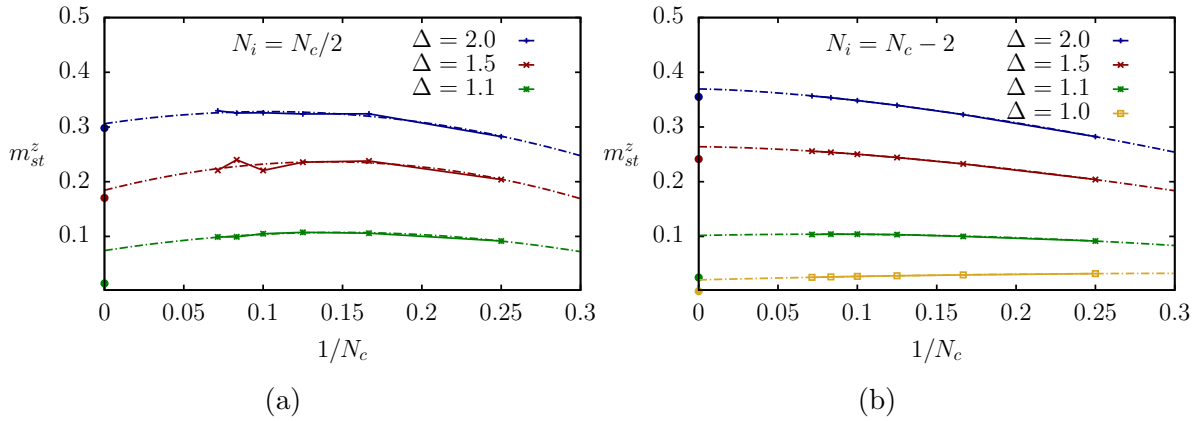

Figure 5.4: Cluster size scaling of m^z_{st} for various Δ with number of impurities (a) $N_i = N_c/2$ and (b) $N_i = N_c - 2$. Average is taken for maximum of 10 random configurations. Dot-dashed lines are power law fits. Solid circles are the results computed using DMRG for corresponding Δ and n_{imp}.

5.3.2 Temperature dependence

In previous section, we have established that antiferromagnetic order is induced in an isotropic spin chain on substitution of a spin-1/2 magnetic impurity resulting in anisotropic neighboring bonds. We now discuss, signatures of phase transition in specific heat (C_v) and susceptibility (χ) with increasing temperature for different values of impurity density n_{imp} and Δ. Fig. 5.5 (a) shows variation of C_v with temperature for different n_{imp} with $\Delta = 2.0$. For a completely isotropic spin chain ($n_{imp} = 0.0$), specific heat changes smoothly with broadened peak near $T = 0.4$. For impurity density as low as $n_{imp} = 0.1$, a small peak emerges as a consequence of phase transition from a Néel phase to a paramagnet. The peak in C_v sharpens when n_{imp} increases. The huge bump in C_v for higher temperature is a consequence of continuously decreasing correlations among spins. The origin of this behaviour is discussed in detail in Section 3.3.2. Fig. 5.5 (b) shows that χ decreases with increase in impurity density. Susceptibility results in the completely Heisenberg limit show an unusual curvature in $T < 0.25$. Susceptibility results differ from the behaviour expected from the ideal 1D antiferromagnetic Heisenberg chain. The result shown here is a consequence of the mixed Néel order with dimer correlations as obtained using CMFT. The susceptibility matches with the one expected from an alternating exchange antiferromagnetic chain (weakly coupled dimers) [201]. A significant deviation appears for high n_{imp} in lower temperature region while the behavior qualitatively remains same in higher T limit.

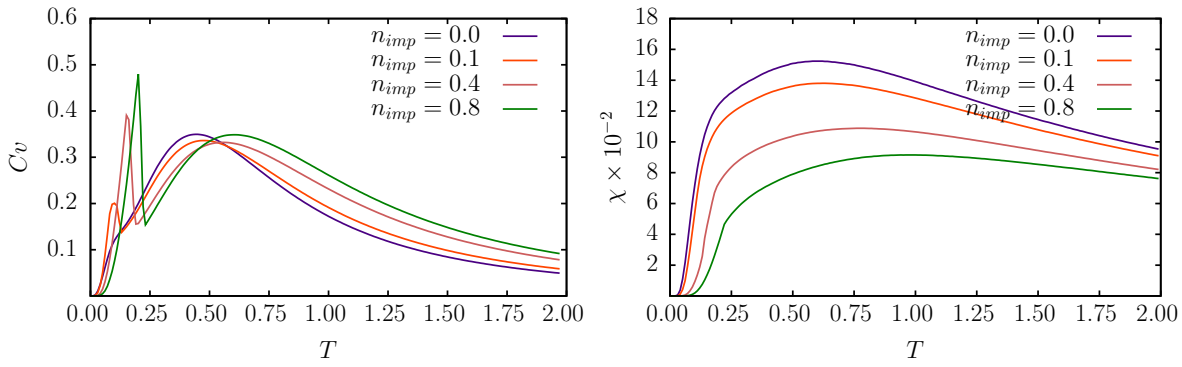

(a) (b)

Figure 5.5: Variation of (a) specific heat and (b) susceptibility with temperature for different values of impurity density while the anisotropy strength is fixed to $\Delta = 2.0$.

In Fig. 5.6, we show the dependence of Δ on specific heat and susceptibility for different impurity densities. Specific heat results reveal that increase in the anisotropy strength (Δ), increases the transition temperature as well as the specific heat peak. This

effect is consistent for all impurity densities $n_{imp} = 0.1, 0.4, 0.8$ shown in Fig. 5.6 (a-c). Susceptibility results of a completely isotropic case ($n_{imp} = 0.0$) calculated using CMFT is similar to that of χ obtained for antiferromagnetic dimer chain [201]. For $n_{imp} = 0.1$ no significant change in susceptibility is identified on increasing Δ. Further increase in impurity density, leads to decrease in χ which is prominent for higher Δ.

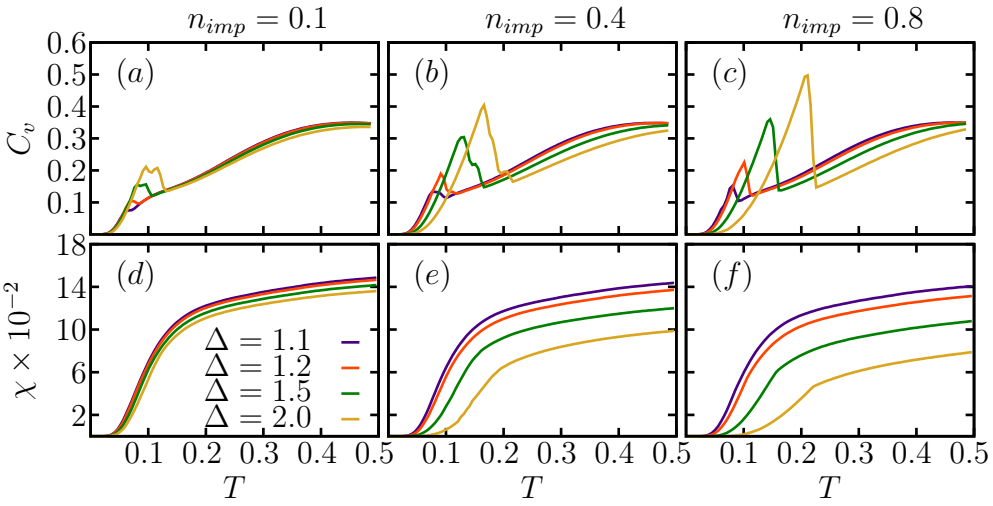

Figure 5.6: Variation of specific heat and susceptibility for different values of Δ. The results are obtained for (a,d) $n_{imp} = 0.1$, (b,e) $n_{imp} = 0.4$ and (c,f) $n_{imp} = 0.8$.

Presence of impurity bonds induce a Néel order which melts to a disordered state with increase in temperature. As this effect is more significant in low temperature regime, Fig 5.7 and 5.8 shows the variation of C_v and χ with temperature for different n_{imp} with fixed $\Delta = 2.0$. Transition temperature increases with increase in n_{imp}. For high n_{imp}, the peak in specific heat is very sharp owing to the Ising like nature of most of the bonds. For intermediate values of impurity densities, number of possible random distribution of the impure spins is huge leading to difference in magnetic order. Different colours in Fig. 5.7 corresponds to different N_{av}. For intermediate values of n_{imp}, specific heat show a broad peak which becomes smooth with further increase in N_{av}. Non-monotonic behaviour in C_v for intermediate n_{imp} are a direct consequence of the distribution of impure spins. We believe these peculiarities might be a finite size effect and will lead to a clear phase transition in thermodynamic limit.

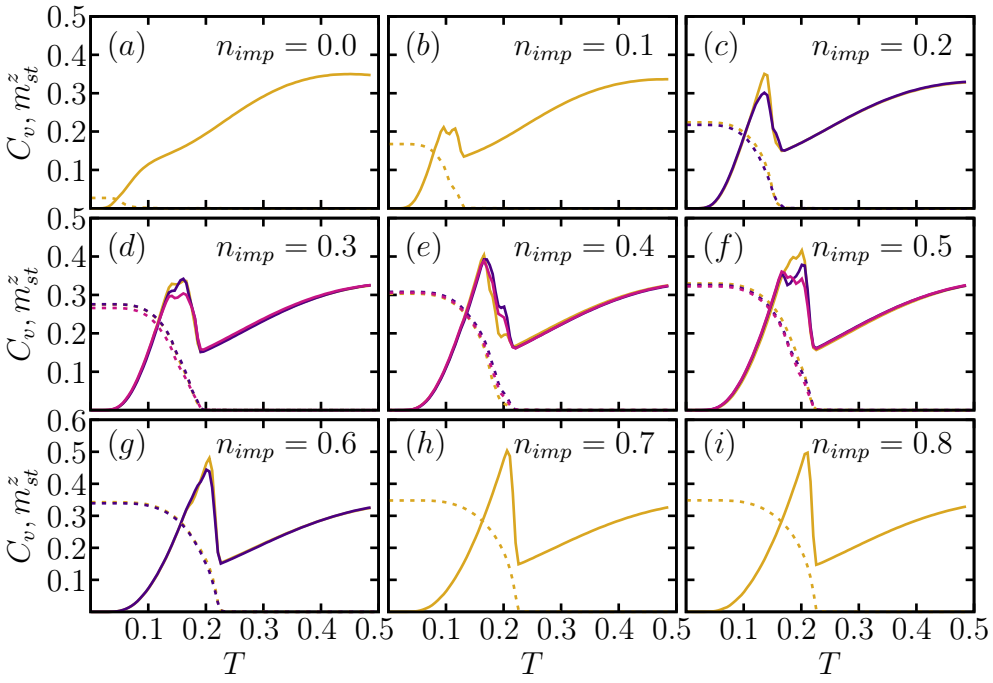

Figure 5.7: Variation of specific heat (solid lines) and staggered magnetization (dashed lines) with temperature obtained using CMFT on a cluster size consisting of 10 spins. Dependence on n_{imp} is shown for various number of random configurations, N_{av})= 10 (yellow), 20(blue), 40 (red).

Fig. 5.8 shows dependence of χ with increasing number of random configurations used for averaging. It is interesting to note that susceptibility decreases with increase in impurity density. Impurity effects in susceptibility are more prevalent for higher n_{imp}, where it shows a discontinuity $T \sim 0.25$ (see Fig. 5.8 (g)-(i)). Susceptibility results on $SrCo_2V_2O_8$ [195] show a signature similar to χ obtained for higher n_{imp}. $SrCo_2V_2O_8$ is expected be described by XXZ model, however inter-chain interactions induce an order in the material at low temperatures. The discontinuity identified in χ is a result of vanishing of Néel order.

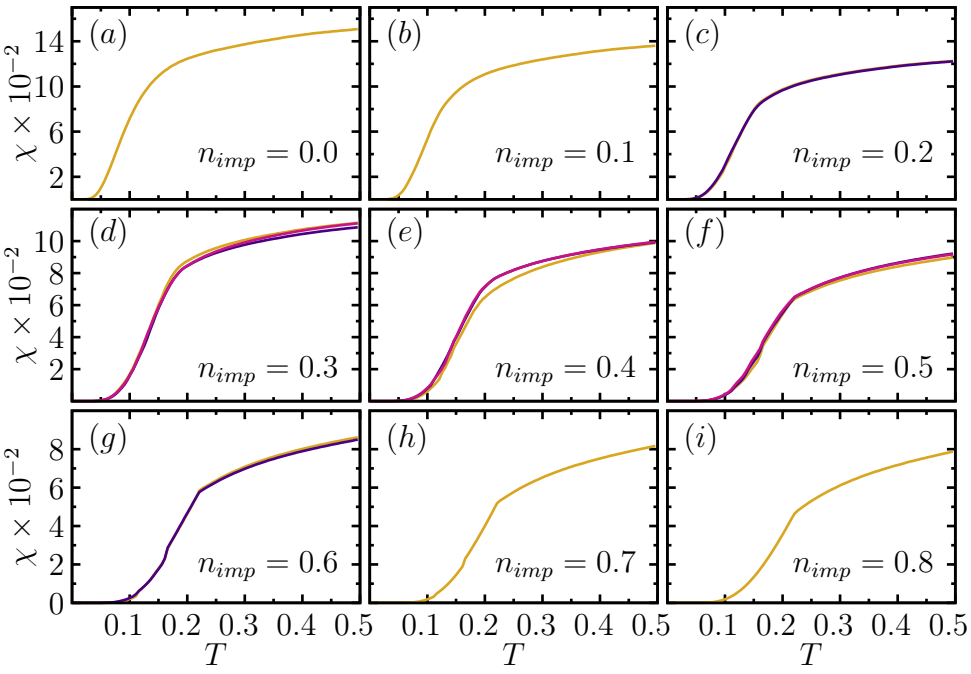

Figure 5.8: Variation of susceptibility with temperature obtained using CMFT on a cluster size consisting of 10 spins ($\Delta = 2.0$). Dependence on n_{imp} is shown for various number of random configurations = 10 (yellow), 20(blue), 40 (red). (update the figure with label a,b,c)

5.3.3 Magnetic Field Dependence

In this section, we discuss the dependence of magnetization as a function of applied magnetic field. We calculate staggered magnetization (m^z_{st}) as well as total magnetization (m^z) for different values of impurity densities. In the absence of impurities ($n_{imp} = 0$), the Hamiltonian Eq. 5.1 reduces to an isotropic Heisenberg model on a 1D chain, while $n_{imp} = 1$ corresponds to the XXZ model. For $n_{imp} = 0$, total magnetization continuously increases with applied field until saturation where all the spins align in the direction of field (see Fig 5.9 (a)). Small step like features obtained in net magnetization is a consequence of finite size effects in CMFT which can be reduced with increasing cluster size. Numerically exact results obtained from DMRG, begins from zero magnetization owing to gapless nature of 1D Heisenberg AFM and continuously increases uptil saturation field. While the intermediate behaviour of m^z obtained by CMFT do not match with the results of DMRG, it is interesting to note that value the saturation field matches very well. Néel order is formed on substitution of impurities, which vanishes above a finite magnetic field. This critical value of field above which Néel order vanishes increases with increase in n_{imp}. This is understood as the closing of the gap existing above the ground

state. This feature is reflected in m^z remaining zero upto a finite strength of magnetic field which is equal to the energy gap above the ground state. In the XXZ limit, this gap is related to the anisotropy in Hamiltonian [202, 203]. Note that results for some field values are omitted as for those applied field values, mean fields did not converge for some random configurations. It is interesting as mean fields converged for all other values of applied field with the same set of random configurations. Further increasing the impurity density, increases the saturation magnetic field strength. For the extreme case, when $n_{imp} = 0.8$, all the bonds except mean field decoupled ones are anisotropic in nature. Disregarding the field values of non-convergence, the behaviour of net magnetization and staggered magnetization reveal formation of Néel order in low fields and fully saturated state in high field limit. The results of m^z with applied field matches with those obtained in $BaCo_2V_2O_8$ [204]. This material is expected to be explained by a quasi-1D XXZ model with $\Delta = 2$. An ideal XXZ chain model will show a quantum phase transition from the Néel ordered phase to Tomonaga Luttinger liquid to saturated state at high fields. Further investigations are required to understand this intermediate order appearing in presence of field using CMFT.

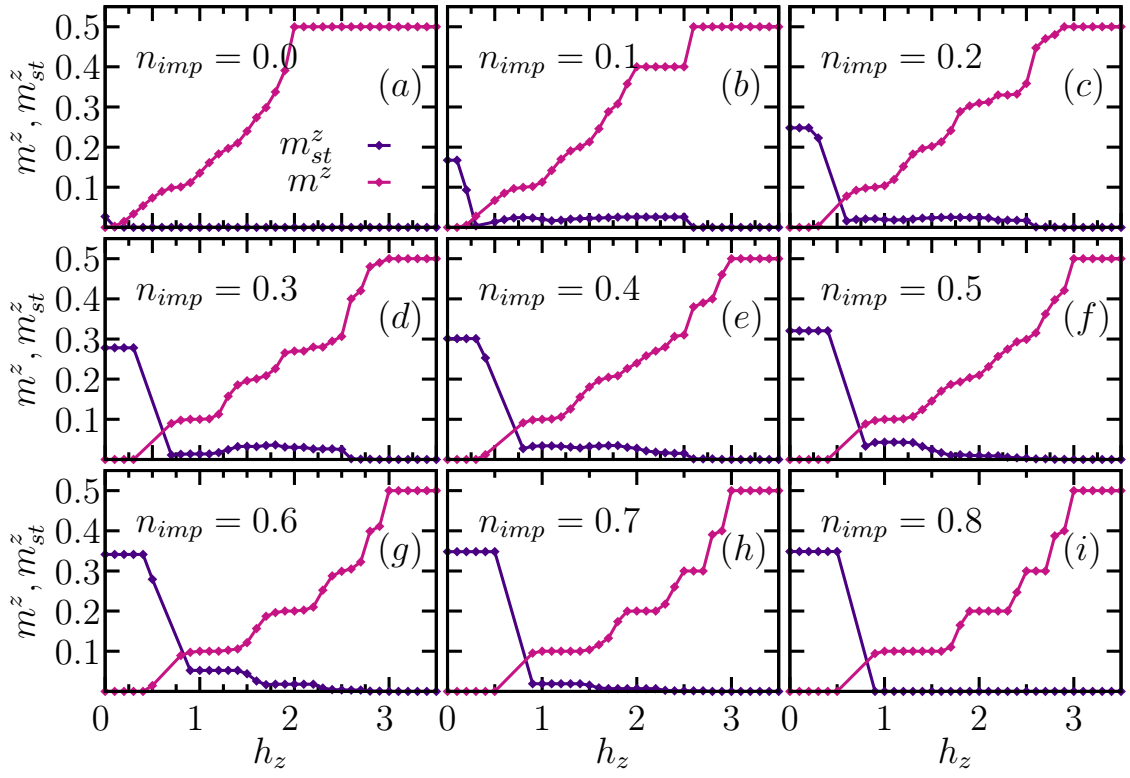

Figure 5.9: Variation of total magnetization, m^z (pink) and staggered magnetization m^z_{st} (purple) with increasing applied magnetic field for different values of n_{imp} as indicated in the panels. Δ is fixed to 2 and N_{av} is set to 10.

5.4 Conclusions

We study a disordered spin chain model using CMFT where a fraction of spin-1/2 magnetic sites are replaced with $S_{imp} = 1/2$ impurities. The effect of the impurity is to introduce an XXZ-type anisotropy in the neighboring bonds. Ground state properties of the model are evaluated for different impurity density and anisotropy strength. We conclude that Néel type magnetic order is induced in the spin chain even in the presence of a single impurity. Staggered magnetization increases with increase in the impurity density as well as the anisotropy strength. Temperature dependence of specific heat and susceptibility reveal a phase transition from a Néel order to a paramagnet. The transition temperature to a paramagnet and the size of peak in specific heat increases with increase in n_{imp} and Δ. In presence of magnetic field, total magnetization remains zero for low values of applied field. This pertains to the spin gap present above the ground state of the XXZ impurity chain. Preliminary calculations using DMRG (not part of this thesis) confirm that the results presented here within CMFT are qualitatively consistent with those of DMRG. One can, therefore, conclude that CMFT approach can prove to be the simplest method of choice for gaining insights into the physics of disordered magnetic systems.

Chapter 6

Summary and Outlook

Understanding the phenomena associated with a large number of interacting quantum particles is challenging as the exact solutions are rarely available and the brute force numerical exact diagonalization of Hamiltonians are practically restricted to few tens of spins. Therefore, various approximate methods are constantly developed in order to make progress towards understanding the physics of such Hamiltonians. Mean field theory is the simplest approximation which ignores spatial and quantum fluctuations among particles. Despite its limitations, it is frequently adopted as a starting point to get qualitative insights about any complex model. Over the years, this approach has been systematically improved by including local correlations. Cluster mean field theory (CMFT), is an extension of Weiss mean field theory which attempts to capture quantum correlations which are otherwise ignored in simple MFT. It treats interactions located within the cluster exactly, while using conventional mean field decoupling interactions among different clusters. The thesis focuses on capturing the magnetic orders and phase transitions appearing in Heisenberg models motivated by low dimensional real materials using CMFT.

We test the applicability of CMFT to Heisenberg model written for quasi-1D tetramer compound $CuInVO_5$. We find that CMFT is able to qualitatively identify the origin of an extra peak observed in low temperature experimental results of specific heat. The careful analysis is performed using correlations of different spin pairs in the parameter space. It reveals an unexpected competition between inter-tetramer and intra-tetramer interactions. Material specific choice of parameter suggests that it lies in the strongly competing regime, therefore, treating inter-tetramer interaction exactly is important to capture the relevant aspects of this system. Magnetic susceptibility calculations confirmed the pres-

ence of three distinct regimes in temperature corresponding to a systematic melting of singlet order. Furthermore, multiple spin-flop transitions are identified in the presence of field which matches with experimental observation of magnetic plateaus. These findings emphasize on the relevance of considering weak (inter-tetramer) interactions in low dimensional systems realized in real magnetic materials.

In the second problem, the CMF approach is utilized to understand experimental results for a frustrated ferromagnetic compound β-$TeVO_4$. With the aim to capture the important features observed in the material, an anisotropic Heisenberg model with nn FM and nnn AFM interactions on weakly coupled zig-zag spin-1/2 chains is investigated. While some of the sophisticated computational approaches like QMC fail in this regime, CMFT is able to identify the series of phase transitions reported experimentally. A detailed analysis on the dependence on anisotropy and inter-chain coupling strength concludes that an appropriate combination of inter-chain coupling and anisotropy in nnn interaction is required in obtaining long range orders relevant for this frustrated system. CMFT was able to uncover complex phases like vector chiral ground state and quadrupolar phases in the presence of magnetic field. Moreover, a specific anomaly of re-entrant transition is also found similar to experimental observations. It is remarkable that some of the experimentally observed features are captured by CMFT, however a complete understanding of this complex material require a 3-dimensional cluster with anisotropic interactions. To this end, we highlight the similarities as well as differences between experimental results and cluster mean field calculations.

The last project discusses the effects of anisotropic impurities in an isotropic spin-1/2 Heisenberg chain system. We conclude that a fraction of impure sites, which modify the anisotropy of interaction with neighboring sites, is able to induce a Néel order. We also discuss the dependence of transition temperature on impurity density as well as anisotropy strength.

While CMFT emerges as a tool to understand experimental features appearing in low dimensional magnets, some interesting inferences drawn from our calculations can motivate experimental studies in future. For instance, experimentally observing the crossover between two distinct singlet orders identified in the tetramer model. Further work on the material suggests that $CuInVO_5$ lies close to the quantum critical point. These features may be studied by applying pressure or synthesizing materials with specific interaction constants. We have studied the dependency of anisotropic strength and interchain coupling in stabilizing vector chiral orders for the problem of coupled zig-zag chains. The competition of the same emerges as signatures in specific heat, which can also be studied

in experiments with an appropriate control parameter. The last problem in the thesis gives a detailed analysis for an impurity problem with variations in impurity density and anisotropy strength. As experimental studies of anisotropic impurities are limited, verification of the results (such as m^z, C_v and χ) obtained numerically should motivate further studies.

In conclusion, the thesis highlights that the CMF approach can become a powerful tool in understanding the nature of magnetic order emerging at low temperatures. CMFT recovers the correlations important for the long range orders which are otherwise lost in computationally possible exact diagonalization results. The technique is useful for frustrated magnets as it can capture subtle competition between different magnetic ordering. In the mean field spirit, the approach allows access to both thermal as well as quantum fluctuations at level of finite-size calculations.

Bibliography

[1] J. George Bednorz and K. Alex Müller. Possible high T_c superconductivity in the Ba-La-Cu-O system. *Zeitschrift für Physik B Condensed Matter*, 64(2):189–193, 1986.

[2] Elbio Dagotto. Correlated electrons in high-temperature superconductors. *Reviews of Modern Physics*, 66(3):763, 1994.

[3] Alexander Vasiliev, Olga Volkova, Elena Zvereva, and Maria Markina. Milestones of low-D quantum magnetism. *npj Quantum Materials*, 3(1):1–13, 2018.

[4] Thierry Giamarchi. *Quantum physics in one dimension*, volume 121. Clarendon press, 2003.

[5] SungBin Lee, Ribhu K. Kaul, and Leon Balents. Interplay of quantum criticality and geometric frustration in columbite. *Nat. Phys.*, 6(9):702–706, 2010.

[6] Stephen J. Blundell and Francis L. Pratt. Organic and molecular magnets. *Journal of Physics: Condensed Matter*, 16(24):R771, 2004.

[7] Florian Meier, Jeremy Levy, and Daniel Loss. Quantum computing with spin cluster qubits. *Physical review letters*, 90(4):047901, 2003.

[8] Jun-Sen Xiang, Cong Chen, Wei Li, Xian-Lei Sheng, Na Su, Zhao-Hua Cheng, Qiang Chen, and Zi-Yu Chen. Criticality-enhanced magnetocaloric effect in quantum spin chain material copper nitrate. *Scientific reports*, 7(1):1–11, 2017.

[9] A. Honecker and S. Wessel. Magnetocaloric effect in quantum spin$-s$ chains. *Condensed Matter Physics*, 12(3):399–410, 2009.

[10] S. Sahling, G. Remenyi, C. Paulsen, P. Monceau, V. Saligrama, C. Marin, A. Revcolevschi, L.P. Regnault, S. Raymond, and J.E. Lorenzo. Experimental realization of long-distance entanglement between spins in antiferromagnetic quantum spin chains. *Nature Physics*, 11(3):255–260, 2015.

[11] Bernhard Keimer, Steven A. Kivelson, Michael R. Norman, Shinichi Uchida, and J Zaanen. From quantum matter to high-temperature superconductivity in copper oxides. *Nature*, 518(7538):179–186, 2015.

[12] Rodney J. Baxter. *Exactly solved models in statistical mechanics*. Elsevier, 2016.

[13] Ernst Ising. Beitrag zur theorie des ferromagnetismus. *Z. Physik*, 31:253–258, 1925.

[14] D. Gignoux and M. Schlenker. Fundamentals, magnetism and de lacheisserie, e du trémolet, 2005.

[15] L.J. De Jongh. Experiments on simple magnetic model systems. *Journal of Applied Physics*, 49(3):1305–1310, 1978.

[16] Hans-Jürgen Mikeska and Alexei K Kolezhuk. One-dimensional magnetism. In *Quantum magnetism*, pages 1–83. Springer, 2004.

[17] Albert Furrer, Joel F Mesot, and Thierry Strässle. *Neutron scattering in condensed matter physics*, volume 4. World Scientific Publishing Company, 2009.

[18] Rudolf Ernst Peierls and Rudolf Peierls. *Surprises in theoretical physics*. Princeton University Press, 1979.

[19] Werner Heisenberg. Zur theorie des ferromagnetismus. In *Original Scientific Papers Wissenschaftliche Originalarbeiten*, pages 580–597. Springer, 1985.

[20] Sabyasachi Chatterjee. Heisenberg and ferromagnetism. *Resonance*, 9(8):57–66, 2004.

[21] John Hubbard. Electron correlations in narrow energy bands. *Proceedings of the Royal Society of London. Series A. Mathematical and Physical Sciences*, 276(1365):238–257, 1963.

[22] Assa Auerbach. *Interacting electrons and quantum magnetism*. Springer Science & Business Media, 2012.

[23] Kerson Huang. *Introduction to statistical physics*. CRC press, 2009.

[24] W.P. Wolf. The Ising model and real magnetic materials. *Brazilian Journal of Physics*, 30(4):794–810, 2000.

[25] Tôru Moriya. Anisotropic superexchange interaction and weak ferromagnetism. *Physical review*, 120(1):91, 1960.

[26] Chen-Ning Yang and Chen-Ping Yang. One-dimensional chain of anisotropic spin-spin interactions. I. proof of Bethe's hypothesis for ground state in a finite system. *Physical Review*, 150(1):321, 1966.

[27] Chanchal K. Majumdar and Dipan K. Ghosh. On next-nearest-neighbor interaction in linear chain. i. *Journal of Mathematical Physics*, 10(8):1388–1398, 1969.

[28] Chanchal K. Majumdar. Antiferromagnetic model with known ground state. *Journal of Physics C: Solid State Physics*, 3(4):911, 1970.

[29] F. Duncan M. Haldane. Continuum dynamics of the 1-D Heisenberg antiferromagnet: Identification with the O(3) nonlinear sigma model. *Physics Letters A*, 93(9):464–468, 1983.

[30] L.D. Faddeev and L.A. Takhtajan. What is the spin of a spin wave? *Physics Letters A*, 85(6-7):375–377, 1981.

[31] D.A. Tennant, T.G. Perring, R.A. Cowley, and S.E. Nagler. Unbound spinons in the $S = 1/2$ antiferromagnetic chain $KCuF_3$. *Physical review letters*, 70(25):4003, 1993.

[32] R. Botet and R. Jullien. Ground-state properties of a spin-1 antiferromagnetic chain. *Physical Review B*, 27(1):613, 1983.

[33] Shaolong Ma, Collin Broholm, Daniel H. Reich, B.J. Sternlieb, and R.W. Erwin. Dominance of long-lived excitations in the antiferromagnetic spin-1 chain NENP. *Physical review letters*, 69(24):3571, 1992.

[34] J.P. Renard, M. Verdaguer, L.P. Regnault, W.A.C. Erkelens, J. Rossat-Mignod, and W.G. Stirling. Presumption for a quantum energy gap in the quasi-one-dimensional S=1 Heisenberg antiferromagnet $Ni(C_2H_8N_2)_2NO_2(ClO_4)$. *Europhysics Letters*, 3(8):945, 1987.

[35] A.P. Ramirez. Strongly geometrically frustrated magnets. *Annual Review of Materials Science*, 24(1):453–480, 1994.

[36] H.T. Diep. *Frustrated spin systems*. World Scientific, 2013.

[37] Claudine Lacroix, Philippe Mendels, and Frédéric Mila. *Introduction to frustrated magnetism: materials, experiments, theory*, volume 164. Springer Science & Business Media, 2011.

[38] G. H. Wannier. Antiferromagnetism. the triangular ising net. *Physical Review*, 79(2):357, 1950.

[39] Y. Tokiwa, T. Radu, R. Coldea, H. Wilhelm, Z. Tylczynski, and F. Steglich. Magnetic phase transitions in the two-dimensional frustrated quantum antiferromagnet Cs_2CuCl_4. *Physical Review B*, 73(13):134414, 2006.

[40] Radu Coldea, D.A. Tennant, A.M. Tsvelik, and Z. Tylczynski. Experimental realization of a 2D fractional quantum spin liquid. *Physical review letters*, 86(7):1335, 2001.

[41] Elbio Dagotto and T. M. Rice. Surprises on the way from one- to two-dimensional quantum magnets: The ladder materials. *Science*, 271(5249):618–623, 1996.

[42] Marko Bosiočić, Fabrice Bert, Siân E Dutton, Robert J. Cava, Peter J. Baker, Miroslav Požek, and Philippe Mendels. Possible quadrupolar nematic phase in the frustrated spin chain licusbo 4: An nmr investigation. *Physical Review B*, 96(22):224424, 2017.

[43] M. Mourigal, M. Enderle, B. Fåk, R.K. Kremer, J.M. Law, A. Schneidewind, A Hiess, and A. Prokofiev. Evidence of a bond-nematic phase in licuvo 4. *Physical Review Letters*, 109(2):027203, 2012.

[44] H Eugene Stanley. Introduction to phase transitions and critical phenomena, 1971.

[45] Pierre Curie. *Propriétés magnétiques des corps a diverses températures*. Number 4. Gauthier-Villars et fils, 1895.

[46] N. D. Mermin and H. Wagner. Absence of ferromagnetism or antiferromagnetism in one- or two-dimensional isotropic Heisenberg models. *Phys. Rev. Lett.*, 17(0):1133–1136, 1966.

[47] Subir Sachdev. *Quantum Phase Transitions*. Cambridge University Press, 2011.

[48] Lincoln Carr. *Understanding quantum phase transitions*. CRC press, 2010.

[49] Shivaji Lal Sondhi, S.M. Girvin, J.P. Carini, and D. Shahar. Continuous quantum phase transitions. *Reviews of modern physics*, 69(1):315, 1997.

[50] H. Alloul, J. Bobroff, M. Gabay, and P.J. Hirschfeld. Defects in correlated metals and superconductors. *Reviews of Modern Physics*, 81(1):45, 2009.

[51] Koushik Karmakar, Markos Skoulatos, Giacomo Prando, Bertran Roessli, Uwe Stuhr, Franziska Hammerath, Christian Rüegg, and Surjeet Singh. Effects of quantum spin-1/2 impurities on the magnetic properties of zigzag spin chains. *Physical review letters*, 118(10):107201, 2017.

[52] Hans Bethe. On the theory of metals. *Z. Physik*, 71:205–226, 1931.

[53] Bill Sutherland. *Beautiful models: 70 years of exactly solved quantum many-body problems*. World Scientific Publishing Company, 2004.

[54] David P. Landau and Kurt Binder. *A guide to Monte Carlo simulations in statistical physics*. Cambridge university press, 2014.

[55] Sei Suzuki, Jun-ichi Inoue, and Bikas K. Chakrabarti. *Quantum Ising phases and transitions in transverse Ising models*, volume 862. Springer, 2012.

[56] Henk W.J. Blöte and Youjin Deng. Cluster monte carlo simulation of the transverse Ising model. *Physical Review E*, 66(6):066110, 2002.

[57] E.Y. Loh Jr., J.E. Gubernatis, R.T. Scalettar, S.R. White, D.J. Scalapino, and R.L. Sugar. Sign problem in the numerical simulation of many-electron systems. *Physical Review B*, 41(13):9301, 1990.

[58] Dominik Hangleiter, Ingo Roth, Daniel Nagaj, and Jens Eisert. Easing the monte carlo sign problem. *Science advances*, 6(33):eabb8341, 2020.

[59] Steven R. White. Density matrix formulation for quantum renormalization groups. *Physical review letters*, 69(19):2863, 1992.

[60] Steven R. White. Density-matrix algorithms for quantum renormalization groups. *Physical Review B*, 48(14):10345, 1993.

[61] Frank Verstraete, Valentin Murg, and J. Ignacio Cirac. Matrix product states, projected entangled pair states, and variational renormalization group methods for quantum spin systems. *Advances in Physics*, 57(2):143–224, 2008.

[62] V.K. Saxena. Effect of dilution on phase transitions in a transverse Ising model. *Physical Review B*, 27(11):6884, 1983.

[63] Román Orús. A practical introduction to tensor networks: Matrix product states and projected entangled pair states. *Annals of Physics*, 349:117–158, 2014.

[64] L.G. Marland. Series expansions for the zero-temperature transverse Ising model. *Journal of Physics A: Mathematical and General*, 14(8):2047, 1981.

[65] Kirill K. Zhuravlev. Molecular-field theory method for evaluating critical points of the Ising model. *Physical Review E*, 72(5):056104, 2005.

[66] Daniel C. Mattis. Molecular-field theory with correlations. *Physical Review B*, 19(9):4737, 1979.

[67] Leo P. Kadanoff. More is the same; phase transitions and mean field theories. *Journal of Statistical Physics*, 137(5-6):777, 2009.

[68] Anders W. Sandvik. Computational studies of quantum spin systems. In *AIP Conference Proceedings*, volume 1297, pages 135–338. American Institute of Physics, 2010.

[69] Pierre Weiss. L'hypothèse du champ moléculaire et la propriété ferromagnétique. 1907.

[70] F. London. On the problem of the molecular theory of superconductivity. *Physical Review*, 74(5):562, 1948.

[71] Nigel Goldenfeld. *Lectures on phase transitions and the renormalization group*. CRC Press, 2018.

[72] Hans A. Bethe. Statistical theory of superlattices. *Proceedings of the Royal Society of London. Series A-Mathematical and Physical Sciences*, 150(871):552–575, 1935.

[73] Lars Onsager. Crystal statistics. i. a two-dimensional model with an order-disorder transition. *Physical Review*, 65(3-4):117, 1944.

[74] Takehiko Oguchi. A theory of antiferromagnetism, II. *Progress of Theoretical Physics*, 13(2):148–159, 1955.

[75] Y. Shibata, S. Nishimoto, and Y. Ohta. Charge ordering in the one-dimensional extended Hubbard model: Implication to the TMTTF family of organic conductors. *Physical Review B*, 64(23):235107, 2001.

[76] Anders W. Sandvik. Multichain mean-field theory of quasi-one-dimensional quantum spin systems. *Physical review letters*, 83(15):3069, 1999.

[77] H.J. Schulz. Dynamics of coupled quantum spin chains. *Physical review letters*, 77(13):2790, 1996.

[78] Lars Onsager. Electric moments of molecules in liquids. *Journal of the American Chemical Society*, 58(8):1486–1493, 1936.

[79] G.M. Wysin and J. Kaplan. Correlated molecular-field theory for Ising models. *Physical Review E*, 61(6):6399, 2000.

[80] Z. Chvoj, J. Kudrnovskỳ, and V. Drchal. Ordering in random overlayers: the correlated cluster mean-field method. *Journal of Physics: Condensed Matter*, 22(39):395005, 2010.

[81] F.M. Zimmer, M. Schmidt, and S.G. Magalhaes. Correlated cluster mean-field theory for spin-glass systems. *Physical Review E*, 89(6):062117, 2014.

[82] F.M. Zimmer, M. Schmidt, and Jonas Maziero. Quantum correlated cluster mean-field theory applied to the transverse Ising model. *Physical Review E*, 93(6):062116, 2016.

[83] Daisuke Yamamoto, Akiko Masaki, and Ippei Danshita. Quantum phases of hard-core bosons with long-range interactions on a square lattice. *Physical Review B*, 86(5):054516, 2012.

[84] J.B. Fouet, P. Sindzingre, and C. Lhuillier. An investigation of the quantum $J_1-J_2-J_3$ model on the honeycomb lattice. *The European Physical Journal B-Condensed Matter and Complex Systems*, 20(2):241–254, 2001.

[85] D.C. Cabra, C.A. Lamas, and H.D. Rosales. Quantum disordered phase on the frustrated honeycomb lattice. *Physical Review B*, 83(9):094506, 2011.

[86] AF Albuquerque, David Schwandt, Balazs Hetenyi, Sylvain Capponi, Matthieu Mambrini, and AM Läuchli. Phase diagram of a frustrated quantum antiferromagnet on the honeycomb lattice: Magnetic order versus valence-bond crystal formation. *Physical Review B*, 84(2):024406, 2011.

[87] Dorota Gotfryd, Juraj Rusnačko, Krzysztof Wohlfeld, George Jackeli, Ji ří Chaloupka, and Andrzej M. Oleś. Phase diagram and spin correlations of the Kitaev-Heisenberg model: Importance of quantum effects. *Phys. Rev. B*, 95(11):024426, 2017.

[88] Katsuhiro Morita, Masanori Kishimoto, and Takami Tohyama. Ground-state phase diagram of the Kitaev-Heisenberg model on a kagome lattice. *Physical Review B*, 98(13):134437, 2018.

[89] Yong-Zhi Ren, Ning-Hua Tong, and Xin-Cheng Xie. Cluster mean-field theory study of $J_1 - J_2$ Heisenberg model on a square lattice. *Journal of Physics: Condensed Matter*, 26(11):115601, 2014.

[90] Daisuke Yamamoto, Giacomo Marmorini, and Ippei Danshita. Magnetization process of spin-1/2 Heisenberg antiferromagnets on a layered triangular lattice. *Journal of the Physical Society of Japan*, 85(2):024706, 2016.

[91] Daisuke Yamamoto, Giacomo Marmorini, and Ippei Danshita. Microscopic model calculations for the magnetization process of layered triangular-lattice quantum antiferromagnets. *Physical review letters*, 114(2):027201, 2015.

[92] S.R. Hassan, L. de Medici, and A-M.S. Tremblay. Supersolidity, entropy, and frustration: t-t'-V model of hard-core bosons on the triangular lattice. *Physical Review B*, 76(14):144420, 2007.

[93] A. Fabricio Albuquerque, Nicolas Laflorencie, Jean-David Picon, and Frédéric Mila. Phase separation versus supersolid behavior in frustrated antiferromagnets. *Physical Review B*, 83(17):174421, 2011.

[94] Masahiro Kadosawa, Satoshi Nishimoto, Koudai Sugimoto, and Yukinori Ohta. Finite-temperature properties of excitonic condensation in the extended Falicov-Kimball Model: Cluster mean-field-theory approach. *Journal of the Physical Society of Japan*, 89(5):053706, 2020.

[95] Akihisa Koga, Shiryu Nakauchi, and Joji Nasu. Ground-state phase diagram in the Kugel-Khomskii model with finite spin-orbit interactions. *Physica B: Condensed Matter*, 536:369–371, 2018.

[96] Akihisa Koga, Shiryu Nakauchi, and Joji Nasu. Role of spin-orbit coupling in the Kugel-Khomskii model on the honeycomb lattice. *Physical Review B*, 97(9):094427, 2018.

[97] V.I. Kuz'min, Yu S. Orlov, A.E. Zarubin, T.M. Ovchinnikova, and S.G. Ovchinnikov. Magnetism in spin crossover systems: Short-range order and effects beyond the Heisenberg model. *Physical Review B*, 100(14):144429, 2019.

[98] Rajyavardhan Ray and Sanjeev Kumar. Switchable multiple spin states in the Kondo description of doped molecular magnets. *Scientific reports*, 7(1):1–10, 2017.

[99] Pieremanuele Canepa, Yves J. Chabal, and T. Thonhauser. When metal organic frameworks turn into linear magnets. *Phys. Rev. B*, 87(5):094407, 2013.

[100] Y. C. Arango, E. Vavilova, M. Abdel-Hafiez, O. Janson, A. A. Tsirlin, H. Rosner, S.-L. Drechsler, M. Weil, G. Nénert, R. Klingeler, O. Volkova, A. Vasiliev, V. Kataev,

and B. Büchner. Magnetic properties of the low-dimensional spin-$\frac{1}{2}$ magnet α-$Cu_2As_2O_7$. *Phys. Rev. B*, 84(9):134430, 2011.

[101] A. W. Kinross, M. Fu, T. J. Munsie, H. A. Dabkowska, G. M. Luke, Subir Sachdev, and T. Imai. Evolution of quantum fluctuations near the quantum critical point of the transverse field ising chain system $CoNb_2O_6$. *Phys. Rev. X*, 4(9):031008, 2014.

[102] A. Oosawa, T. Takamasu, K. Tatani, H. Abe, N. Tsujii, O. Suzuki, H. Tanaka, G. Kido, and K. Kindo. Field-induced magnetic ordering in the quantum spin system $KCuCl_3$. *Phys. Rev. B*, 66(7):104405, 2002.

[103] Hidekazu Tanaka, Akira Oosawa, Tetsuya Kato, Hidehiro Uekusa, Yuji Ohashi, Kazuhisa Kakurai, and Andreas Hoser. Observation of field-induced transverse néel ordering in the spin gap system $TlCuCl_3$. *Journal of the Physical Society of Japan*, 70(4):939–942, 2001.

[104] T. Nikuni, M. Oshikawa, A. Oosawa, and H. Tanaka. Bose-einstein condensation of dilute magnons in $TlCuCl_3$. *Phys. Rev. Lett.*, 84(0):5868–5871, 2000.

[105] Akira Oosawa, Kazuhisa Kakurai, Toyotaka Osakabe, Mitsutaka Nakamura, Masayasu Takeda, and Hidekazu Tanaka. Pressure-induced successive magnetic phase transitions in the spin gap system $TlCuCl_3$. *Journal of the Physical Society of Japan*, 73(6):1446–1449, 2004.

[106] A. B. Christian, S. H. Masunaga, A. T. Schye, A. Rebello, J. J. Neumeier, and Yi-Kuo Yu. Magnetic field influence on the néel, dimer, and spin-liquid states of the low-dimensional antiferromagnets $nita_2o_6$ and $CoSb_2O_6$. *Phys. Rev. B*, 90(10):224423, 2014.

[107] M.G. Banks, F. Heidrich-Meisner, A. Honecker, H. Rakoto, J.M. Broto, and R.K. Kremer. High field magnetization of the frustrated one-dimensional quantum antiferromagnet $LiCuVO_4$. *Journal of Physics: Condensed Matter*, 19(14):145227, 2007.

[108] I. Cabrera, J. D. Thompson, R. Coldea, D. Prabhakaran, R. I. Bewley, T. Guidi, J. A. Rodriguez-Rivera, and C. Stock. Excitations in the quantum paramagnetic phase of the quasi-one-dimensional ising magnet $CoNb_2O_6$ in a transverse field: Geometric frustration and quantum renormalization effects. *Phys. Rev. B*, 90(10):014418, 2014.

[109] J. Ma, C. D. Dela Cruz, Tao Hong, W. Tian, A. A. Aczel, Songxue Chi, J.-Q. Yan, Z. L. Dun, H. D. Zhou, and M. Matsuda. Magnetic phase transition in the low-dimensional compound $BaMn_2Si_2O_7$. *Phys. Rev. B*, 88(8):144405, 2013.

[110] J. L. Gavilano, E. Felder, D. Rau, H. R. Ott, P. Millet, F. Mila, T. Cichorek, and A. C. Mota. Unusual magnetic properties of the low-dimensional quantum magnet $Na_2V_3O_7$. *Phys. Rev. B*, 72(10):064431, 2005.

[111] Bella Lake, D. Alan Tennant, Chris D. Frost, and Stephen E. Nagler. Quantum criticality and universal scaling of a quantum antiferromagnet. *Nature materials*, 4(4):329–334, 2005.

[112] M. B. Stone, D. H. Reich, C. Broholm, K. Lefmann, C. Rischel, C. P. Landee, and M. M. Turnbull. Extended quantum critical phase in a magnetized spin-$\frac{1}{2}$ antiferromagnetic chain. *Phys. Rev. Lett.*, 91(4):037205, 2003.

[113] A. A. Nersesyan and A. M. Tsvelik. One-dimensional spin-liquid without magnon excitations. *Phys. Rev. Lett.*, 78(0):3939–3942, 1997.

[114] Yukihiro Yoshida, Hiroshi Ito, Mitsuhiko Maesato, Yasuhiro Shimizu, Hiromi Hayama, Takaaki Hiramatsu, Yuto Nakamura, Hideo Kishida, Takashi Koretsune, Chisa Hotta, et al. Spin-disordered quantum phases in a quasi-one-dimensional triangular lattice. *Nature Physics*, 11(8):679–683, 2015.

[115] P. Lecheminant. One-dimensional quantum spin liquids. In *Frustrated spin systems*, pages 321–381. World Scientific, 2013.

[116] Masanori Kohno, Oleg A. Starykh, and Leon Balents. Spinons and triplons in spatially anisotropic frustrated antiferromagnets. *Nature Physics*, 3(11):790–795, 2007.

[117] M. Skoulatos, M. Månsson, C. Fiolka, K. W. Krämer, J. Schefer, J. S. White, and Ch. Rüegg. Dimensional reduction by pressure in the magnetic framework material $CuF_2(D_2O)_2(pyz)$: From spin-wave to spinon excitations. *Phys. Rev. B*, 96(5):020414, 2017.

[118] Zhe Wang, Jianda Wu, Wang Yang, Anup Kumar Bera, Dmytro Kamenskyi, ATM Nazmul Islam, Shenglong Xu, Joseph Matthew Law, Bella Lake, Congjun Wu, et al. Experimental observation of bethe strings. *Nature*, 554(7691):219–223, 2018.

[119] A. K. Bera, B. Lake, F. H. L. Essler, L. Vanderstraeten, C. Hubig, U. Schollwöck, A. T. M. N. Islam, A. Schneidewind, and D. L. Quintero-Castro. Spinon confinement in a quasi-one-dimensional anisotropic Heisenberg magnet. *Phys. Rev. B*, 96(16):054423, 2017.

[120] A. Harrison, M. F. Collins, J. Abu-Dayyeh, and C. V. Stager. Magnetic structures and excitations of $CsMnI_3$: A one-dimensional Heisenberg antiferromagnet with easy-axis anisotropy. *Phys. Rev. B*, 43(0):679–688, 1991.

[121] Michael Karbach and Gerhard Müller. Line-shape predictions via bethe ansatz for the one-dimensional spin-$\frac{1}{2}$ Heisenberg antiferromagnet in a magnetic field. *Phys. Rev. B*, 62(0):14871–14879, 2000.

[122] Haruhiko Kuroe, Kouhei Kusakabe, Akira Oosawa, Tomoyuki Sekine, Fumiko Yamada, Hidekazu Tanaka, and Masashige Matsumoto. Magnetic field induced one-magnon raman scattering in the magnon bose-einstein condensation phase of $TlCuCl_3$. *Phys. Rev. B*, 77(5):134420, 2008.

[123] R. Coldea, D. A. Tennant, E. M. Wheeler, E. Wawrzynska, D. Prabhakaran, M. Telling, K. Habicht, P. Smeibidl, and K. Kiefer. Quantum criticality in an ising chain: Experimental evidence for emergent E8 symmetry. *Science*, 327(5962):177–180, 2010.

[124] C. M. Morris, R. Valdés Aguilar, A. Ghosh, S. M. Koohpayeh, J. Krizan, R. J. Cava, O. Tchernyshyov, T. M. McQueen, and N. P. Armitage. Hierarchy of bound states in the one-dimensional ferromagnetic ising chain $CoNb_2O_6$ investigated by high-resolution time-domain terahertz spectroscopy. *Phys. Rev. Lett.*, 112(5):137403, 2014.

[125] M. Matsuda, S. E. Dissanayake, D. L. Abernathy, K. Totsuka, and A. A. Belik. Magnetic excitations in an $s = \frac{1}{2}$ diamond-shaped tetramer compound Cu_2PO_4OH. *Phys. Rev. B*, 92(6):184428, 2015.

[126] Masashi Hase, Masashige Matsumoto, Akira Matsuo, and Koichi Kindo. Magnetism of the antiferromagnetic spin-$\frac{1}{2}$ tetramer compound $\mathbf{CuInVO_5}$. *Phys. Rev. B*, 94(7):174421, 2016.

[127] Masashi Hase, Akira Matsuo, Koichi Kindo, and Masashige Matsumoto. Magnetism of the spin-1 tetramer compound $A_2Ni_2Mo_3O_{12}$ (A = Rb or K). *Phys. Rev. B*, 96(8):214424, 2017.

[128] Andrew G. Green, Gareth Conduit, and Frank Krüger. Quantum order-by-disorder in strongly correlated metals. *Annual Review of Condensed Matter Physics*, 9(1):59–77, 2018.

[129] J. D. M. Champion, M. J. Harris, P. C. W. Holdsworth, A. S. Wills, G. Balakrishnan, S. T. Bramwell, E. Čižmár, T. Fennell, J. S. Gardner, J. Lago, D. F. McMorrow, M. Orendáč, A. Orendáčová, D. McK. Paul, R. I. Smith, M. T. F. Telling, and A. Wildes. $Er_2Ti_2O_7$: Evidence of quantum order by disorder in a frustrated antiferromagnet. *Phys. Rev. B*, 68(4):020401, 2003.

[130] P. C. Guruciaga, M. Tarzia, M. V. Ferreyra, L. F. Cugliandolo, S. A. Grigera, and R. A. Borzi. Field-tuned order by disorder in frustrated ising magnets with antiferromagnetic interactions. *Phys. Rev. Lett.*, 117(5):167203, 2016.

[131] Thomas Maier, Mark Jarrell, Thomas Pruschke, and Matthias H. Hettler. Quantum cluster theories. *Rev. Mod. Phys.*, 77(0):1027–1080, 2005.

[132] Oleg A. Starykh. Unusual ordered phases of highly frustrated magnets: a review. *Reports on Progress in Physics*, 78(5):052502, 2015.

[133] C. Balz, B. Lake, H. Luetkens, C. Baines, T. Guidi, M. Abdel-Hafiez, A. U. B. Wolter, B. Büchner, I. V. Morozov, E. B. Deeva, O. S. Volkova, and A. N. Vasiliev. Quantum spin chain as a potential realization of the nersesyan-tsvelik model. *Phys. Rev. B*, 90(5):060409, 2014.

[134] David C. Johnston and K.H.J. Buschow. Handbook of magnetic materials. *Elsevier, Amsterdam*, 10:1237, 1997.

[135] Daisuke Yamamoto. Correlated cluster mean-field theory for spin systems. *Phys. Rev. B*, 79(9):144427, 2009.

[136] F. M. Zimmer, M. Schmidt, and S. G. Magalhaes. Correlated cluster mean-field theory for spin-glass systems. *Phys. Rev. E*, 89(7):062117, 2014.

[137] F. M. Zimmer, M. Schmidt, and Jonas Maziero. Quantum correlated cluster mean-field theory applied to the transverse ising model. *Phys. Rev. E*, 93(8):062116, 2016.

[138] Gerhard Müller, Harry Thomas, Hans Beck, and Jill C. Bonner. Quantum spin dynamics of the antiferromagnetic linear chain in zero and nonzero magnetic field. *Physical Review B*, 24(3):1429, 1981.

[139] Felix Bloch. Zur theorie des ferromagnetismus. *Zeitschrift für Physik*, 61(3-4):206–219, 1930.

[140] Jacques Des Cloizeaux and J.J. Pearson. Spin-wave spectrum of the antiferromagnetic linear chain. *Physical Review*, 128(5):2131, 1962.

[141] B. Keimer and J. E. Moore. The physics of quantum materials. *Nat. Phys.*, 13(11):1045–1055, 2017.

[142] Thierry Giamarchi, Christian Rüegg, and Oleg Tchernyshyov. Bose–Einstein condensation in magnetic insulators. *Nat. Phys.*, 4(3):198–204, 2008.

[143] Leon Balents. Spin liquids in frustrated magnets. *Nature*, 464(7286):199–208, 2010.

[144] Max Hirschberger, Jason W. Krizan, R. J. Cava, and N. P. Ong. Large thermal hall conductivity of neutral spin excitations in a frustrated quantum magnet. *Science*, 348(6230):106–109, 2015.

[145] Takashi Kurumaji, Taro Nakajima, Max Hirschberger, Akiko Kikkawa, Yuichi Yamasaki, Hajime Sagayama, Hironori Nakao, Yasujiro Taguchi, Taka-hisa Arima, and Yoshinori Tokura. Skyrmion lattice with a giant topological hall effect in a frustrated triangular-lattice magnet. *Science*, 365(6456):914–918, 2019.

[146] A. Ramirez. Strongly Geometrically Frustrated Magnets. *Annu. Rev. Mater. Res.*, 24(1):453–480, 1994.

[147] P. Chandra and P. Coleman. Quantum spin nematics: Moment-free magnetism. *Phys. Rev. Lett.*, 66(1):100–103, 1991.

[148] Daichi Hirobe, Masahiro Sato, Takayuki Kawamata, Yuki Shiomi, Ken-ichi Uchida, Ryo Iguchi, Yoji Koike, Sadamichi Maekawa, and Eiji Saitoh. One-dimensional spinon spin currents. *Nat. Phys.*, 13(1):30–34, 2016.

[149] S.-H. Lee, C. Broholm, W. Ratcliff, G. Gasparovic, Q. Huang, T. H. Kim, and S.-W. Cheong. Emergent excitations in a geometrically frustrated magnet. *Nature*, 418(6900):856–858, 2002.

[150] Oleg A. Starykh and Leon Balents. Excitations and quasi-one-dimensionality in field-induced nematic and spin density wave states. *Phys. Rev. B*, 89(10):104407, 2014.

[151] Eron Cemal, Mechthild Enderle, Reinhard K. Kremer, Björn Fåk, Eric Ressouche, Jon P. Goff, Mariya V. Gvozdikova, Mike E. Zhitomirsky, and Tim Ziman. Field-induced states and excitations in the quasicritical spin-1/2 chain linarite. *Phys. Rev. Lett.*, 120(6):067203, 2018.

[152] B. Willenberg, M. Schäpers, K. C. Rule, S. Süllow, M. Reehuis, H. Ryll, B. Klemke, K. Kiefer, W. Schottenhamel, B. Büchner, B. Ouladdiaf, M. Uhlarz, R. Beyer, J. Wosnitza, and A. U. B. Wolter. Magnetic frustration in a quantum spin chain: The case of linarite $PbCuSO_4(OH)_2$. *Phys. Rev. Lett.*, 108(5):117202, 2012.

[153] Kazuhiro Nawa, Makoto Yoshida, Masashi Takigawa, Yoshihiko Okamoto, and Zenji Hiroi. Collinear spin density wave order and anisotropic spin fluctuations in the frustrated $J_1 - J_2$ chain magnet $NaCuMoO_4(OH)$. *Phys. Rev. B*, 96(9):174433, 2017.

[154] M. Enderle, B. Fåk, H.-J. Mikeska, R. K. Kremer, A. Prokofiev, and W. Assmus. Two-spinon and four-spinon continuum in a frustrated ferromagnetic spin-1/2 chain. *Phys. Rev. Lett.*, 104(4):237207, 2010.

[155] M. Enderle, C. Mukherjee, B. Fåk, R. K Kremer, J.-M Broto, H Rosner, S.-L. Drechsler, J. Richter, J. Malek, A. Prokofiev, W. Assmus, S. Pujol, J.-L. Raggazzoni, H Rakoto, M. Rheinstädter, and H. M. Rønnow. Quantum helimagnetism of the frustrated spin-1/2 chain $LiCuVO_4$. *Europhysics Letters (EPL)*, 70(2):237–243, 2005.

[156] Yu. Savina, O. Bludov, V. Pashchenko, S. L. Gnatchenko, P. Lemmens, and H. Berger. Magnetic properties of the antiferromagnetic spin-1/2 chain system β-$TeVO_4$. *Phys. Rev. B*, 84(10):104447, 2011.

[157] M. Pregelj, A. Zorko, O. Zaharko, H. Nojiri, H. Berger, L. C. Chapon, and D. Arčon. Spin-stripe phase in a frustrated zigzag spin-1/2 chain. *Nat. Commun.*, 6(1):7255, 2015.

[158] M. Pregelj, O. Zaharko, M. Herak, M. Gomilšek, A. Zorko, L. C. Chapon, F. Bourdarot, H. Berger, and D. Arčon. Exchange anisotropy as mechanism for spin-stripe formation in frustrated spin chains. *Phys. Rev. B*, 94(8):081114, 2016.

[159] F. Weickert, N. Harrison, B. L. Scott, M. Jaime, A. Leitmäe, I. Heinmaa, R. Stern, O. Janson, H. Berger, H. Rosner, and A. A. Tsirlin. Magnetic anisotropy in the frustrated spin-chain compound β-$TeVO_4$. *Phys. Rev. B*, 94(6):064403, 2016.

[160] M. Pregelj, O. Zaharko, U. Stuhr, A. Zorko, H. Berger, A. Prokofiev, and D. Arčon. Coexisting spinons and magnons in the frustrated zigzag spin- 1/2 chain compound β-$TeVO_4$. *Phys. Rev. B*, 98(9):094405, 2018.

[161] M. Pregelj, A. Zorko, M. Klanjšek, O. Zaharko, J. S. White, O. Prokhnenko, M. Bartkowiak, H. Nojiri, H. Berger, and D. Arčon. Magnetic ground state of the frustrated spin-$\frac{1}{2}$ chain compound β–$TeVO_4$ at high magnetic fields. *Phys. Rev. B*, 100(7):094433, 2019.

[162] Matej Pregelj, Andrej Zorko, Matjaž Gomilšek, Martin Klanjšek, Oksana Zaharko, Jonathan S. White, Hubertus Luetkens, Fiona Coomer, Tomislav Ivek, David Rivas Góngora, Helmuth Berger, and Denis Arčon. Elementary excitation in the spin-stripe phase in quantum chains. *npj Quantum Materials*, 4(1), 2019.

[163] Raymond F. Bishop, Damian J. J. Farnell, and John B. Parkinson. Phase transitions in the spin-half $J_1 - J_2$ model. *Phys. Rev. B*, 58(10):6394–6402, 1998.

[164] J. Sirker, V. Y. Krivnov, D. V. Dmitriev, A. Herzog, O. Janson, S. Nishimoto, S.-L. Drechsler, and J. Richter. $J_1 - J_2$ Heisenberg model at and close to its z=4 quantum critical point. *Phys. Rev. B*, 84(14):144403, 2011.

[165] D. V. Dmitriev and V. Ya. Krivnov. Weakly anisotropic frustrated zigzag spin chain. *Phys. Rev. B*, 77(2):024401, 2008.

[166] F. Heidrich-Meisner, A. Honecker, and T. Vekua. Frustrated ferromagnetic spin-1/2 chain in a magnetic field: The phase diagram and thermodynamic properties. *Phys. Rev. B*, 74(2):020403, 2006.

[167] T. Vekua, A. Honecker, H.-J. Mikeska, and F. Heidrich-Meisner. Correlation functions and excitation spectrum of the frustrated ferromagnetic spin-1/2 chain in an external magnetic field. *Phys. Rev. B*, 76(17):174420, 2007.

[168] Masahiro Sato, Toshiya Hikihara, and Tsutomu Momoi. Spin-Nematic and Spin-Density-Wave Orders in Spatially Anisotropic Frustrated Magnets in a Magnetic Field. *Phys. Rev. Lett.*, 110(7):077206, 2013.

[169] Toshiya Hikihara, Lars Kecke, Tsutomu Momoi, and Akira Furusaki. Vector chiral and multipolar orders in the spin-1/2 frustrated ferromagnetic chain in magnetic field. *Phys. Rev. B*, 78(14):144404, 2008.

[170] H.-J. Grafe, S. Nishimoto, M. Iakovleva, E. Vavilova, L. Spillecke, A. Alfonsov, M.-I. Sturza, S. Wurmehl, H. Nojiri, H. Rosner, et al. Signatures of a magnetic field-induced unconventional nematic liquid in the frustrated and anisotropic spin-chain cuprate $LiCuSbO_4$. *Scientific reports*, 7(1):1–16, 2017.

[171] Andrey V. Chubukov. Chiral, nematic, and dimer states in quantum spin chains. *Phys. Rev. B*, 44(9):4693–4696, 1991.

[172] Fabio Cinti, Alessandro Cuccoli, and Angelo Rettori. Vector chiral spin liquid phase in quasi-one-dimensional incommensurate helimagnets. *Phys. Rev. B*, 83(6):174415, 2011.

[173] A. Saúl and G. Radtke. Density functional approach for the magnetism of β -$TeVO_4$. *Phys. Rev. B*, 89(10):104414, 2014.

[174] Ayushi Singhania and Sanjeev Kumar. Cluster mean-field study of the Heisenberg model for $CuInVO_5$. *Phys. Rev. B*, 98(10):104429, 2018.

[175] Katarína Karľová, Jozef Strečka, and Tomáš Madaras. The schottky-type specific heat as an indicator of relative degeneracy between ground and first-excited states: The case study of regular ising polyhedra. *Physica B: Condensed Matter*, 488:49–56, 2016.

[176] Dayasindhu Dey, Manoranjan Kumar, Siân E. Dutton, Robert J. Cava, and Zoltán G. Soos. Spin-specific heat determination of the ratio of competing first- and second-neighbor exchange interactions in frustrated spin-$\frac{1}{2}$ chains. *Phys. Rev. B*, 97(5):064407, 2018.

[177] Hiroaki Ishizuka and Yukitoshi Motome. Thermally induced phases in an Ising Kondo lattice model on a triangular lattice: Partial disorder and Kosterlitz-Thouless state. *Phys. Rev. B*, 87(15):155156, 2013.

[178] M. E. Zhitomirsky and H. Tsunetsugu. Magnon pairing in quantum spin nematic. *Europhysics Lett.*, 92(3):37001, 2010.

[179] Julien Sudan, Andreas Lüscher, and Andreas M. Läuchli. Emergent multipolar spin correlations in a fluctuating spiral: The frustrated ferromagnetic spin-1/2 Heisenberg chain in a magnetic field. *Phys. Rev. B*, 80(14):140402, 2009.

[180] John Sydney Dugdale. *The electrical properties of disordered metals*. Cambridge University Press, 2005.

[181] A. Maeda, T. Yabe, S. Takebayashi, M. Hase, and K. Uchinokura. Substitution of $3d$ metals for Cu in $Bi_2(Sr_{0.6}Ca_{0.4})_3Cu_2O_y$. *Physical Review B*, 41(7):4112, 1990.

[182] Philip W. Anderson. Absence of diffusion in certain random lattices. *Physical review*, 109(5):1492, 1958.

[183] Tianping Ying, Yueqiang Gu, Xiao Chen, Xinbo Wang, Shifeng Jin, Linlin Zhao, Wei Zhang, and Xiaolong Chen. Anderson localization of electrons in single crystals: Lixfe7se8. *Science advances*, 2(2):e1501283, 2016.

[184] Yoseph Imry and Michael Wortis. Influence of quenched impurities on first-order phase transitions. *Physical Review B*, 19(7):3580, 1979.

[185] Sebastian Eggert and Ian Affleck. Magnetic impurities in half-integer-spin Heisenberg antiferromagnetic chains. *Physical Review B*, 46(17):10866, 1992.

[186] Masayuki Hagiwara, Koichi Katsumata, Ian Affleck, Bertrand I. Halperin, and J.P. Renard. Observation of $S = 1/2$ degrees of freedom in an $S = 1$ linear-chain Heisenberg antiferromagnet. *Physical review letters*, 65(25):3181, 1990.

[187] M. Hase, I. Terasaki, Y. Sasago, K. Uchinokura, and H. Obara. Effects of substitution of Zn for Cu in the spin-peierls cuprate, $CuGeO_3$: the suppression of the spin-peierls transition and the occurrence of a new spin-glass state. *Physical review letters*, 71(24):4059, 1993.

[188] B. Grenier, L.P. Regnault, J.E. Lorenzo, J. Bossy, J.P. Renard, G. Dhalenne, and A. Revcolevschi. Effect of magnetic field and Si-doping on the spin-peierls phase of $CuGeO_3$. *Physica B: Condensed Matter*, 234:534–535, 1997.

[189] M. Azuma, Y. Fujishiro, M. Takano, M. Nohara, and H. Takagi. Switching of the gapped singlet spin-liquid state to an antiferromagnetically ordered state in $Sr(Cu_{1-x}Zn_x)_2O_3$. *Physical Review B*, 55(14):R8658, 1997.

[190] N. Motoyama, H. Eisaki, and S. Uchida. Magnetic susceptibility of ideal spin 1/2 Heisenberg antiferromagnetic chain systems, Sr_2CuO_3 and $SrCuO_2$. *Physical review letters*, 76(17):3212, 1996.

[191] K.M. Kojima, J. Yamanobe, H. Eisaki, S. Uchida, Y. Fudamoto, I.M. Gat, M.I. Larkin, A. Savici, Y.J. Uemura, P.P. Kyriakou, et al. Site-dilution in the quasi-one-dimensional antiferromagnet $Sr_2(Cu_{1-x}Pd_x)O_3$: reduction of néel temperature and spatial distribution of ordered moment sizes. *Physical Review B*, 70(9):094402, 2004.

[192] Gediminas Simutis, S. Gvasaliya, M. Månsson, Alexander L. Chernyshev, Ananthanarayanan Mohan, S. Singh, C. Hess, Andrei T. Savici, Alexander I. Kolesnikov, A. Piovano, et al. Spin pseudogap in ni-doped $SrCuO_2$. *Physical review letters*, 111(6):067204, 2013.

[193] Koushik Karmakar, Rabindranath Bag, Markos Skoulatos, Christian Rüegg, and Surjeet Singh. Impurities in the weakly coupled quantum spin chains Sr_2CuO_3 and $SrCuO_2$. *Physical Review B*, 95(23):235154, 2017.

[194] S. Kimura, M. Matsuda, T. Masuda, S. Hondo, K. Kaneko, N. Metoki, M. Hagiwara, T. Takeuchi, K. Okunishi, Z. He, et al. Longitudinal spin density wave order in a quasi-1d ising-like quantum antiferromagnet. *Physical review letters*, 101(20):207201, 2008.

[195] A.K. Bera, B. Lake, W.-D. Stein, and S. Zander. Magnetic correlations of the quasi-one-dimensional half-integer spin-chain antiferromagnets $srm_2v_2o_8$ (m= co, mn). *Physical Review B*, 89(9):094402, 2014.

[196] Sebastian Eggert, David P. Gustafsson, and Stefan Rommer. Phase diagram of an impurity in the Spin-1/2 chain: Two-channel Kondo effect versus Curie law. *Physical review letters*, 86(3):516, 2001.

[197] J. Bobroff, N. Laflorencie, L.K. Alexander, A.V. Mahajan, B. Koteswararao, and P. Mendels. Impurity-induced magnetic order in low-dimensional spin-gapped materials. *Physical review letters*, 103(4):047201, 2009.

[198] L.K. Alexander, J. Bobroff, A.V. Mahajan, B. Koteswararao, N. Laflorencie, and F. Alet. Impurity effects in coupled-ladder $BiCu_2PO_6$ studied by NMR and quantum monte carlo simulations. *Physical Review B*, 81(5):054438, 2010.

[199] Weijie Zhang, Jun-ichi Igarashi, and Peter Fulde. Thermodynamics of an impurity coupled to a Heisenberg chain: Density-matrix renormalization group and monte carlo studies. *Journal of the Physical Society of Japan*, 66(7):1912–1915, 1997.

[200] W. Zhang, J. Igarashi, and P. Fulde. Magnetic impurity coupled to a Heisenberg chain: Density-matrix renormalization-group study. *Physical Review B*, 56(2):654, 1997.

[201] D.C. Johnston, R.K. Kremer, Matthias Troyer, X. Wang, A. Klümper, S.L. Bud'ko, A.F. Panchula, and P.C. Canfield. Thermodynamics of spin $S = 1/2$ antiferromagnetic uniform and alternating-exchange Heisenberg chains. *Physical Review B*, 61(14):9558, 2000.

[202] Stefan Wessel and Stephan Haas. Three-dimensional ordering in weakly coupled antiferromagnetic ladders and chains. *Physical Review B*, 62(1):316, 2000.

[203] Jacques Des Cloizeaux and Michel Gaudin. Anisotropic linear magnetic chain. *Journal of Mathematical Physics*, 7(8):1384–1400, 1966.

[204] S. Kimura, T. Takeuchi, K. Okunishi, M. Hagiwara, Z. He, K. Kindo, T. Taniyama, and M. Itoh. Novel ordering of an $S = 1/2$ quasi-1d ising-like antiferromagnet in magnetic field. *Physical review letters*, 100(5):057202, 2008.